AD A073475

DDC ACCESSION NUMBER

II

LEVEL

DATA SHEET

PHOTOGRAPH

THIS SHEET

1

INVENTORY

WT-724

DOCUMENT IDENTIFICATION

DISTRIBUTION STATEMENT A

Approved for public release;
Distribution Unlimited

per telecon w/Betty Fox (DNA Tech Libr, Chief), the classified references contained herein may remain.

N. LaChance (DDA-2)
9-5-79

Accession For

NTIS GRA&I [X]
DDC TAB [ ]
Unannounced [ ]
Justification per Doc.

By

Distribution/

Availability Codes

Dist	Avail and/or special
A	

DISTRIBUTION STAMP

DDC
RECEIVED
SEP 5 1979
E

DATE ACCESSIONED

79 08 21 048

DATE RECEIVED IN DDC

PHOTOGRAPH THIS COPY

WT-724

Copy No. 173 A

Operation UPSHOT-KNOTHOLE

NEVADA PROVING GROUNDS

March - June 1953

Project 3.5

TESTS ON THE RESPONSE OF WALL AND ROOF PANELS AND THE TRANSMISSION OF LOAD TO SUPPORTING STRUCTURE

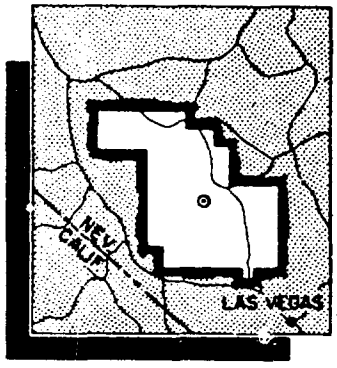

[redacted]

as
54.

Statement A
Approved for public release;
Distribution unlimited.

HEADQUARTERS FIELD COMMAND, ARMED FORCES SPECIAL WEAPONS PROJECT
SANDIA BASE, ALBUQUERQUE, NEW MEXICO

[redacted]

Reproduced Direct from Manuscript Copy by
AEC Technical Information Service
Oak Ridge, Tennessee

Inquiries relative to this report may be made to

Chief, Armed Forces Special Weapons Project

Washington, D. C.

[redacted] UNCLASSIFIED

WT-724

This document consists of 182 pages

No. 173 of 270 copies, Series A

OPERATION UPSHOT-KNOTHOLE

Project 3.5

TESTS ON THE RESPONSE OF WALL AND ROOF PANELS AND THE TRANSMISSION OF LOAD TO SUPPORTING STRUCTURES

UNCLASSIFIED

REPORT TO THE TEST DIRECTOR

[redacted]

[redacted] DH Form 1575 27 Jul 24 ICAG-2 dtd 6 Aug 63

[redacted] By Wade, 23 Sep 64

Eugene Sevin

CONFIDENTIAL

[redacted] DOWNGRADED [redacted] BY AUTHORITY OF AG-2 18 dtd 23 Feb 60

WADC-TN-55-109

May 1955

[redacted]

Air Materiel Command
Wright-Patterson Air Force Base
Dayton, Ohio

Statement A
Approved for public release;
Distribution unlimited.

[redacted] UNCLASSIFIED

[redacted] CONFIDENTIAL [redacted]

ABSTRACT

This report deals with the pre- and post-test work on the Air Force Structures Test, Project 3.5 of Operation UPSHOT-KNOTHOLE, Tests on the Response of Wall and Roof Panels. Ten wall and seven roof panels, representing typical construction practice (e.g., masonry, reinforced concrete, metal, and wood siding, etc.) were positioned in three overpressure regions in Shot 9. Instrumentation consisted of pressure gages, motion picture cameras, and a strain gage system which measured the blast forces transmitted by the panels to the supporting structure.

All but two of the wall panels were destroyed (the three brick walls showed a definite gradation of damage from light through severe) and all of the roof panels were at least partially destroyed. The test results indicate that, when a wall panel remains intact, the predicted applied load represents reasonably well the average load transmitted by the panel to the supporting frame. With the exception of the reinforced concrete panel, the walls that failed transmitted only a small percentage of the applied loading; initial structural failure occurred during the first 20 ms or so, and complete failure in 50 to 100 ms.

Peak pressure damage criteria appear to be justified for most of the roof and wall panels tested and, where possible, critical pressures above which failure of the panel is reasonably assured have been deduced. An attempt is made to correlate the impulse of the transmitted force with the diffraction impulse of the predicted critical loading for the panel with the view toward incorporating the test results into existing building response analyses. According to this scheme, masonry construction (and apparently wood construction of the type tested) will transmit 150 per cent of the critical diffraction impulse, while the other lightweight materials tested will transmit only from 20 to 40 per cent of this impulse. The force transmitted by most of the roof structures appeared to be in substantial agreement with the predicted applied loading during the first 50 to 100 ms.

The pressure gage located behind the brick wall which failed indicated a remarkably slow buildup time for the incoming pressure wave. From this it is inferred that even though a wall fails structurally quite early in the loading period, the debris may not clear from the opening until a relatively long time has passed. In such cases, the peak forces in the interior of a building are expected to be considerably lower that if the wall debris were not present. The effect of wall debris thus may be of considerably greater importance than had previously been anticipated in

reducing the loading on interior equipment, downstream wall, columns, and trusswork. Comparison of measured pressures with predicted loadings on several of the roofs indicates that predictions are fair to good in most respects for the Mach reflection region, but are poor in certain respects for the regular reflection region.

FOREWORD

This report is one of the reports presenting the results of the 78 projects participating in the Military Effects Tests Program of Operation UPSHOT-KNOTHOLE, which included 11 test detonations. For readers interested in other pertinent test information, reference is made to WT-782, Summary Report of the Technical Director, Military Effects Program. This summary report includes the following information of possible general interest.

a. An over-all description of each detonation, including yield, height of burst, ground zero location, time of detonation, ambient atmospheric conditions at detonation, etc., for the 11 shots.

b. Compilation and correlation of all project results on the basic measurements of blast and shock, thermal radiation, and nuclear radiation.

c. Compilation and correlation of the various project results on weapons effects.

d. A summary of each project, including objectives and results.

e. A complete listing of all reports covering the Military Effects Tests Program.

PREFACE

In a letter dated 12 March 1952, the Air Materiel Command was requested by Air Research & Development Command to submit for testing in Operation UPSHOT/KNOTHOLE existing requirements for a structures program which would be based on the needs of the Air Force for Target Analysis and Indirect Bomb Damage Assessment information. Within the Air Materiel Command the responsibility for designing and executing such a program was delegated to the Special Studies Office, Engineering Branch of the Installations Division. The requirements which were submitted and approved became part of Program Three of the Operation and were designated as Projects 3.1, 3.3, 3.4, 3.5, 3.6, and 3.26.1. Mr. B. J. O'Brien of Special Studies Office was appointed project officer and as such coordinated and successfully directed the planning and operation phases of the six projects.

Armour Research Foundation (ARF) of the Illinois Institute of Technology was awarded a contract to assist the Special Studies Office in planning and designing the experiments, and in analysis and reporting of test results.. During the period of planning, close liaison was maintained with other interested Air Force agencies, particularly the Physical Vulnerability Division, Directorate of Intelligence, Headquarters USAF. Many valuable suggestions were contributed by Colonel John Weltman, USAF, Lt Col John Ault, USAF, Messrs. R. G. Grassy and S. White, Dr. F. Genevese and others of that Division, and by Mr. Louis A. Nees, Chief of the Engineering Branch, Installations Division, Air Materiel Command.

Personnel of the Special Studies Office who were intimately connected with the program were Mr. Eric H. Wang, Chief, Special Studies, who was the technical and scientific monitor for the Air Force Program, Mr. Arthur Stansel (now with Landing Gear Development Section, Equipment Laboratory, Wright Air Development Center), and Mrs. Maisie G. Ridgeway, secretary to Mr. Wang. Other members of the office who were associated with the program were Messrs. R. R. Birukoff, P. A. Cooley, J. C. Noble, and Lts. T. M. Murray, and G. A. Rockwell, USAF.

The atomic effects work of the Special Studies Office is now being performed by the Blast Effects Research Group, Mechanics Branch, Aeronautical Research Laboratory, Wright Air Development Center. The personnel of this group are those formerly associated with the Special Studies Office.

Most of the introduction section of this report was taken from the preface of the Preliminary Report, Operation UPSHOT-KNOTHOLE project 3.5 authored by Eric H. Wang and Bernard J. O'Brien.

ACKNOWLEDGMENTS

This report covers the activities of the Armour Research Foundation in connection with the Air Force Structures Program, Project 3.5, of Operation UPSHOT-KNOTHOLE. The work reported herein was sponsored by the Air Research and Development Command, and performed for Air Materiel Command, Wright-Patterson Air Force Base, Dayton, Ohio, under the terms of Air Force Contract No. AF33(038)-30029. This program was technically monitored by the Special Studies Office of Installations Division, AMC.

Personnel who have contributed to this report include: R. L. Calvin, S. J. Fraenkel, K. C. Gandy, H. Himelblau, R. L. Janes, E. L. McDowell, K. E. McKee, R. W. Sauer, A. Sherman, T. Schiffman, L. A. Schmidt, E. Sevin, M. R. Smith, A. H. Wiedermann, and T. A. Zaker.

CONTENTS

ILLUSTRATIONS

TABLES

CHAPTER I

INTRODUCTION

1.1 PURPOSE OF AIR FORCE TEST PROGRAMS

The series of tests conducted by the Air Force in Operation UPSHOT-KNOTHOLE is part of a continuing Air Force program designated as "Determination of Blast Effects on Buildings and Structures." The United States Air Force is mainly interested in the offensive aspects of such research.

The UPSHOT-KNOTHOLE projects sponsored by the Air Force and their specific objectives cannot be fully understood without some knowledge of the general objectives of the over-all program. The research results emanating from these studies and experiments conducted by the Air Force are used by a number of government agencies to improve their own systems of determining blast effects, or to further their own research.

One of these agencies is the Directorate of Intelligence, Headquarters, USAF, which feeds results as they are obtained into its own system of vulnerability classes, thereby making it possible to analyze prospective enemy targets with greater accuracy, and to recommend the desired ground zero. Another principal user of the research results is the Strategic Air Command, which applies them toward improvement of an existing indirect bomb damage assessment system. The purpose of this system is to make it possible to dispense with the usual reconnaissance after a strike, using instead information on the actual ground zero, height of burst, and yield of the weapon which is brought back to the operational base by the strike aircraft to determine the damage inflicted.

The task of determining the effect of blast on various types of building structures and tactical equipment is a rather formidable one. However, its difficulty is somewhat relieved by the fact that, for the offensive purposes in which the Air Force is interested, it is not necessary to determine the effect of transient loads on these items with the same accuracy as would normally be employed for static design purposes. In fact, even if it were possible to solve the dynamic problems satisfactorily, Intelligence information would be far too sketchy to furnish the information necessary to justify the use of an accurate analysis for items located in prospective enemy countries. From the experience that is so far available it is expected that it will be

possible within the foreseeable future to determine blast damage within broad limits with sufficient accuracy for planning as well as for operational purposes.

In view of the complex phenomena attending shock waves emanating from various types of atomic blasts and the uncertainties inherent in determining significant parameters, an investigator's first idea would be to obtain solutions through a long series of very elaborate and properly designed full-scale tests. However, neither funds nor time will allow such an approach. It has therefore been the objective of the agencies involved to obtain sufficiently accurate results by judicious use of theoretical analyses, laboratory tests, high explosive field tests, and a small number of full-scale atomic tests.

Three of these research projects have involved full-scale atomic testing. The first was GREENHOUSE, the second was JANGLE (the first, and so far only, underground burst of an atomic weapon to which an Air Force structures program was subjected) and the third the present UPSHOT-KNOTHOLE program.

From previous analysis, laboratory tests, and full-scale tests (the latter especially as conducted in GREENHOUSE), methods of damage prediction have been developed by Armour Research Foundation (ARF) and others. These prediction methods have attempted to describe the character of the blast loads acting on a variety of items. Response computations based on the predicted loadings permit, in turn, an estimate of physical damage. However, the relation between the deflection or movement of a body and significant military damage has never been clearly established except for extreme cases, e.g., total destruction or no destruction. Another aim of these tests is, therefore, to establish the relationship between deflection and functional damage. A full-scale test also affords an excellent opportunity to determine scaling check points for laboratory tests.

In addition to the scientific aspects of the tests, most of the results of the Air Force projects can be used by other government agencies such as the Directorate of Intelligence to furnish "rough and ready" experimental answers to the behavior of various kinds of structures under blast. In many cases there is a statistically significant number of items involved which, added to previous experimental data such as those gathered at Hiroshima and Nagasaki, will help round out the present vulnerability picture. In other cases, mathematical analysis may have to rely on ad hoc information to furnish parameters which cannot be obtained in any other way.

The foregoing remarks are designed to furnish the background necessary for a full understanding of the objectives of this and other of the Air Force projects. The full significance and value of the results of each test will be realized only when they are correlated with results of past, current, and future analyses, laboratory tests, high explosive field tests, and full-scale atomic investigations.

1.2 SPECIFIC OBJECTIVES

The response of structures to blast loading is an important phase of over-all target analysis. One of the greatest uncertainties in this

problem from the point of view of analytical treatment is knowledge of the actual forces that serve to distort and damage the structural frame of a building. Load prediction methods have in the past served only to identify the character of loading acting on the exterior roof and wall panels. However, as a result of the action of these components, this loading is distorted and modified to yield the actual forces that excite the structural frame. In the majority of cases, intelligent engineering guesses had to replace factual knowledge in order to incorporate this factor into response calculations.

The specific objectives of this test are as follows:

1. To determine the percentage of applied load that walls and roofs transmit to the supporting frames.

2. To determine the modes of failure of various types of wall and roof panels.

3. To determine as many as possible of the loading changes on the inside of buildings due to the failure of roofs and walls.

4. To determine pressures which will insure damage to typical roof and wall panels which are not amenable to analysis at present.

1.3 RESPONSIBILITIES

Armour Research Foundation was retained by the Air Materiel Command (AMC) of the United States Air Force to carry out the following work:

1. Consultation on the selection of the test items.
2. Design of the test items.
3. Specification of instrumentation requirements.
4. Location of the structures at the test site.
5. Supervision of construction of the test items.
6. Theoretical and experimental analyses concerning pretest predictions of blast loading and response of the test items where required.
7. Analysis of the test results.
8. Submission of reports accounting for the ARF's activities pursuant to the objectives of the program.

Detailed statements of the duties and obligations of the contracting parties can be found in the Statement of Work in Air Force Contract AF33(038)-30029.

Preparation of construction drawings for most of the test items was subcontracted by the ARF to the firm of Holabird and Root and Burgee. A member of this organization supervised the actual construction under the general direction of the ARF. As-built drawings of all the test items

were prepared by the Silas Mason Company, which was also in charge of the construction work.

All electronic instrumentation was installed and operated by the Ballistic Research Laboratories (BRL) under Project 3.28.1 Structures Instrumentation, WT-738. The BRL was also responsible for the reduction and presentation of the instrument records. Motion picture photography was handled by personnel connected with Project 9.1, Technical Photography, WT-779.

CHAPTER 2

GENERAL DESCRIPTION OF TEST

2.1 TEST ITEMS

Ten wall panels and seven roof panels, all but one representing typical construction practice, were included in Shot 9 at ground ranges where the blast was expected to cause major damage or total destruction to most of the items. (One roof, 3.5ba, was a geometrically scaled model of a 50 ft span wood bowstring roof designed for 40 psf live load.) The panels were grouped together at three locations, the groups being designated as 3.5a (at 6700 ft), 3.5b (at 4500 ft), and 3.5c (at 2200 ft). The test panels are described briefly in Table 2.1; as-built construction drawings are included in Appendix C of this report. Pretest and postshot photographs are shown in Figs. 4.1 through 4.31.

The test wall panels, measuring 8 ft 9 in. high by 13 ft 9 in. wide, were mounted in cells of reinforced concrete construction designed to rigidly withstand the effects of the blast. The cells housing the wall panels each measured approximately 16 ft wide, 10 ft high, and 7 ft deep. The rear and side walls of the cell were approximately 16 in. thick, and the frontal area facing ground zero was left open to accommodate the test panel. The front ends of the side walls were notched in order to house the sensor bars which supported the panel and measured the blast loads transmitted by it to the frame. In order to prevent pressure buildup on the back side of the walls, the openings between the frame and wall panel were sealed with 1/4 in. steel plates bolted to the concrete (see Fig. 4.7). In general, all of the test cells at each location were placed adjacent to one another and poured monolithically.

In the interests of economy, two groups of test cells (3.5a and 3.5b) were attached to similar structures built for Project 3.29 (Federal Civil Defense Administration test). It is expected that the results of this project will be of value to Project 3.29, inasmuch as several of the test panels in the latter project were withdrawn because of their similarity to the Project 3.5 panels. Project 3.29 panels were much less extensively instrumented than were the 3.5 structures.

The roof panels, each approximately 27 ft long and 15 ft wide, were also supported in test cells of reinforced concrete measuring approximately 15 ft wide, 10 ft high, and 30 ft deep. The front and rear walls of these structures each had two openings measuring 3 ft by 4 ft which comprised about 17 per cent of the gross frontal area. The purpose of this design was to simulate the loading on roofs of structures having wall openings (e.g., windows or doors). The walls and sides of the test cells were 16 in. thick and were reinforced by pilasters every 7-1/2 ft. In addition, horizontal bracing was placed at the top and bottom of the walls. The tops of the walls were notched in order to accommodate the sensor elements which supported the roof panel and measured the blast force transmitted by it to the frame.

2.2 INSTRUMENTATION

2.2.1 General

The instrumentation provided was designed to meet the following objectives:

1. To determine the modes of response of the roof and wall panels i.e., the type and degree of failure.

2. To determine the actual forces transmitted by these panels to their supporting frames.

3. To determine the pressure distribution on the roof panels and behind a failing wall.

Objective (1) was to be achieved by means of motion picture photography and time-of-break measurements; objective (2) was to be achieved by means of a specially designed force measurement system utilizing strain gage data. The strain gages were located on so-called sensor bars which supported the roof and wall panels in the test cells; objective (3) was to be achieved by means of pressure gage measurements taken on the roof panels and behind one of the wall panels. No pressure gages were provided on the outside surfaces of the wall panels since recording channels were at a premium, and it was felt that this loading could be adequately determined from knowledge of the free stream pressure-time data provided by other of the UPSHOT-KNOTHOLE Projects.

2.2.2 Photographic Measurements

Motion picture photography was provided for each wall and roof panel at the two farthest ground range locations. Two cameras were installed at each of these locations, and the film record covered the entire response period of interest. No cameras were provided at the closest location (3.5c at 2200 feet) since visibility was expected to be practically zero and, in addition, the camera towers probably would have been destroyed by the blast at this distance.

Bell and Howell Gun Sight Aiming Point Cameras (GSAP) with special-order Eastman Kodak film (Type 918 Emulsion) were used exclusively. Nominal film speed of the cameras was 64 frames per second, although this actually varied from 59 to 66 frames per second. The cameras were calibrated by observing well-defined shock phenomena recorded on the film, since no timing marks were provided. More detailed information as to the equipment and field layout can be obtained from Project 9.1, Technical Photography, WT-779.

2.2.3 Time-of-Break Measurements

In order to aid in the study of modes of failure, time-of-break gages were placed on roof panels 3.5bb, 3.5bc, 3.5ca, and 3.5cb (see Table 2.1). Two types of break gages were employed. One consisted of a stretched wire which closed a set of electrical contacts when displaced about 1/2 in. from its original position (see Fig. 4.29). The resulting electrical signal was superimposed upon a highly accurate time base and recorded on a simplified magnetic tape recorder.

The other type of gage consisted of either aluminum foil strips or thin wires crisscrossed over the test panel (see Figs. 4.25 and 4.28). Breakage of the strips provided an electrical signal by opening a contact. Complete details of these installations are contained in the final report on Project 3.28.1, Structures Instrumentation, WT-738.

2.2.4 Sensor Measurements (Strain Gage Measurements)

Special sensing elements were provided in order to measure the forces transmitted by the panels to the supporting frame. These sensors were intended not only to permit measurement of the transmitted forces, but to model as closely as possible the actual connection details of the panels. A complete schedule of the sensor instrumentation is shown in Figs. 2.1 through 2.6. The wall and roof sensor designs are shown schematically in Figs. 2.7 and 2.8. An actual wall sensor installation is shown in Fig. 2.9.

The sensor elements were constructed from steel bars of square cross section spaced equidistantly around the perimeter of the test panels. The ends of the bars were welded to steel plates, one of which was securely bolted to the supporting structure and the other attached to the test panel. Details of this construction are shown in Appendix C. The forces in the sensor bars were recorded by means of strain gages connected so as to yield average direct strains in the bars. The free length of the sensor bars was made about eight times the cross section dimension in order to achieve a uniform stress distribution across the section at which the strain gages were mounted.

The sensor design provides for the measurement of a thrust force (i.e., a force in the plane of the wall) in addition to the measurement of a direct compressive force. The thrust bars were provided since current theories concerning wall action indicate that such forces are developed as a result of deformation of the panel.

Standard SR4 strain gages were used in four active arm bridge configurations to measure strain. The output of each bridge was fed into a Webster-Chicago recording system through a coupling unit and recorded on magnetic tape. The calibration of the strain gages was accomplished electrically by shunting the proper arm of each gage installation with an accurately known resistance to simulate actual strain. Complete details of the strain gage installations are contained in the final report on Project 3.28.1, Structures Instrumentation, WT-738.

2.2.5 Air Pressure Measurements

The primary aim of the pressure measurements was to provide data which would aid in evaluating current prediction methods for blast forces on roofs of structures with front and rear wall openings. In particular, data are needed concerning the pressures on inside roof surfaces during the time the initial interior shock sweeps down the building and is reflected back to the front.

Other factors of interest include: (1) the period of time which elapses before the interior pressure begins to follow the outside free stream pressure decay; (2) whether or not the pressures on the inside roof surface are disturbed seriously by protuberances (such as purlins and trusswork) on or close to this surface; and (3) whether the pressure on the inside roof surface tends to follow closely the pressures on the floor of the building. (In field tests floor pressures are frequently easier to measure than inside roof pressures.)

Twenty pressure gages were used for blast loading studies on the roof panels, as shown schematically in Figs. 2.1, 2.3, and 2.5. Seventeen gages were arranged to record pressures on the inside surfaces of the roofs; one was located on the floor beneath a roof, and two were located to read pressures on the outside of one roof. Six of the seven roof panels had at least one pressure gage. One additional pressure gage was placed behind a brick wall panel (3.5ce) in an attempt to obtain some information as to the change in loading on the inside of a structure as a result of wall failure.

Gages were mounted flush with the surface whenever possible. Typical installations can be seen in Figs. 4.21 and 4.29. Gage cables for inside pressure measurements were led through a U-pipe fixed to the outside of the roof and returned through the roof to the interior about 3 ft away from the gage face. This method prevented gage cable connections from creating local and undesired pressure disturbances which could affect the gage.

On the corrugated steel roof, 3.5ab, the gages could not be mounted as noted above. A smooth mounting surface was made for these gages by bolting a plate about 12 in. wide (in the flow direction) and 1 in. thick against the underside of the corrugated steel roof surface. The gage face was mounted flush with this plate. This method of mounting can be seen in Fig. 4.19. Details of the dimensional locations of the gages are given in Table 5.2 and in the construction drawings of Appendix C.

All air pressure versus time measurements were obtained by the use of Wiancko type gages, a differential inductance type bridge actuated by a pressure-sensitive Bourdon tube. The gage output was fed into modified Webster-Chicago magnetic type recorders. The circuitry is described as a phase modulated system.

Just prior to the test the pressure gages were calibrated statically in conjunction with the recording system. A regulated air pressure system was used for positive pressures and a vacuum pump was used for negative pressures. Accurately known steps of pressure were applied in increments of 10 per cent of full-scale deflection for each gage. The resulting record was then played back and a calibration curve established.

The accuracy of the pressure values is estimated by the BRL at 3 per cent of full-scale readings. The time resolution is in every case within 2 ms. Complete details of the pressure gage installations are contained in WT-738.

2.2.6 Instrument Records

The BRL handled all of the instrumentation with the exception of the photographic measurements. The output of the strain and pressure gages was recorded initially on magnetic tape, and later played back onto oscillographic paper. The records in this form exhibit certain undesirable characteristics (e.g., the ordinate scale is markedly nonlinear) which make them ill-suited for purposes of interpretation and comparison. For this reason all the records were subsequently converted to linear form.

The BRL reduced, calibrated, and plotted to linear scales all of the instrument records, and also submitted tabulated listings of the points, as well as ozalid copies of the original playbacks. The ARF was responsible for fairing curves through the linearized plotted points.

2.3 LOCATION OF TEST STRUCTURES

The location of the structures at the site is shown in Fig. 2.10. Ground range, actual orientation, and measured overpressures are given in Table 2.1. Other pertinent information is given in Table B.1. Because of the bombing error in Shot 9, the test structures were not struck head-on by the blast wave as intended. The actual angle of incidence varied from about 21 deg at the closest location (3.5c) to only about 7 deg at the farthermost location (3.5a). In other respects the test as conducted did not deviate significantly from the test specifications given in Part VII of the final pretest report on Contract No. AF33(038)-30029, Test of Roof and Wall Panels.

TABLE 2.1 - Description and Actual Location of Test Items

Item	Description[a]	Distance from Ground Zero (ft)		Overpressure (psi)		Actual Orientation (Angle of Incidence)[c] (deg)
		Actual	Expected	Expected	Actual[b]	
3.5ac	8 in. brick wall	6700	6500	5	4.2	7
3.5ad	Corrugated steel siding over steel girt	6700	6500	5	4.2	7
3.5ae	Corrugated asbestos board over wood girt	6700	6500	5	4.2	7
3.5af	Wood siding over plaster board nailed to studs	6700	6500	5	4.2	7
3.5bd	8 in. cinder block wall[d]	4500	4200	10	7.1	10
3.5be	12 in. cinder block wall	4500	4200	10	7.1	10
3.5bf	8 in. brick wall	4500	4200	10	7.1	10
3.5cc	8 in. cinder block with 4 in. brick facing	2200	1700	15	12	21
3.5cd	6 in. concrete with 1/4 per cent reinforcing steel	2200	1700	15	12	21
3.5ce	8 in. brick wall	2200	1700	15	12	21
3.5aa	Corrugated asbestos board over wood truss rafters	6700	6500	5	4.2	7
3.5ab	Corrugated steel panels over wood truss rafters	6700	6500	5	4.2	7
3.5ba	Bowstring truss with wood decking, tar and gravel roofing	4500	4200	10	7.1	10
3.5bb	3-1/2 in. precast concrete channels on steel purlins, tar and gravel roofing	4500	4200	10	7.1	10
3.5bc	Laminated 2 x 4's, flat wood deck, tar and gravel roofing	4500	4200	10	7.1	10
3.5ca	4 in. reinforced concrete roof, tar and gravel roofing	2200	1700	15	12	21
3.5cb	Holorib steel channels with gypsum fill, tar and gravel roofing	2200	1700	15	12	21

a/ All wall panels were 8 ft - 9 in. by 13 ft - 9 in., and supported on four sides. All roof panels were approximately 15 ft wide by 27 ft long, and supported on either two opposite sides or all four sides.

b/ Actual pressures have the following uncertainties: 4.2 ± 0.1 psi, 7.1 ± 0.3 psi, (Mach region), and 12 ± 0.8 psi (regular reflection region).

c/ Expected orientation was head-on (zero angle of incidence) for all test items.

d/ Cinder block was erroneously referred to as a concrete block in the preliminary post-test report, UKP-15.

Note: All pressure gages facing inside

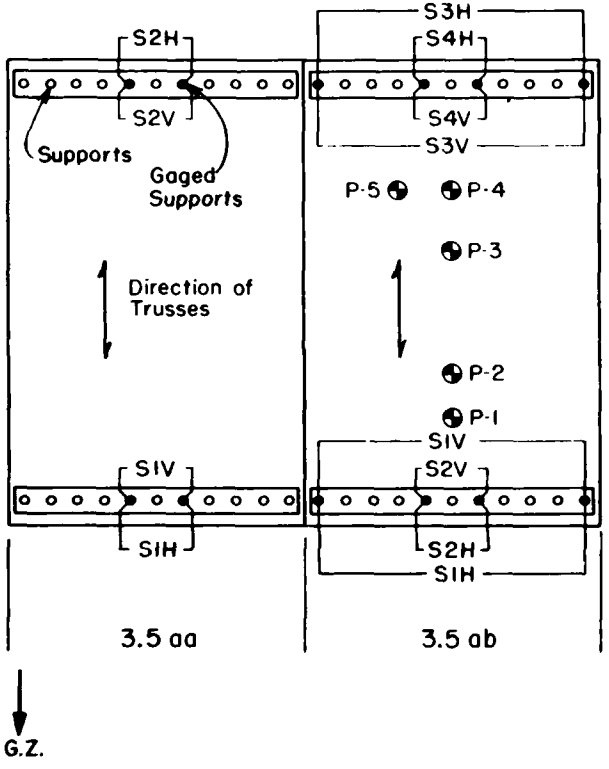

Note: See Fig. 2.8 for gage notation

Fig. 2.1 Strain and Pressure Gage Locations, 3.5 a Roof Panels

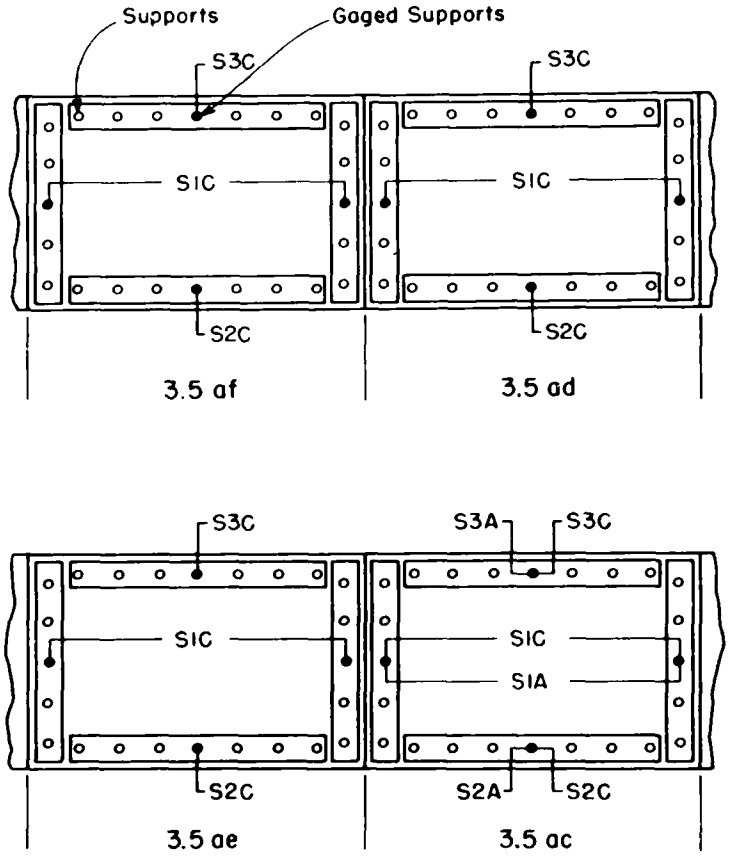

Note: See Fig. 2.7 for gage notation

Fig. 2.2 Strain Gage Locations, 3.5 a Wall Panels

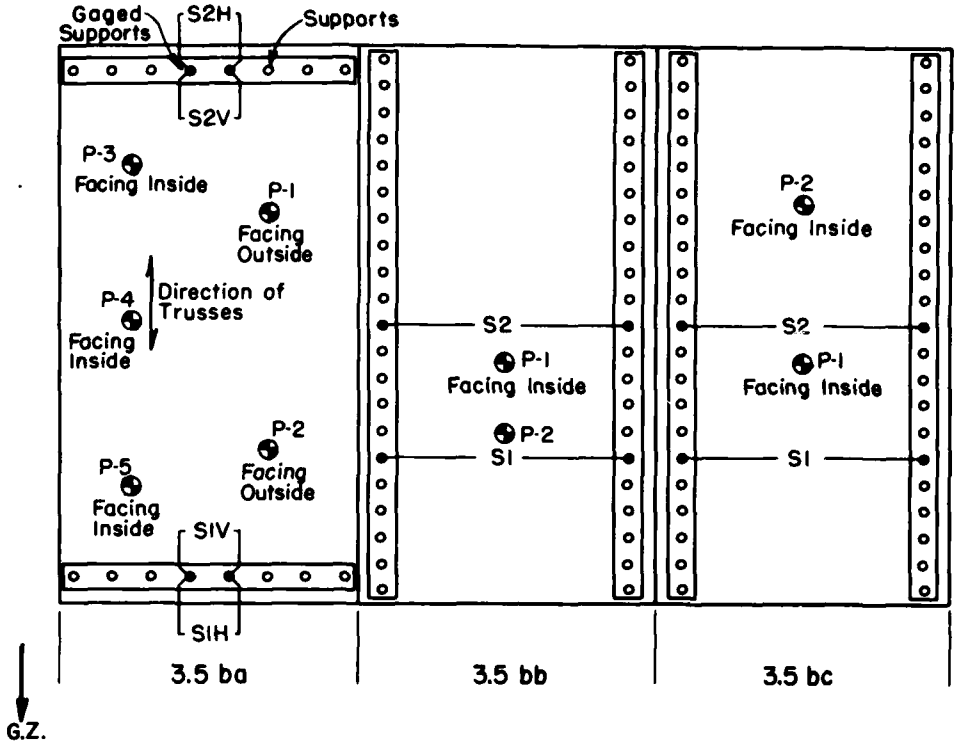

Fig. 2.3 Strain and Pressure Gage Locations, 3.5 b Roof Panels

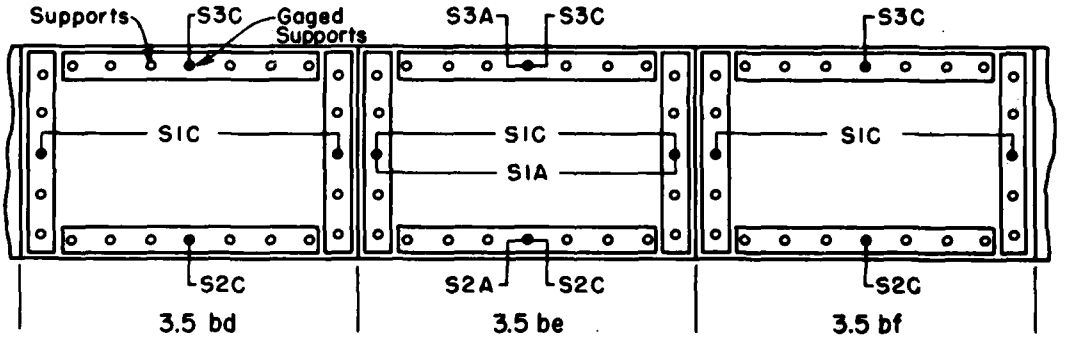

Note: See Fig. 2.7 for gage notation

Fig. 2.4 Strain Gage Locations, 3.5 b Wall Panels

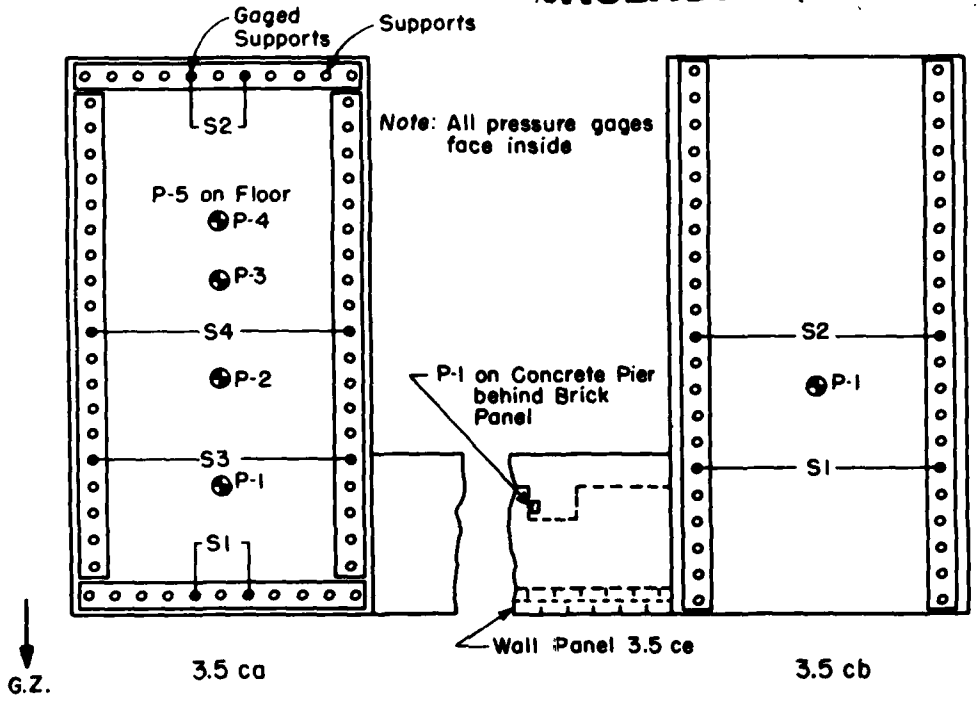

Note: See Fig. 2.8 for gage notation

Fig. 2.5 Strain and Pressure Gage Locations, 3.5 c Roof Panels

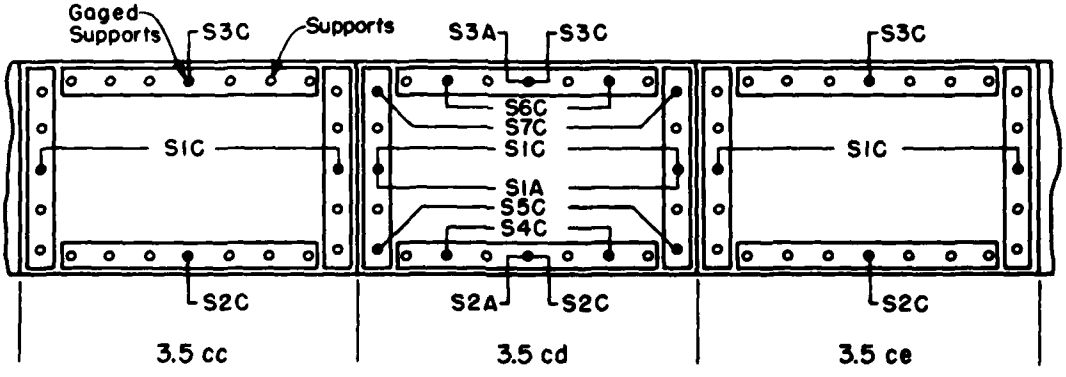

Note: See Fig. 2.7 for gage notation

Fig. 2.6 Strain Gage Locations, 3.5 c Wall Panels

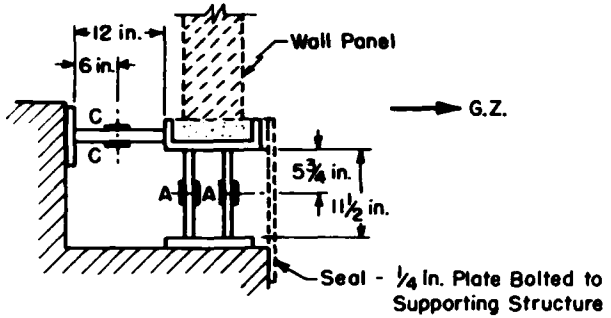

C - Strain Gages on Compression Sensors
A - Strain Gages on Thrust Sensors

Fig. 2.7 Schematic Design of Wall Sensors

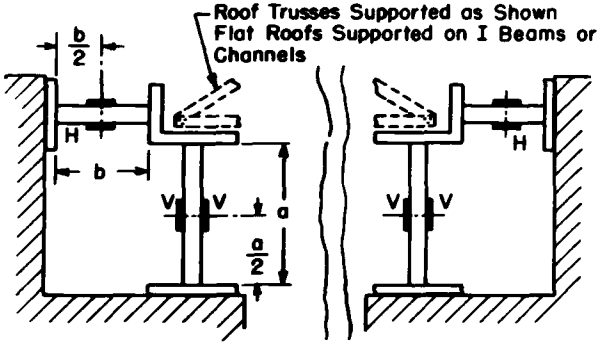

Note: See Appendix C for schedule of a, b dimensions

Fig. 2.8 Schematic Design of Roof Sensors

Fig. 2.9 Typical Wall Sensor Installation (Thrust bars)

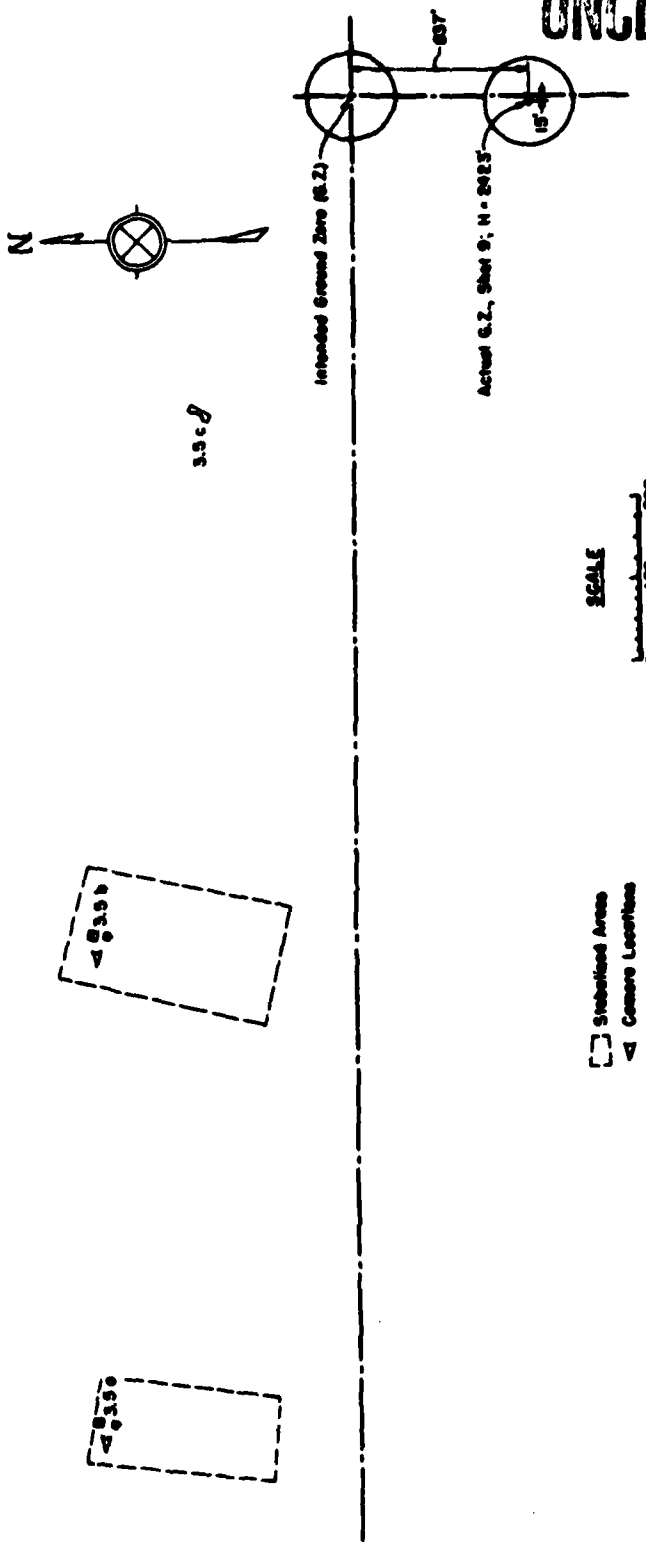

Fig. 2.10 Location of Structures at Test Site

CHAPTER 3

PRETEST CONSIDERATIONS

3.1 BLAST LOADING AND STRUCTURAL DESIGN

The pretest work was concerned primarily with load prediction methods for the wall and roof panels in both the conventional Mach and regular reflection regions. The wall loadings pertain to solid panels; the roof loadings take into account partial openings in the front and rear walls. This work is given in detail in the final pretest report, Tests on Roof and Wall Panels, Planning Program for Air Force Structures Tests, and is summarized in Appendix B of this report.

The load prediction methods were utilized to establish (a) the pressure regions in which the desired damage to the test panels was expected to occur, and (b) the design of the test cells so that they would rigidly withstand the effects of the blast. The latter analysis assumed that the wall panels would transmit all their load in the form of an impulse to the structure, and that the mode of response of the cell would be either rigid body sliding or overturning. The walls of the roof test cells (and roofs of the wall test cells) were assumed to act as simple beams and designed to develop only elastic stresses in bending. Impulse-momentum techniques were also utilized in these analyses. While this approach resulted in an extremely conservative design (which proved successful during the test), it was considerably more economical than a design based on static application of twice[1/] the peak loads.

The wall and roof test panels were intended to be representative of typical size and construction practice. All of the test panels, with the exception of one, were built accordingly. The Air Force was interested in the behavior of curved roofs typical of heavy industrial

1/ For design purposes when the dynamic characteristics of the system and the loading are not well defined, it is common practice to assume a factor of 2 to account for the effects of suddenly applied loads. The factor 2 corresponds to the well-known response of a simple undamped elastic system subjected to a suddenly applied constant load wherein the system attains the same displacement as if it were statically loaded with twice the force.

construction. In practice such a roof might have bowstring trusses spanning up to 100 feet. It was not practical to include a structure of this size in the test, so an attempt was made to construct a scale model of this type of roof.

At best, true structural scaling can be done in relatively few and idealized cases. The major difficulties are concerned with the incompatability of dead weight and inertial scaling, and the uncertainty of modeling the action of connection details. In the present case, it was decided to scale the wood bowstring roof (3.5ba) geometrically at a ratio of one-half true size. The scaling pertained principally to the truss members and certain deviations were made in order to permit the use of standard lumber sizes. It was hoped that the results of the model test would serve as an indication of the behavior of the prototype roof.

No attempt was made in the pretest work to carry out detailed predictions of the behavior of the test panels based on existing theories. However, the test design was such as to provide information relating to these theories (e.g., the measurement of suspected thrust forces).

3.2 SENSOR DESIGN

A major portion of the pretest work was concerned with the design of the instrumentation system which would permit measurement of the forces transmitted by the test panels to the supporting structure. The design conditions were the following:

1. The supporting system should permit representative connection details for the test panels.

2. The period of vibration of the sensor bars should be appreciably less than that of the test panels in order to adequately resolve the transmitted forces.

3. The strains in the sensor bars should be large enough to produce an adequate signal from the strain gages.

4. The sensor bars should be long enough so as to cause a uniform strain distribution at the cross section where the gages were mounted, since adequate pretest calibration was impractical.

5. The required recording channels should be held to a minimum.

It is seen that these requirements are not all compatible. Conditions (3) and (4) must, of course, be satisfied. However, they both tend to make the bars more flexible and hence tend to violate condition (2). Conditions (1) and (5) severely limit the arrangement of the measuring system. Nevertheless, an adequate compromise design was evolved that has proved to be quite successful.

CHAPTER 4

EXPERIMENTAL RESULTS

4.1 VISUAL OBSERVATIONS

Some failure of all of the test panels occurred, as had been desired. The behavior of the three unreinforced brick panels was particularly gratifying since a definite gradation of damage from minor through severe through total destruction took place. The following subsections give a general description of the panel failures. Whenever possible, information obtained from the motion picture films is also included. Pre- and postshot photographs are shown in Figs. 4.1 through Fig. 4.31.

4.1.1 Wall Panel, 3.5ac, 8 in. Brick (4.2 psi Overpressure)

The panel was still in place and almost completely free of damage. Close inspection revealed hairline cracks in several bricks at the center of the panel, in the mortar joints at the bottom of the top course, and along the diagonals near the corners. No additional information was obtained from the motion picture films.

4.1.2 Wall Panel, 3.5bf, 8 in. Brick (7.1 psi Overpressure), Fig. 4.6

The panel was still in place, although some damage was noted. Two center courses of brick were pushed in about 3/4 in. with a general dishing in all around. Cracks through the joints started in the corners and progressed at approximately 45 deg toward the center of the panel.

Some indications of failure are visible in the films. Toward the end of the positive loading period, a crack appeared at the top and sides and seemed to move downward. This line of failure was observed on films from each of the cameras recording the action.

4.1.3 Wall Panel, 3.5ce, 8 in. Brick (12 psi Overpressure), Fig. 4.7

The panel was blown out with only fringes of the brick remaining. The rear portions of the bricks remaining in place showed evidence of crushing.

4.1.4 Wall Panel, 3.5ad, Corrugated Steel Siding Over Steel Girt (4.2 psi Overpressure), Fig. 4.8

The panel, including the 6 in. channel girt, was blown completely inward. The siding was wrapped around the girt, which in turn was badly bent. The end connections of the girt to the supporting frame also failed. On the right side (viewed from ground zero) the welded clip angle failed at the wall, while on the left side the bolts tying the girt to the clip angle sheared.

The film showed that failure of the steel siding started almost immediately after shock arrival. The first indication of failure was a dishing in of the siding between supports. The individual panels then failed and finally the girt was observed to distort and fail.

4.1.5 Wall Panel, 3.5ae, Corrugated Asbestos Board Over Wood Girt (4.2 psi Overpressure), Fig. 4.9

The siding was blown in and completely shattered, as was the 4 by 6 in. wood girt to which the siding was nailed. The wood girt had been toe-nailed to its support.

The films showed that individual panels failed by cracking across the supports and across the center of the panels. Initially the lap between adjacent panels remained in place. The lapped sections then failed and the girt failed immediately afterward.

4.1.6 Wall Panel, 3.5af, Wood Siding (4.2 psi Overpressure), Figs. 4.10 and 4.11

The wood siding was blown out and completely shattered. The supporting studding was completely broken up. The films showed that the wood siding was initially charred by thermal radiation but the smoke had almost entirely dissipated prior to shock arrival. Subsequent cracking of the wood was clearly visible against the charred background. The wall failed by bending in the long direction with cracks first appearing at the center of the span. The mode of failure was such that the studs must have failed prior to any visible crack on the front of the wall.

4.1.7 Wall Panel, 3.5bd, 8 in. Cinder Block (7.1 psi Overpressure), Figs. 4.12 and 4.13

The panel was destroyed. The edge blocks which remained in place were crushed along all four edges of the panel. From the films, the initial sign of failure appeared to be the formation of a crack across the top and down the sides. This crack first appeared approximately one block from the edge of the panel. Cracking then occurred within this area and failure was brought about by a dishing action which left some blocks hanging onto the edge supports. During this action cracks at 45 deg were observed to progress from the corners toward the center of the panel.

4.1.8 Wall Panel, 3.5cc, 8 in. Cinder Block with 4 in. Brick Facing (12 psi Overpressure), Figs. 4.14 and 4.15

The panel was completely blown out with only a small amount of the brick and concrete block still clinging to the frame. Crushing on the rear of these blocks was observed.

4.1.9 Wall Panel, 3.5be, 12 in. Cinder Block (7.1 psi Overpressure), Fig. 4.16

The panel was completely broken out in a manner identical to the 8 in. cinder block panel (3.5bd) described above. Evidence of crushing of the rear surfaces of the blocks was also observed. The films, too, showed a behavior similar to panel 3.5bd.

4.1.10 Wall Panel, 3.5cd, 6 in. Reinforced Concrete (1/4 per cent Steel) (12 psi Overpressure), Fig. 4.17

The wall was blown out bodily and came to rest at the rear wall of the test cell. Cracks from the corner progressing at 45 deg toward the center were observed. The vertical crack clearly evident in Fig. 4.17 indicates that possibly much of the cracking resulted from impact with the rear of the test cell.

4.1.11 Roof Panel, 3.5aa, Corrugated Asbestos Roofing on Wood Trusses (4.2 psi Overpressure), Fig. 4.18

The asbestos covering was completely shattered. The floor of the structure was covered with small fragments of asbestos toward the front, while the rear was comparatively clear of debris. The asbestos cover on the rear portion of the roof was blown out and was found lying on the ground just behind the structure. The pieces of asbestos lying in the rear outside the structure were larger than those found on the inside. The purlins were still in place and, except for one, were undamaged. The trusses were still in place and probably could have been repaired, although the upper and lower chords in the front half of the trusses had failed.

4.1.12 Roof Panel, 3.5ab, Corrugated Steel Roofing on Wood Trusses (4.2 psi Overpressure), Figs. 4.19 and 4.20

The corrugated steel covering was lifted off the trusses in large sections. The covering from the rear portion of the roof was found lying on the ground just behind the structure, and a portion of the covering from the front of the roof was found in front of the structure. One section of the roofing remained in place on the front slope of the roof. The trusses were completely broken and out of place with more severe damage to the front half. The purlins were all broken and were found to the rear of the structure.

4.1.13 Roof Panel, 3.5ba, Scaled Wood Bowstring Truss, Wood Decking, Tar and Gravel Roofing (7.1 psi Overpressure), Figs. 4.21, 4.22, and 4.23

The roof was completely destroyed. Most of the 2 in. sheathing was found inside the structure on the floor. Some of the sheathing was found intact behind the structure. The trusses were very heavily damaged and off their supports. Most severe damage was observed on the front half of the trusses, where complete failure occurred. The rear half of the trusses was less severely damaged with only partial failures to the upper and lower chords.

4.1.14 Roof Panel, 3.5bb, 3-1/2 in. Precast Concrete Channels on Steel Purlins, Tar and Gravel Roofing (7.1 psi Overpressure), Fig. 4.24

The roof was partially destroyed. The rear half of the channels was still in place and undamaged. The purlins supporting the front half of the roof suffered large permanent deformations. The front quarter purlin had the largest permanent set with approximately 14-1/2 in. deflection which permitted some of the precast sections to fall directly to the floor. The precast sections on the front portion of the roof near the side walls, where the purlin deflection was not so great, apparently remained in place long enough to fail partially in shear before they dropped to the floor. The end connection of the purlins did not fail.

4.1.15 Roof Panel, 3.5bc, Laminated 2 by 4 in. Flat Wood Deck, Tar and Gravel Roofing (7.1 psi Overpressure), Figs. 4.25, 4.26, and 4.27

The roof was still in place, although the front half was heavily damaged. The maximum deflection at the centerline was slightly over 1 ft. This occurred at a point one-quarter of the distance from the front to the back walls. The damage decreased at points farther from the front wall. The rear half of the roof suffered almost no damage. The front half of the roof was lifted upward and forward about 4 in., coming to rest on the front wall of the structure.

4.1.16 Roof Panel, 3.5ca, 4 in. Reinforced Concrete Slab, Tar and Gravel Roofing (12 psi Overpressure), Fig. 4.28

The roof was severely cracked and deflected inward a maximum of 7 in. at about one-third the distance from the front wall.

4.1.17 Roof Panel, 3.5cb, Holorib Steel Channels with Gypsum Fill, Tar and Gravel Roofing (12 psi Overpressure), Figs. 4.29 and 4.30

The roof failed completely. However, the steel channels remained whole, despite being wrapped around purlins in the rear half of the

structure. The front channels fell to the floor. The purlins at the one-quarter and one-half points from the front of the structure were deflected approximately 16 in. each, while the purlin at the three-quarter point was deflected only about 6 in.

4.2 INSTRUMENTATION RESULTS

4.2.1 Photographic Measurements

Films were obtained from each of the 11 motion picture cameras. While the films provided considerable general information, it was not possible to obtain many quantitative data since dust and smoke interference caused an appreciable loss of clarity. The mode of failure of the various wall panels could be observed, but most of the roof action was obscured.

An attempt was made to establish the breaking time of the wall panels from the films. Due to uncertainties in determining such quantities as true camera speed, shock arrival time, and (principally) the frame of the film at which breaking first occurred, the break times found in this manner indicate only order of magnitude values. The probable error in locating the instant of break on the film is estimated to be approximately one frame (i.e., about 16 ms), which, unfortunately, is of the order of magnitude of the break time itself. The results obtained are listed in Table 4.1. The condition of the films precluded the possibility of determining break times for the roof panels. No cameras were provided for the 3.5c test items.

4.2.2 Strain Measurement

All but 12 of the 69 strain gage channels provided records. Of these, an additional 6 were discarded because they appeared to give erroneous information. Thus, 74 per cent of the strain instrumentation was available for analysis. Only the reinforced concrete roof (3.5ca) provided no usable strain data. A breakdown of the remaining 26 per cent of the records is shown in Table 4.2.

It is felt that the usable strain gage data are generally acceptable for the purposes of this test. However, it was not possible to determine a probable error associated with these data since a number of the linearized gage records were found to require corrections before they could be accepted for analysis purposes. In general it was found necessary to modify many of these records by comparing them with the original playbacks in order to ascertain whether (1) all significant features of the records had been reproduced, (2) the zero and base line positions had been chosen properly, and (3) any gross inaccuracies were present.

Representative records are shown in Figs. 4.32 through 4.43.

TABLE 4.1 - Break Time of Wall Panels from Motion Picture Film

Wall Panel	Film No.a/	Break Time (sec)b/
3.5ad, Corrugated Steel	16522	0.016
	16630	0.017
3.5ae, Corrugated Asbestos Board	16521	0.033
	16522	0.031
3.5af, Wood Siding	16522	0.031
	16630	0.034
3.5bd, 8 in. Cinder Block	16519	0.015
	16520	0.016
	16610	0.017
3.5be, 12 in. Cinder Block	16519	0.031
	16520	0.032

a/ See Final Report on Project 9.1, Technical Photography, WT-779, for camera data.

b/ The probable error associated with each of the values is ± 0.016 sec.

4.2.3 Time-of-Break Measurements

Five of the six time-of-break indicators installed on the roof panels provided readings. The data obtained refer to elapsed time between zero time (i.e., detonation time) and the break time of the strips. The actual time of break was obtained by subtracting the time of shock arrival from the above time. These results are shown in Table 4.3.

Inspection of the table points out several discrepancies in these results. First, panel 3.5bb is indicated to break prior to the shock arrival. This error is due either to (a) inaccuracies in the break time readings, (b) an early failure of the aluminum foil strip, or (c) the circuit was opened in some other fashion at an early time. Another possible explanation is that the post-test plot survey was in error wit. respect to the 3.5b test cell. However, this error would have to be of the order of 100 ft in order to yield a positive break time and is considered extremely unlikely inasmuch as the survey was independently checked by project personnel.

TABLE 4.2 - Strain Gage Data Not Used

Structure	Gage No.	Doubtful Data	No Data
3.5ad, Corrugated Steel Siding Wall	S3C (1 of 3 gages)	X	
3.5af, Wood Siding Wall	S2C, S3C } 2 of 3 gages	X	X
3.5bc, Laminated 2 by 4 in. Wood Roof	S2 (1 of 2 gages)		X
3.5be, 12 in. Cinder Block Wall	S2A, S3A } 2 of 6 gages		X X
3.5bf, 8 in. Brick Wall	S3C (1 of 3 gages)		X
3.5ca, 4 in. Reinforced Concrete Roof	S1, S2, S3, S4 } 4 of 4 gages	X X	 X X
3.5cd, 6 in. Reinforced Concrete Wall	S1A, S3A, S4C, S5C, S6C, S7C } 6 of 10 gages	 X X	X X X X
3.5cc, 8 in. Cinder Block with 4 in. Brick Wall	S1C (1 of 3 gages)		X
Total		6	12
Percentages		9%	17%

TABLE 4.3 - Break Time of Roof Panels

Roof Panel	Reading (sec)	Shock Arrival Time a/ (sec)	Break Time (sec)
3.5bb, Precast Concrete Channels	3.064	3.133	--
3.5bc, Laminated 2 by 4 in. Wood	3.134	3.133	0.001
	No Record	3.133	--
3.5ca, 4 in. Reinforced Concrete Slab	2.115	1.628	0.487
3.5cb, Holorib Steel Channel	2.115	1.628	0.487
	2.126	1.628	0.498

a/ From Projects 1.1a and 1.1b pretest reports.

The break times found for the 3.5c roofs are surprisingly large considering the extreme damage that occurred. The films of 3.5bc showed a large section of the roof in the air about 0.3 sec after the shock. Thus it seems rather surprising, if not unreasonable, that roofs at a higher loading would require such a long time to fail, even considering the differences in construction.

The installation of the wire break strips on 3.5cb is shown in Fig. 4.29. Since the wires are suspended below the roof, it is possible that the gage system was actuated some time after the initial roof failure. A random behavior of this type would partly explain the discrepancies in break time between the two values obtained for roof 3.5cb.

Two types of circuitry were employed on this roof, one normally open, and one normally closed. It is also possible that differences in the action of these arrangements contributed to the time differences.

All things considered, it is felt that the break times shown in Table 4.3 can be accepted only with reservation, if at all.

4.2.4 Air Pressure Measurements

Twenty of the 21 pressure gages installed on the test structures provided records (the missing record was gage 3.5bb P2). Representative records are shown in Figs. 4.44 through 4.50. All but one of the 20 records were analyzed as described below and in section 5.2, (record 3.5ba P1 appears to be erroneous and was discarded). Table 5.4 is

relevant here since it summarizes a rather detailed analysis of the accuracy and credibility of the plots of these 19 records. The table lists the following five categories in which many of these plots were found to be, or are believed to be, unsatisfactory.

1. Pressure scales: A few plots are obviously in error in this respect. The remaining errors noted in the table were deduced by fairly convincing reasoning as described in section 5.2.2.

2. Baseline prior to shock arrival: These observations were made from copies of the original playbacks of the records. Roughness in the baseline indicates the magnitude of nonpressure hash which may be present throughout the record.

3. Meaningfulness of plotted record after stated time: A number of the plots are believed to be meaningless after values of time which lie variously between about 90 and 800 ms after shock arrival. Nearly all of these effects seemed to be caused by relatively permanent baseline shifts in the original record. Such shifts could presumably be caused by failures in the roofs on which many of the gages were located, or by debris striking the gage or the gage cabling. However, as noted in (2) above, some baselines were rough prior to shock arrival; the same nonpressure effects might be acting in the case described here. Furthermore, there was a general tendency throughout many of the records for identical appearing baseline shifts and sudden dips, oscillations, and pips to occur on records of gages which were connected to the same recorder unit. Such identical and unusual signals sometimes appeared even on both strain and pressure records and on records obtained from gages located on entirely different structures; always, however, such gages were connected to the same recorder unit. Identical signals did not appear on any nearby gages on the same test structure if these gages were connected to a different recorder unit. For these reasons and for an additional reason cited in (4) below, these signals are not felt to be either pressure signals or signals due to roof failures[1] and they have been classified as meaningless signals which were disregarded in the analysis of the records.

1/ Of course, it is conceivable that some such signals were due to roof failures near one gage and appeared on other gages on other structures through interaction between electrical signals at the recorder unit. However, it does not seem to be possible to determine for which gages the signals might be "real" and for which they are meaningless. Also, from preshock appearance of some baselines it would not seem surprising for these signals to occur without being due in any way to the blast wave or damage caused by the blast.

4. Major features of plot which should be ignored: This category refers to temporary baseline shifts, dips, and pips which appear on the final plots prior to the times indicated in item (3) above. On the original records such effects tend to correlate between different records on the basis of the recorder unit used rather than on the basis of the structure or member on which the gages were located. Furthermore, where these effects appeared on several different records, the effects generally occurred at the same absolute values of time indicating velocities of movement between gages far in excess of any velocities at which pressure disturbances could travel here. A number of such dips and pips were correctly ignored by the BRL in the reading of the records during reduction to linear plots.

5. Miscellaneous comments: Entries in this category are self-explanatory in Table 5.4. The majority of the plotted records faithfully correspond to the significant features of the original records; however, some records were read at intervals of time which were quite coarse and, hence, the plots fail to reproduce some significant aspects of the record. This category, of course, does not include nonpressure effects mentioned in item (4) above.

Despite the difficulties enumerated above, it has been possible to abstract a considerable amount of information from the 3.5 pressure records as described later in section 5.2. Of course, with pressure scales uncertain in many cases, and with the lowered degree of confidence in the records resulting from this study of their accuracy, the conclusions which are drawn must often be less definite, or subject to more doubt, than if the records had been more satisfactory.

Fig. 4.1 Preshot, 3.5a, Wall Panels

Fig. 4.2 Preshot, 3.5a, Roof Panels (Visible conduit contains leads from pressure gages on inside of roof)

[redacted]

Fig. 4.3 Preshot, 3.5b, Wall Panels

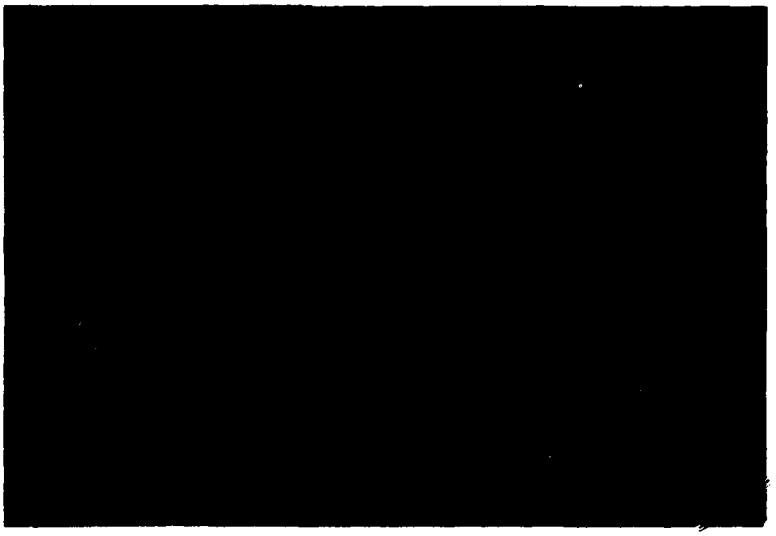

Fig. 4.4 Preshot, 3.5b, Roof Panels

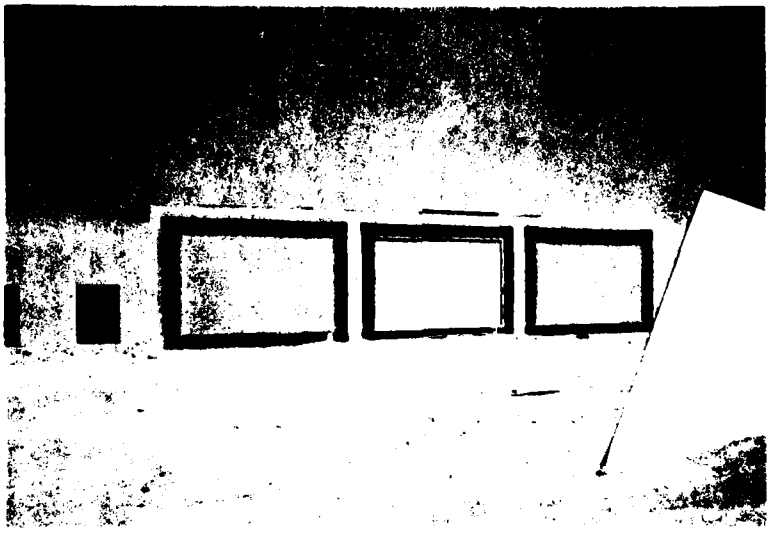

Fig. 4.5 Preshot, 3.5e, Wall and Roof Panels

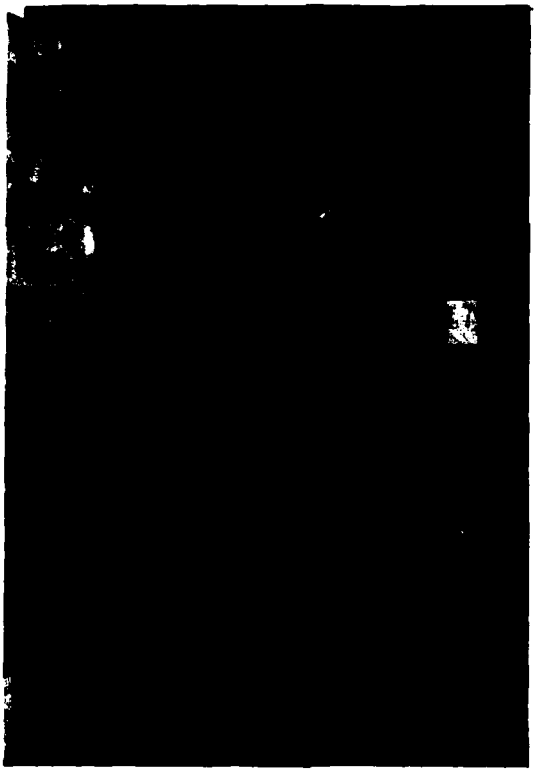

Fig. 4.6 Postshot, 3.5bf, Rear of 8 in. Brick Wall Panel Showing Center Crack

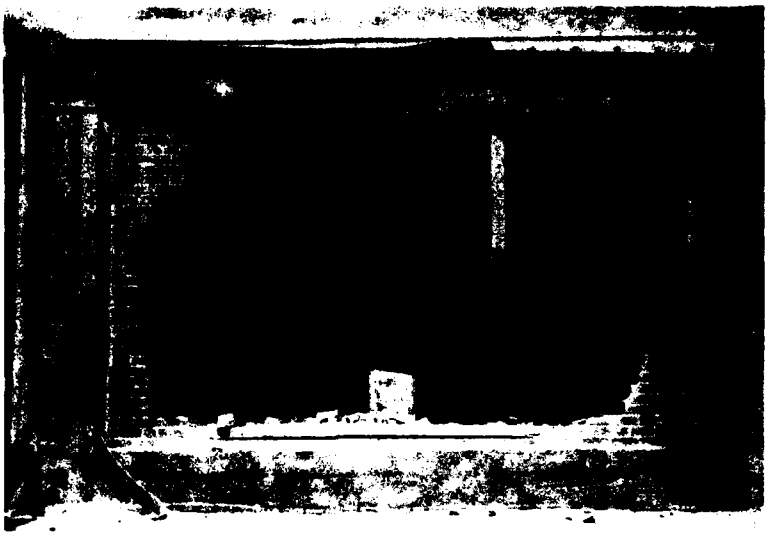

Fig. 4.7 Postshot, 3.5ce, Damaged 8 in. Brick Wall Panel (Note similarity to failure of other masonry panels)

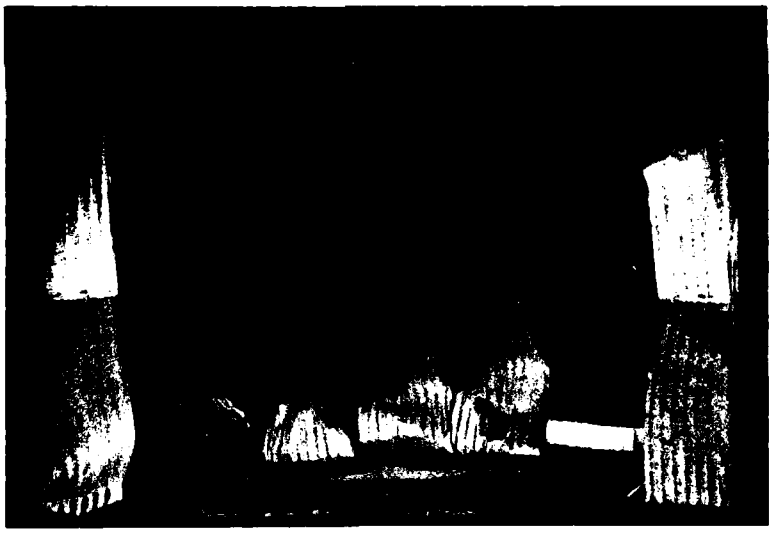

Fig. 4.8 Postshot, 3.5ad, Damaged Corrugated Steel Wall Panel (Individual panels, although bent and twisted, adhered to steel girts)

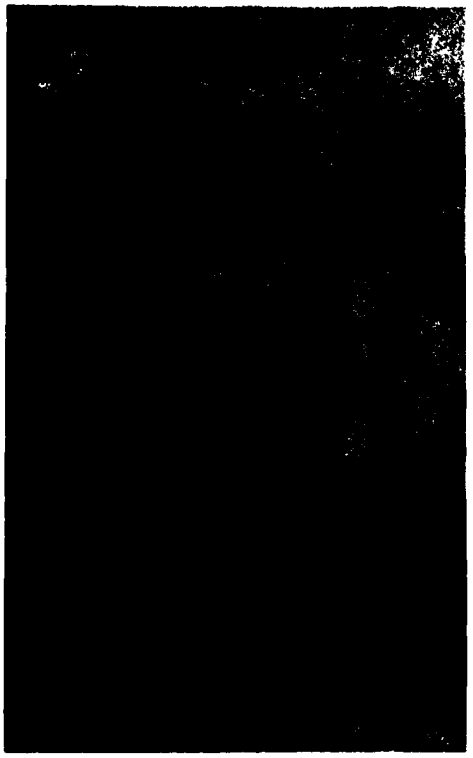

Fig. 4.9 Movie Film, 3.5ae, Breaking of Corrugated Asbestos Board Wall Panel (Cracks appear over support and at center of panel)

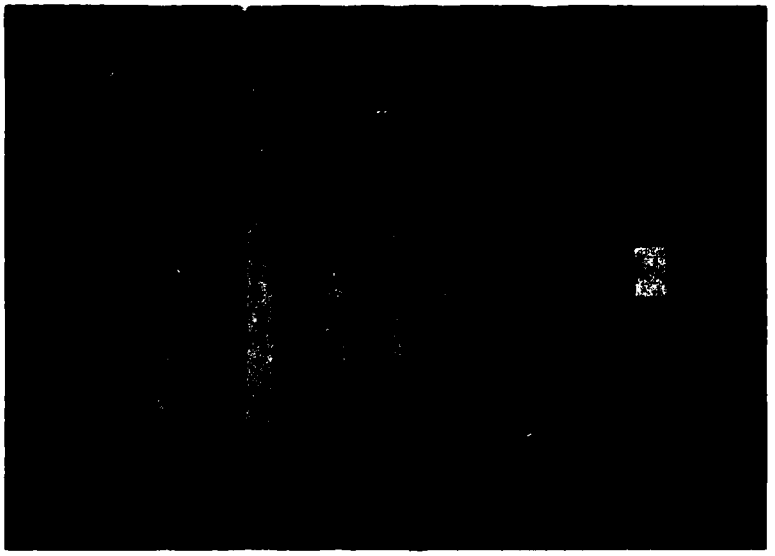

Fig. 4.10 Preshot, 3.5af, Rear of Wood Siding Wall Panel (Interior construction showing framing behind wood sheathing and plaster board)

Fig. 4.11 Postshot, 3.5af, Damaged Wood Siding Wall Panel

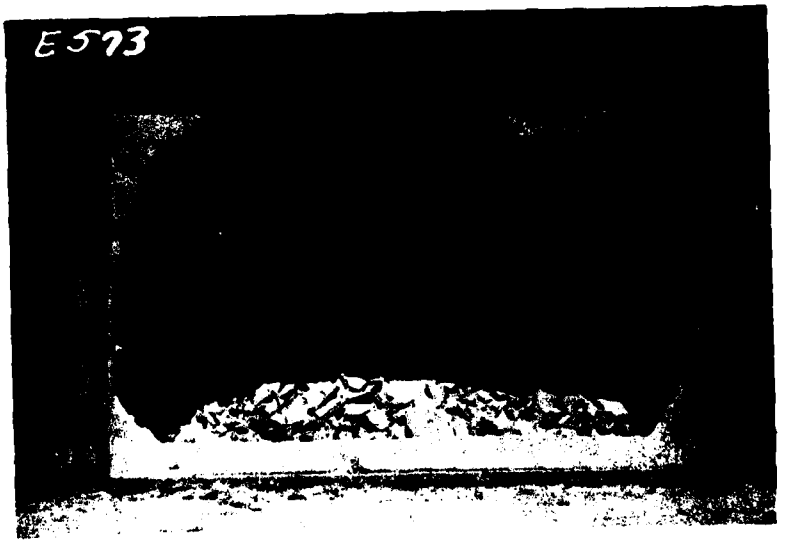

Fig. 4.12 Postshot, 3.5bd, Damaged 8 in. Cinder Block Wall Panel

Fig. 4.13 Postshot, 3.5bd, Edge Blocks Showing Crushing Failure

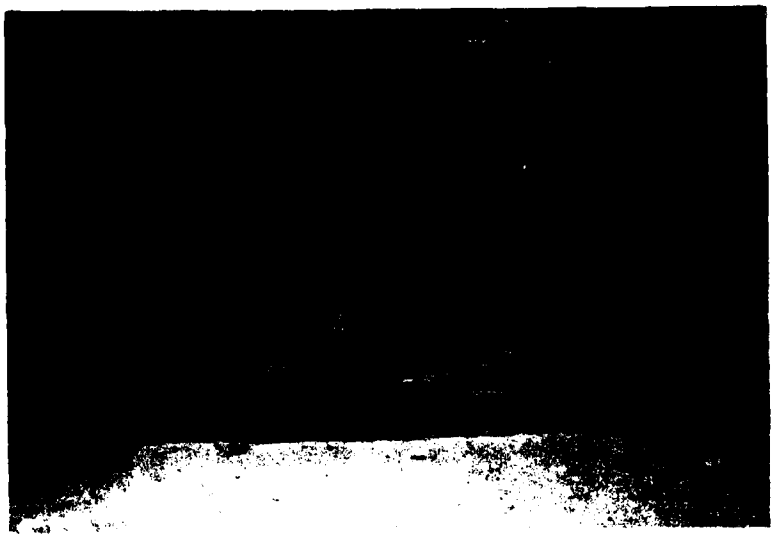

Fig. 4.14 Postshot, 3.5cc, Damaged 4 in. Brick, 8 in. Cinder Block Wall Panel

Fig. 4.15 Postshot, 3.5cc, Edge Brick and Block Showing Crushing Failure

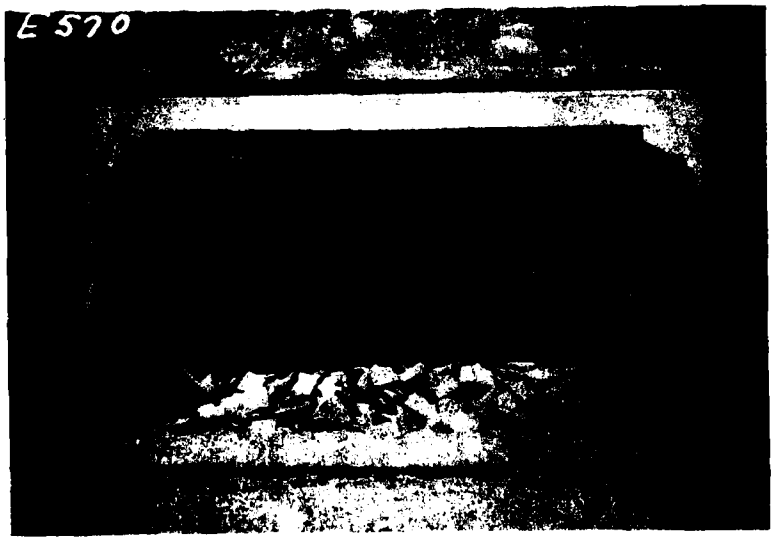

Fig. 4.16 Postshot, 3.5be, Damaged 12 in. Cinder Block Wall Panel (Note similarity to failure of 8 in. concrete block panel, Fig. 4.12)

Fig. 4.17 Postshot, 3.5cd, Damaged 6 in. Reinforced Concrete Wall Panel (Note 45 deg cracks emanating from corners)

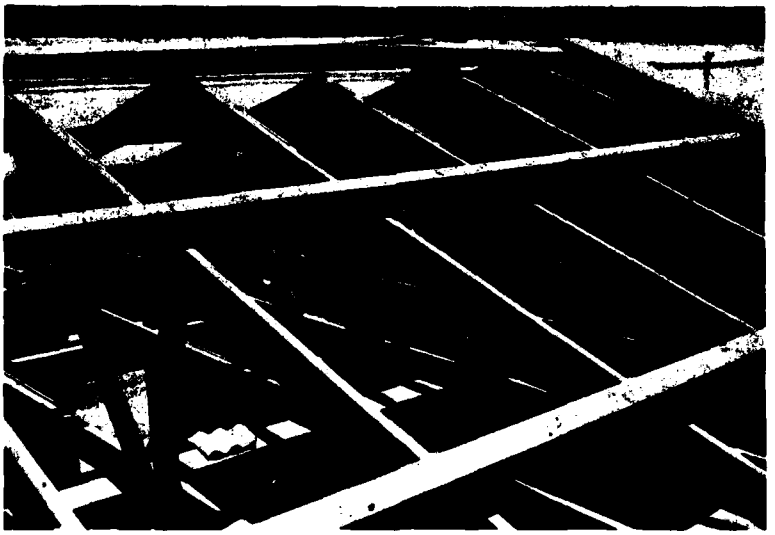

Fig. 4.18 Postshot, 3.5aa, Damaged Corrugated Asbestos Board Roof Panel (Note damage to top purlin and to top chord of trusses)

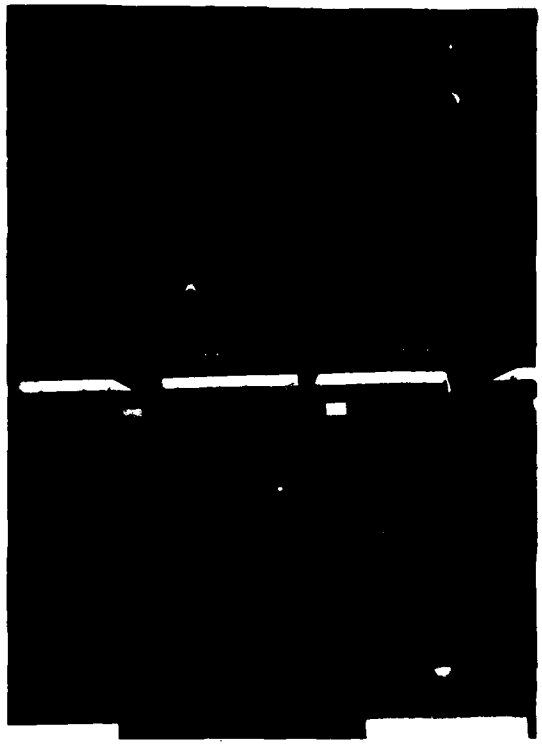

Fig. 4.19 Preshot, 3.5ab, Interior of Corrugated Steel Roof Panel (Note pressure gages. Open area sealed before test.)

Fig. 4.20 Postshot, 3.5ab, Damaged Corrugated Steel Roof Panel (Note greater damage to trusses and purlins as compared to 3.5aa, Fig. 4.18)

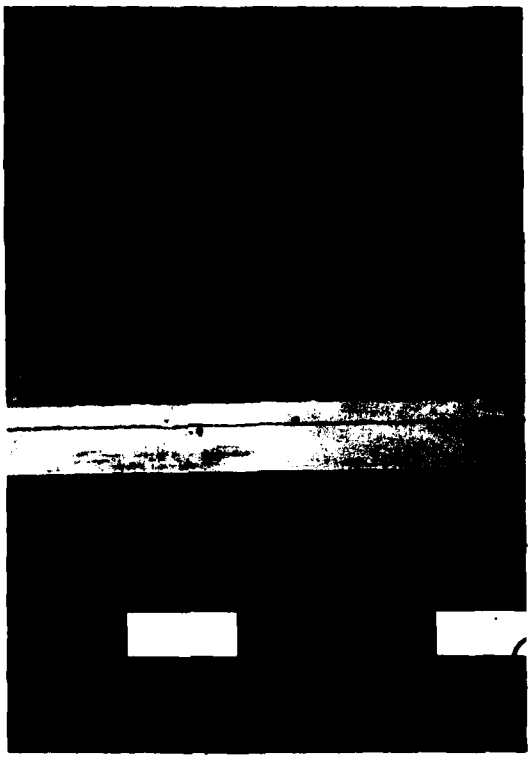

Fig. 4.21 Preshot, 3.5ba, Interior of Scaled Bowstring Roof Panel (Note truss and pressure gages)

Fig. 4.22 Postshot, 3.5ba, Damaged Bowstring Trusses (Note certain trusses remained intact)

Fig. 4.23 Postshot, 3.5ba, Interior of Test Cell

Fig. 4.24 Postshot, 3.5bb, Damage to Precast Concrete Channel Roof (Note severe damage to purlin nearest blast)

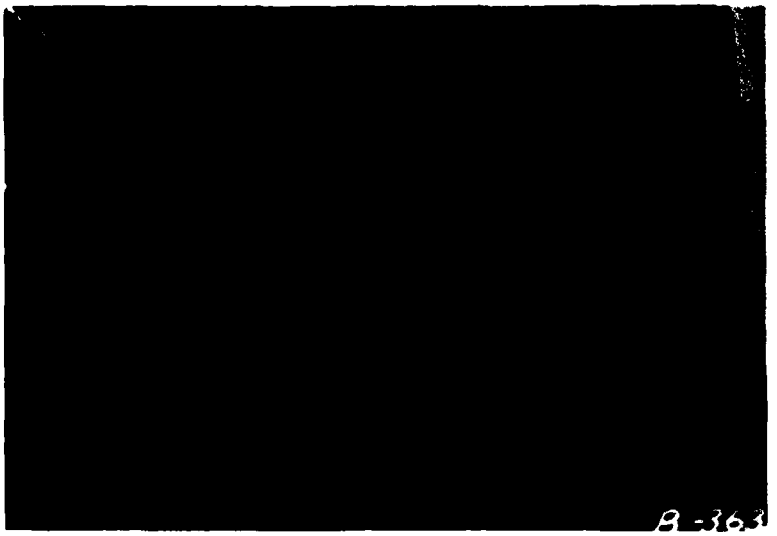

Fig. 4.25 Preshot, 3.5bc, Interior of Laminated Wood Roof Panel Showing Aluminum Foil Break Strip

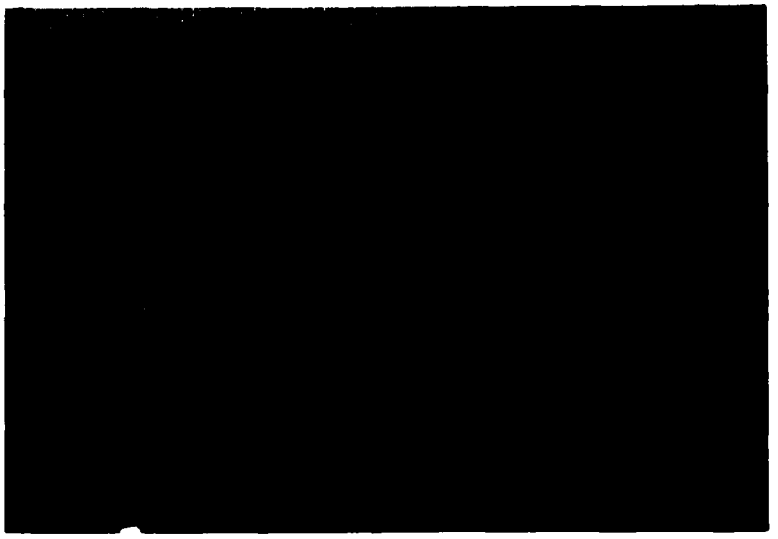

Fig. 4.26 Postshot, 3.5bc, Exterior of Damaged Laminated Wood Roof Panel

Fig. 4.27 Postshot, 3.5bc, Interior of Damaged Laminated Wood Roof Panel (cf similar preshot view, Fig. 4.25)

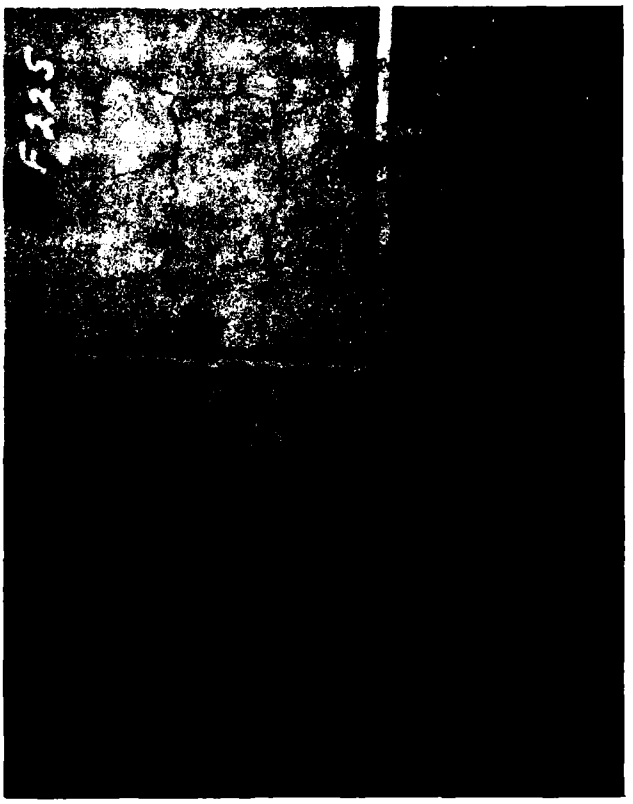

Fig. 4.28 Postshot, 3.5ca, Underside of Cracked 4 in. Reinforced Concrete Roof Panel (Note aluminum foil break strips)

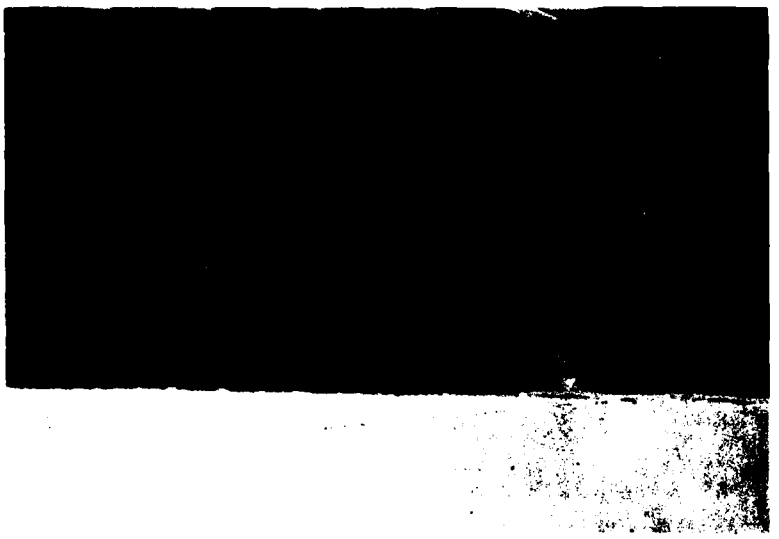

Fig. 4.29 Preshot, 3.5cb, Steel Channel Roof Panel Showing Sensor Supports and Wire Break Strips

Fig. 4.30 Postshot, 3.5cb, Damage to Steel Channel Roof Beams

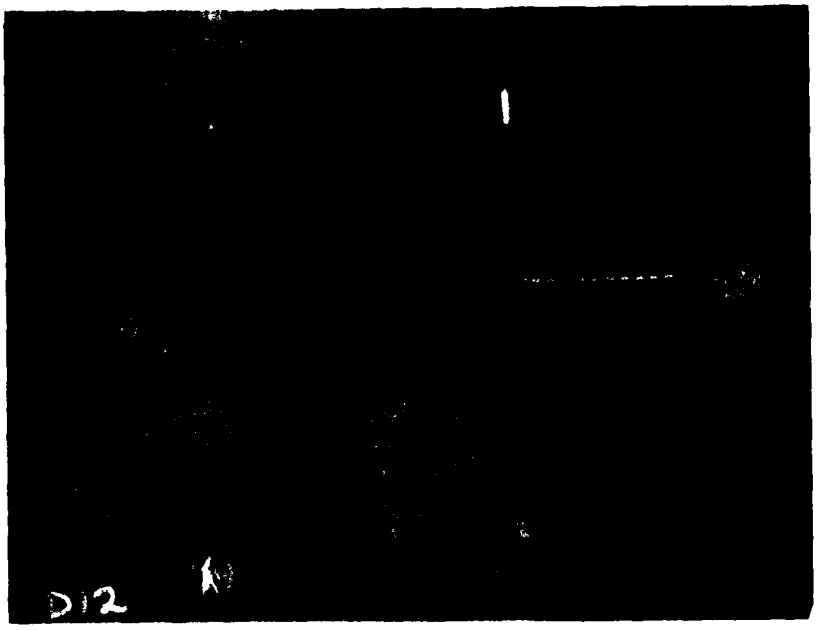

Fig. 4.31 Installation of Pressure Gage 3.5cePl
Behind Brick Wall 3.5ce

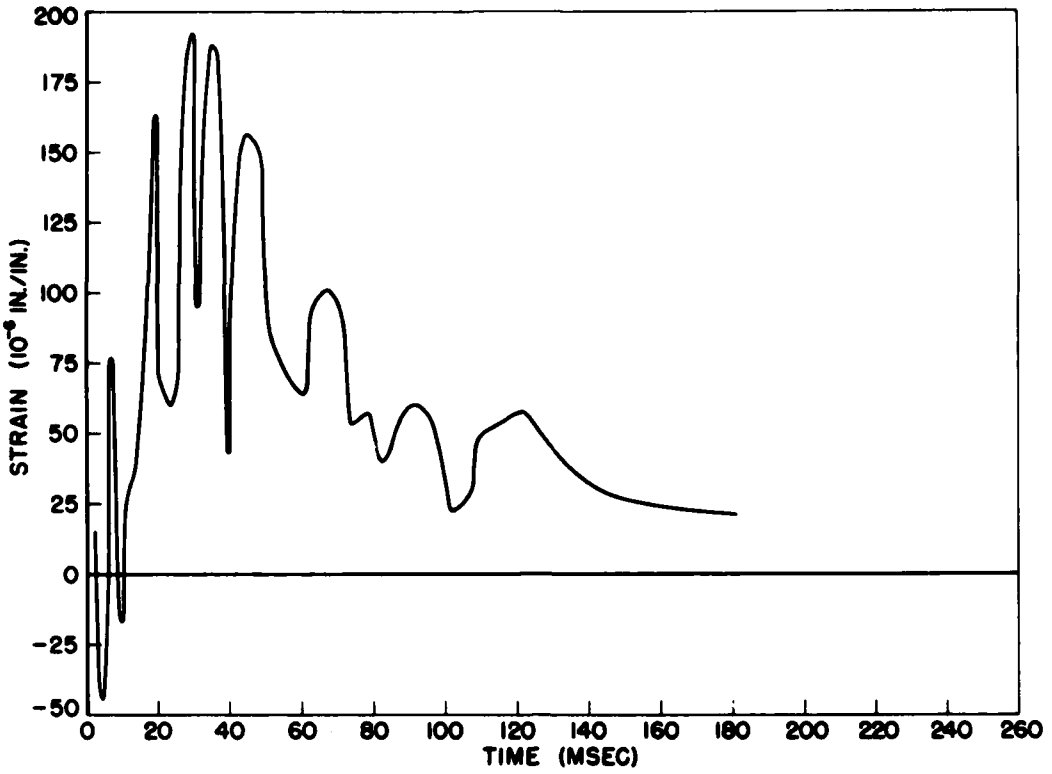

Fig. 4.32 Linearized Strain Record 3.5 ab SIH
(For Gage Location See Fig. 2.1)

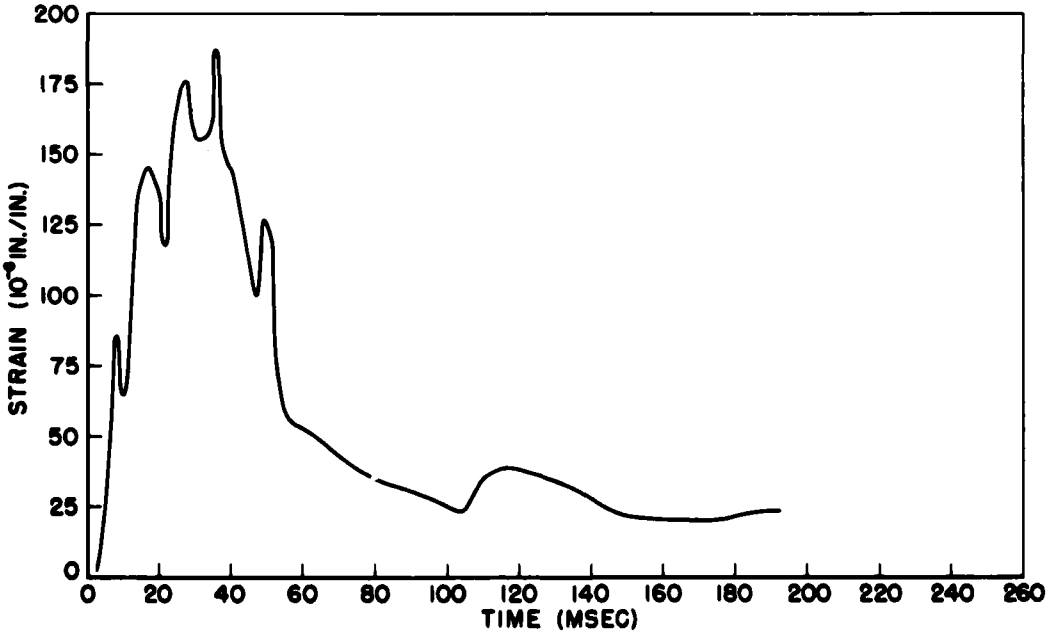

Fig. 4.33 Linearized Strain Record 3.5 ab SIV
(For Gage Location See Fig. 2.1)

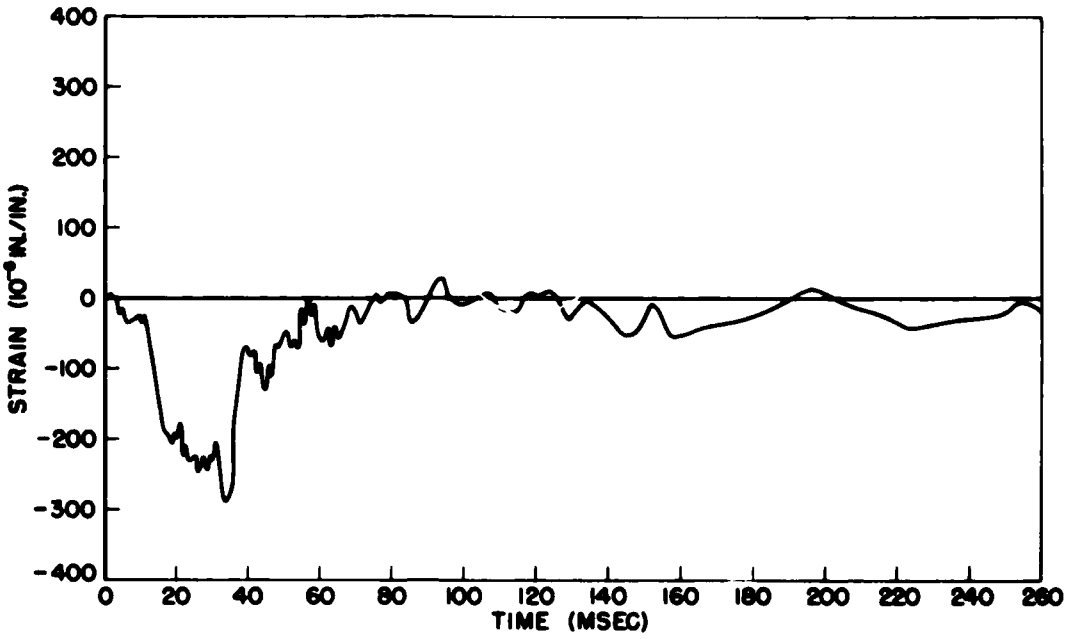

Fig. 4.34 Linearized Strain Record 3.5 ab S4H
(For Gage Location See Fig. 2.1)

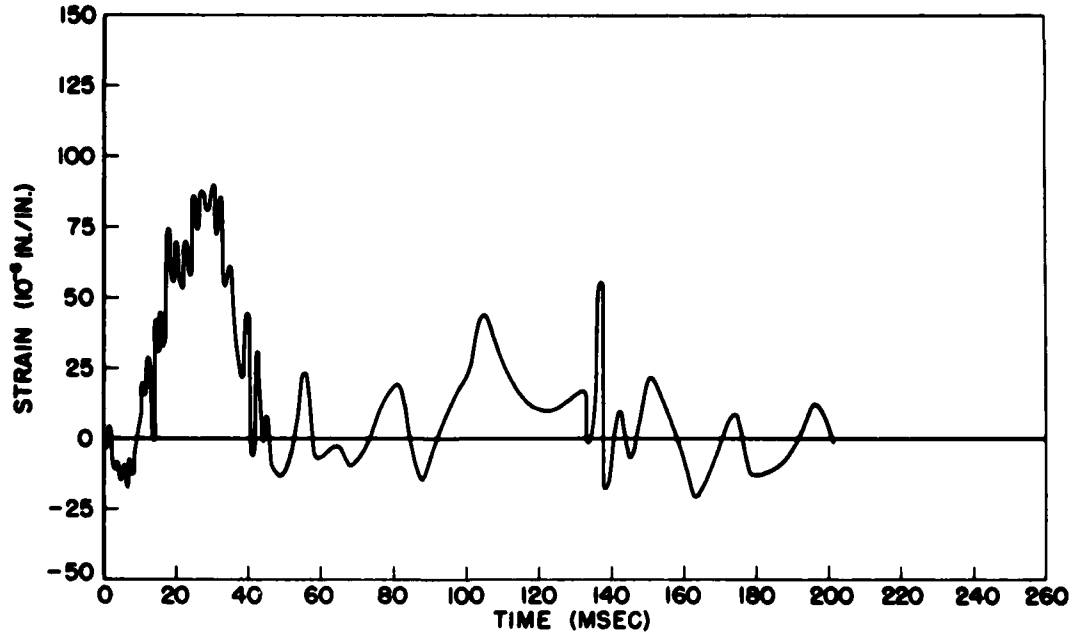

Fig. 4.35 Linearized Strain Record 3.5 ab S4V
(For Gage Location See Fig. 2.1)

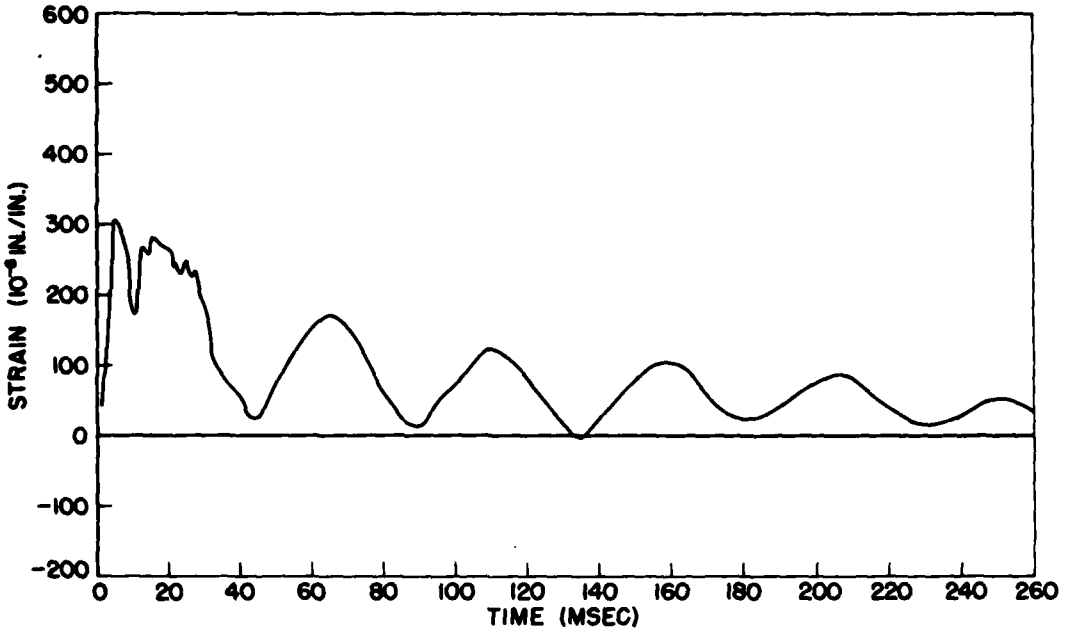

Fig. 4.36 Linearized Strain Record 3.5 ac SIA
(For Gage Location See Fig. 2.2)

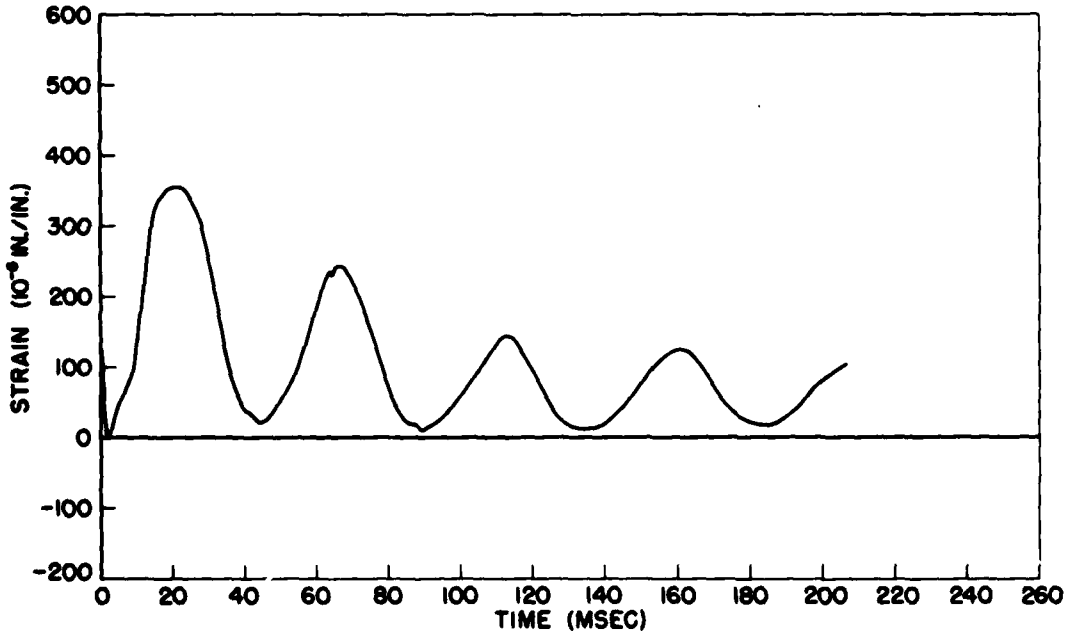

Fig. 4.37 Linearized Strain Record 3.5 ac SIC
(For Gage Location See Fig. 2.2)

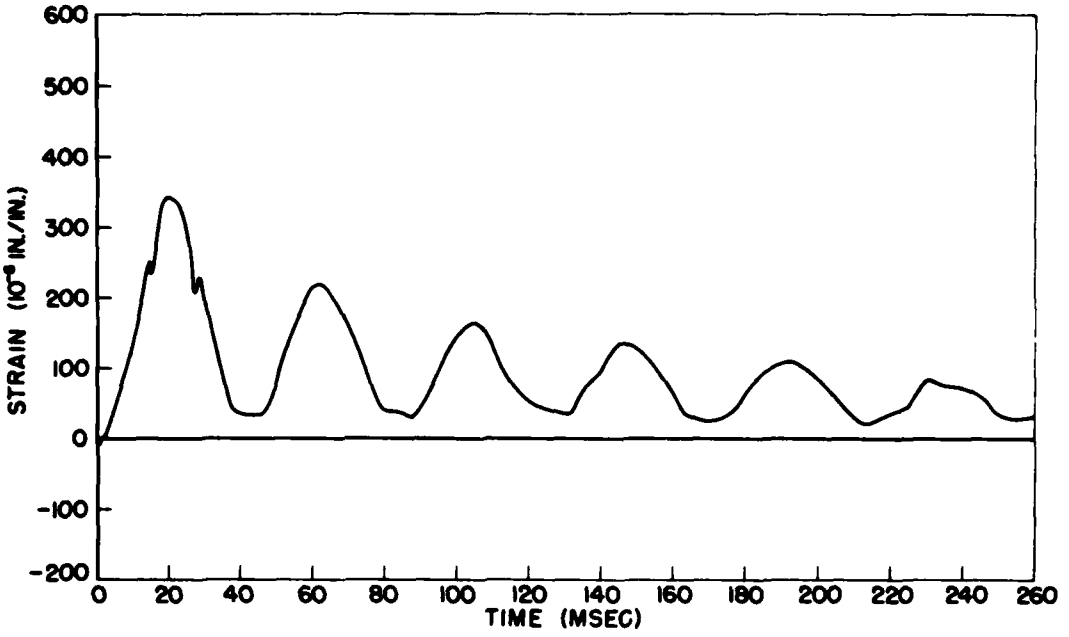

Fig. 4.38 Linearized Strain Record 3.5 ac S3C
(For Gage Location See Fig. 2.2)

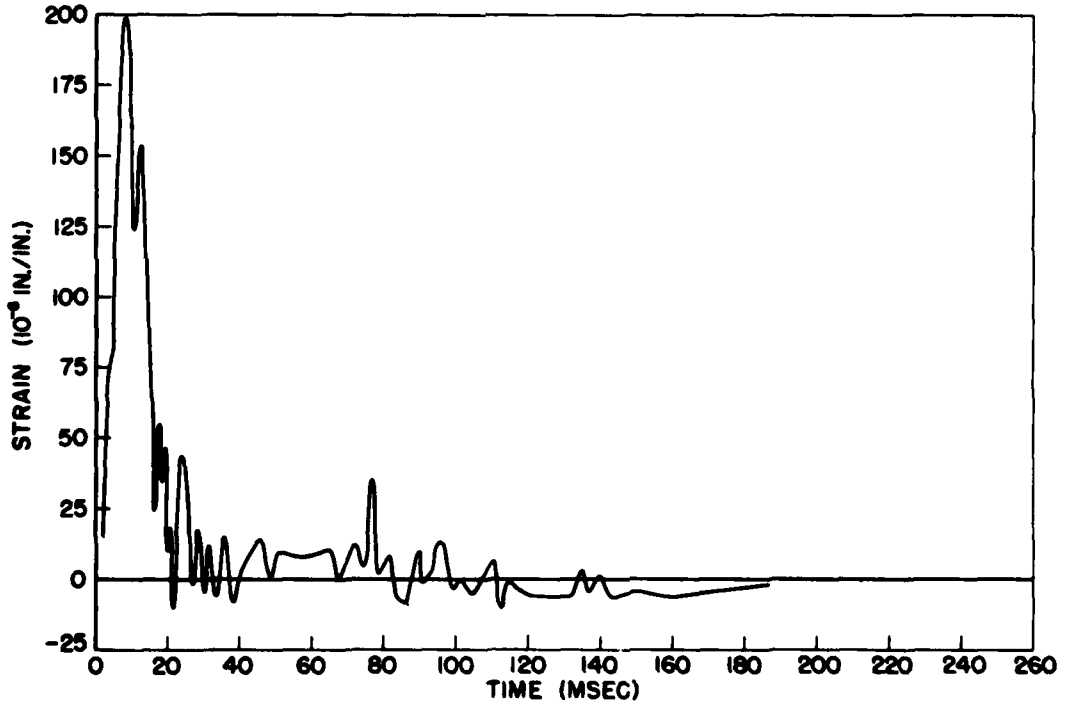

Fig. 4.39 Linearized Strain Record 3.5 ad S1C
(For Gage Location See Fig. 2.2)

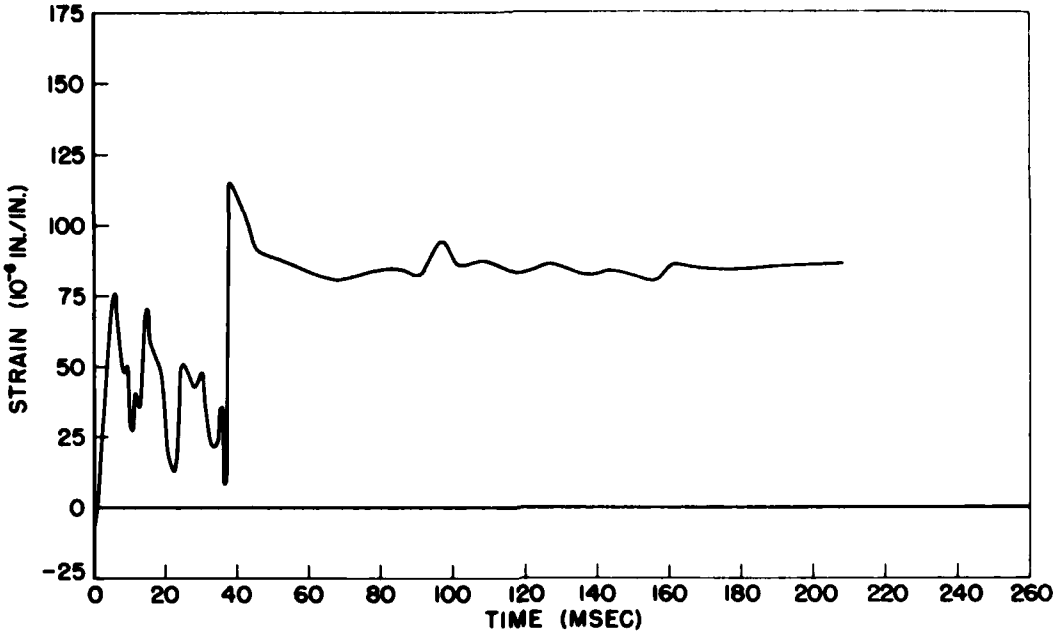

Fig. 4.40 Linearized Strain Record 3.5 af SIC
(For Gage Location See Fig. 2.2)

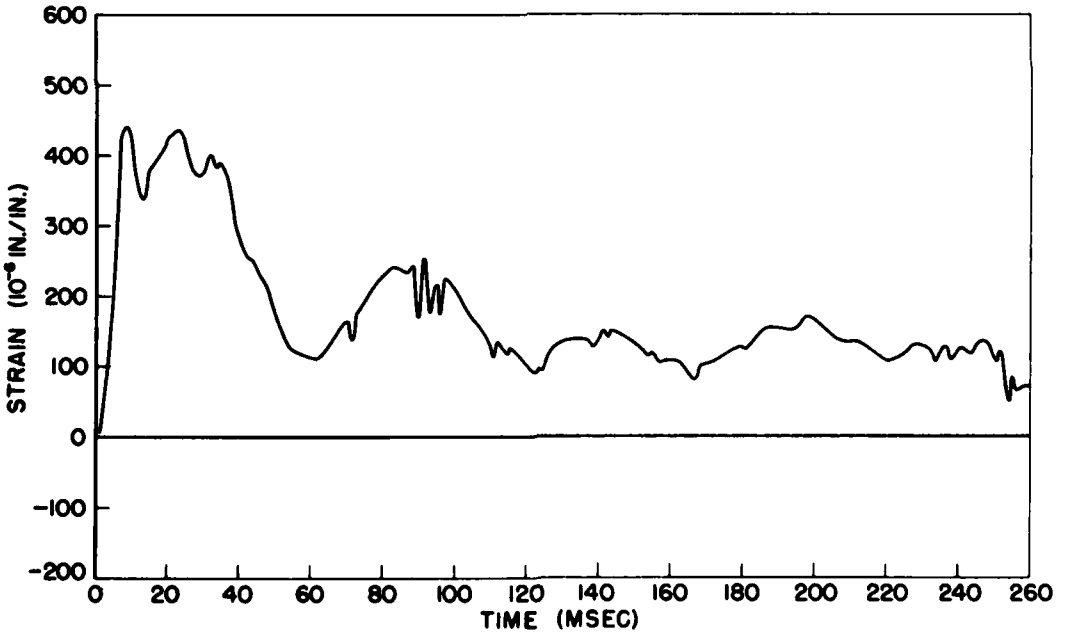

Fig. 4.41 Linearized Strain Record 3.5 bf SIC
(For Gage Location See Fig. 2.4)

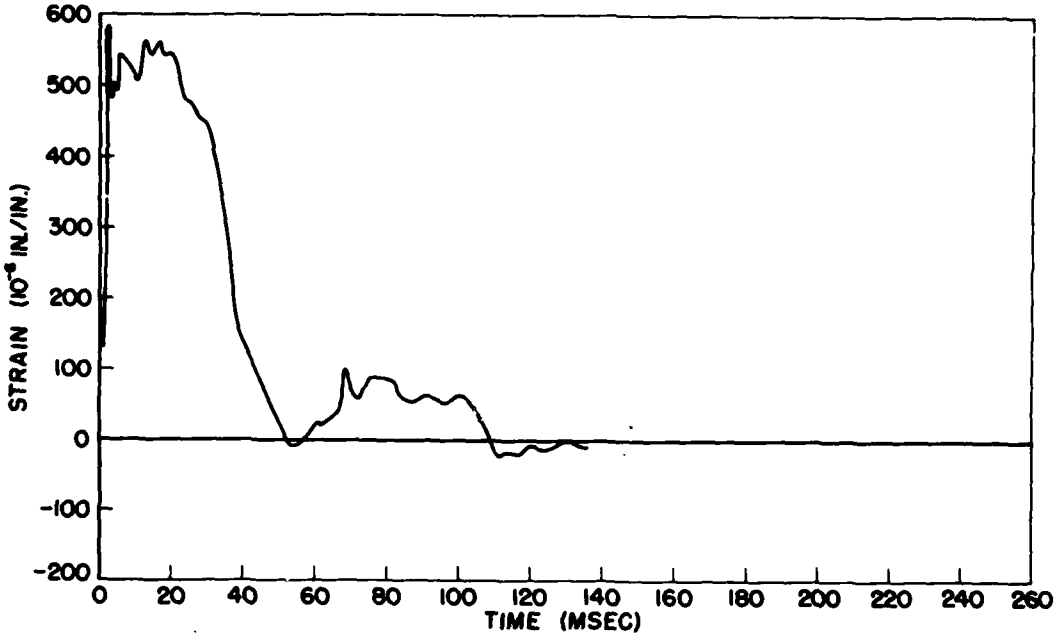

Fig. 4.42 Linearized Strain Record 3.5 cd S2C
(For Gage Location See Fig. 2.6)

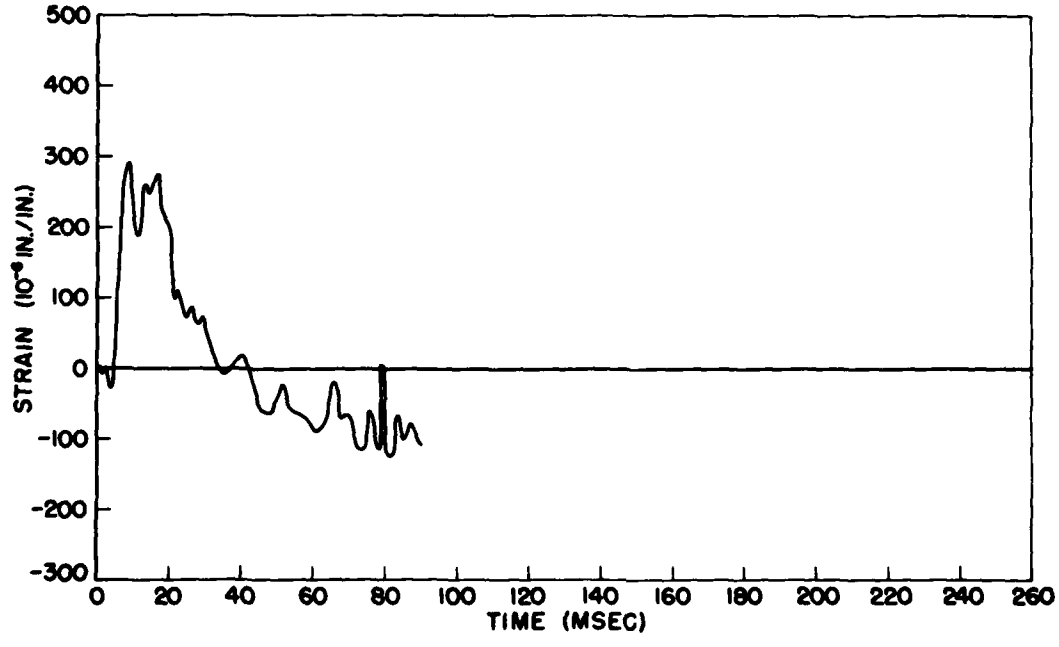

Fig. 4.43 Linearized Strain Record 3.5 ce S3C
(For Gage Location See Fig. 2.6)

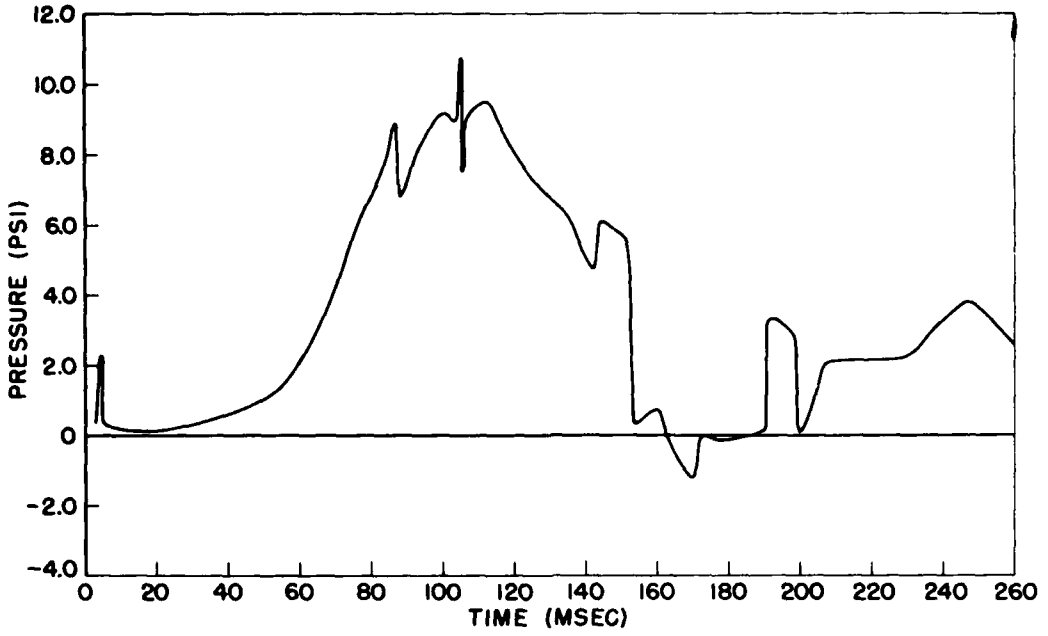

Fig. 4.44 Linearized Pressure Record 3.5 ce PI
(For Gage Location See Fig. 2.5)

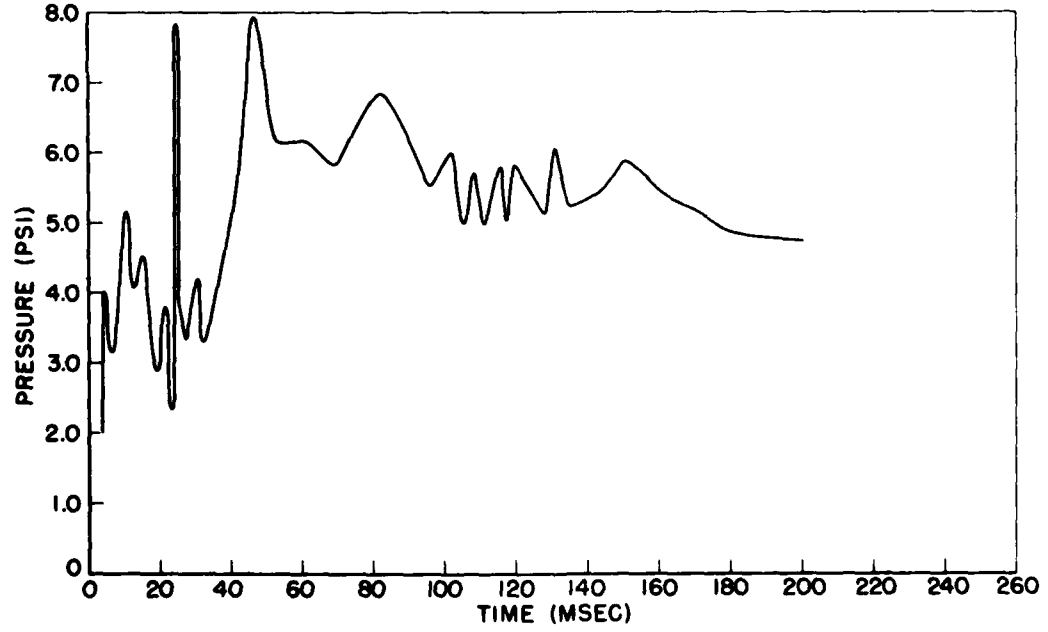

Fig. 4.45 Linearized Pressure Record 3.5 ab PI
(For Gage Location See Fig. 2.1)

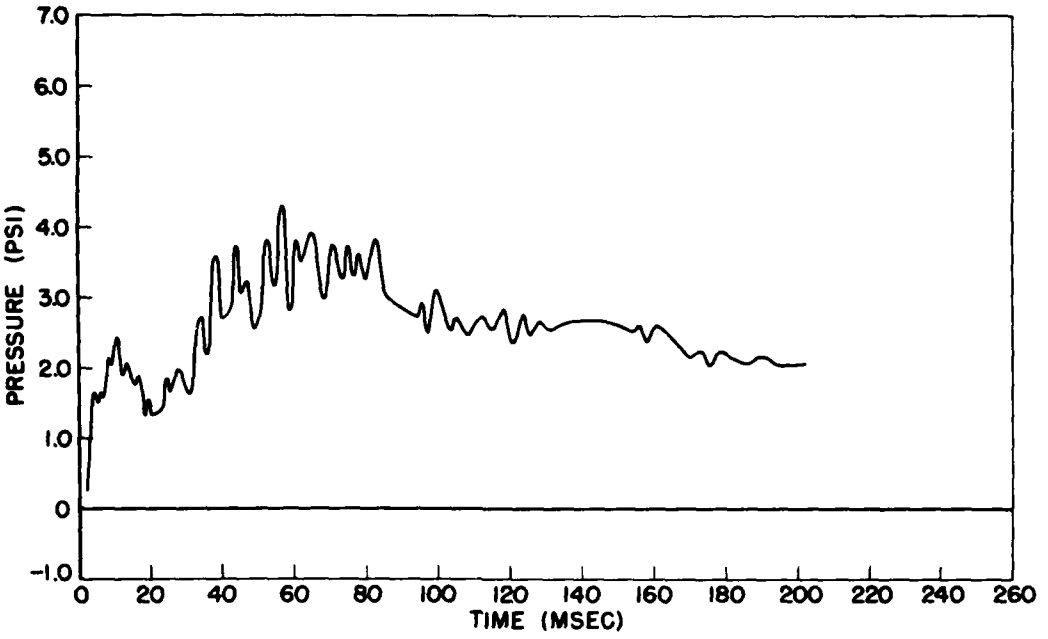

Fig. 4.46 Linearized Pressure Record 3.5 ab P2
(For Gage Location See Fig. 2.1)

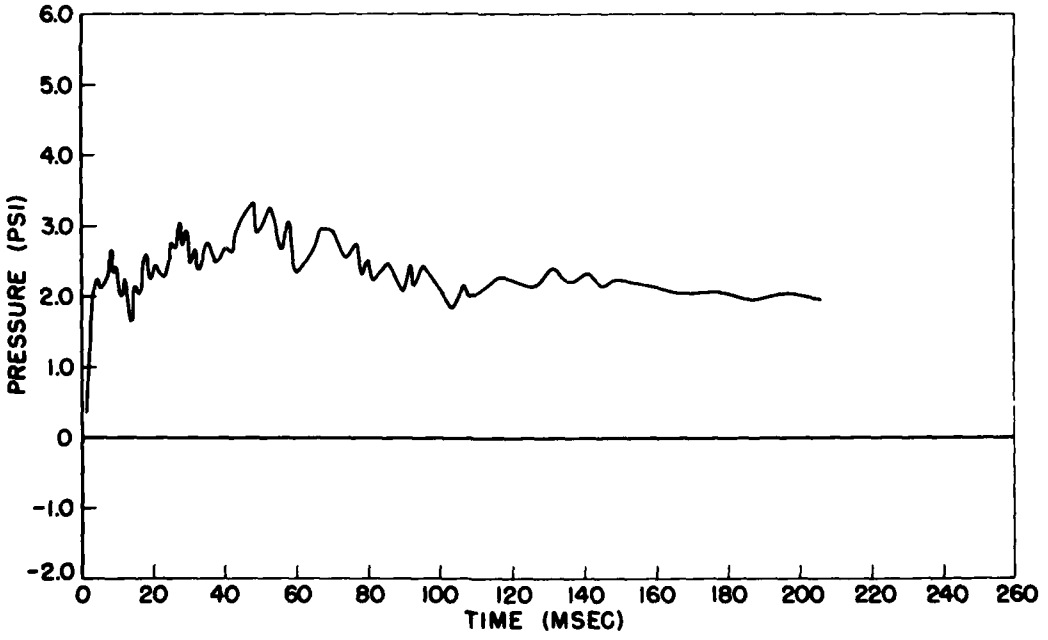

Fig. 4.47 Linearized Pressure Record 3.5 ab P3
(For Gage Location See Fig. 2.1)

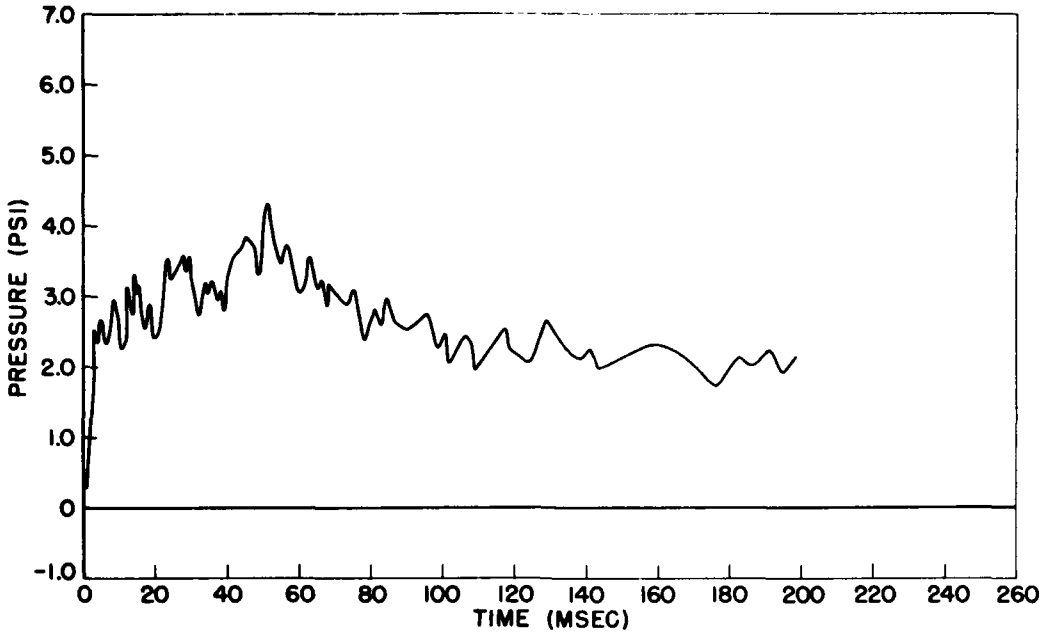

Fig. 4.48 Linearized Pressure Record 3.5 ab P4
(For Gage Location See Fig. 2.1)

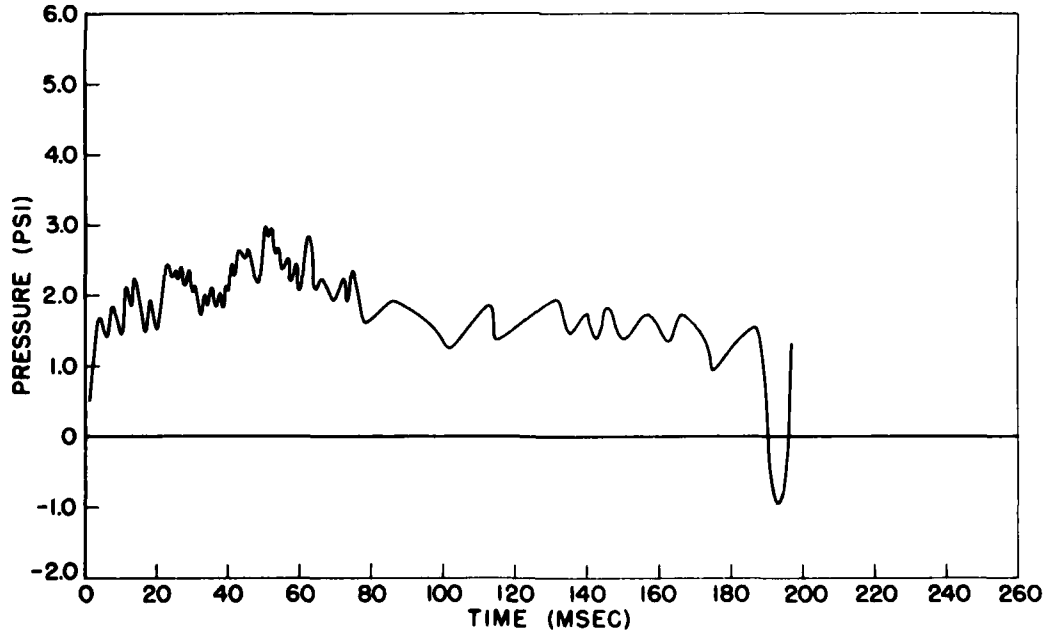

Fig. 4.49 Linearized Pressure Record 3.5 ab P5
(For Gage Location See Fig. 2.1)

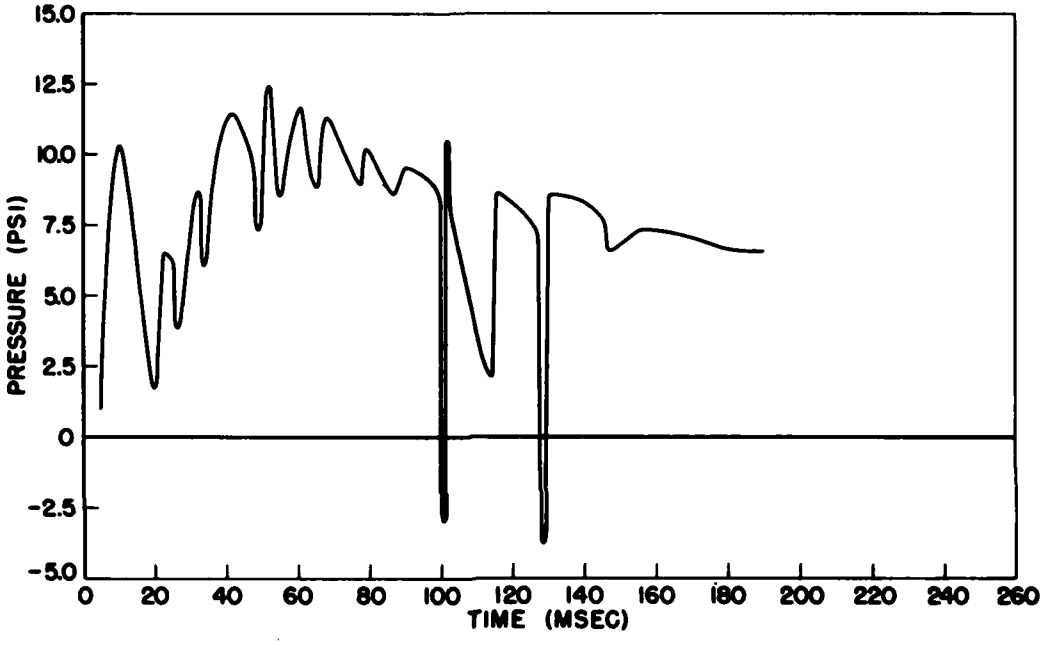

Fig. 4.50 Linearized Pressure Record 3.5 cb PI
(For Gage Location See Fig. 2.5)

CHAPTER 5

DISCUSSION OF RESULTS

5.1 WALL ACTION

5.1.1 Blast Loading

5.1.1.1 Predicted Loads on Walls

The post-test predictions of blast loading on the wall panels are discussed in Appendix B. Essentially, these predictions utilize the pretest prediction method, but use the observed free stream conditions to describe the incident blast wave. The angle of incidence of the blast wave as seen in the horizontal plane differed from the planned head-on incidence because of the bombing error on Shot 9; this error varied from 21 deg at cell 3.5c to 7 deg at cell 3.5a (see Fig. 2.10). The orientation effect was not incorporated in the predictions given in Appendix B, but it can be shown that the error in applied forces probably does not exceed about 10 to 20 per cent at any instant of time for the 3.5c panels (predicted loads are high) and is considerably less for the other wall panels.[1/] A comparison of the predicted applied loads with the transmitted loads as determined from strain gage measurements is given in Figs. 5.1 through 5.10 and discussed in section 5.1.3. The predicted loads were computed as if the walls remained in place for all time.

5.1.1.2 Analysis of Pressure Record from Wall Panel 3.5ce

Only one pressure gage was utilized in connection with the wall panels. This gage was located in the interior of cell 3.5ce behind an 8 in. brick wall in the region of regular reflection at a ground range of about 2160 ft, and at an incident blast overpressure of about 12 psi.

1/ This estimate is based on shock tube and analytical studies of the effects of orientation on blast loading of simple shapes struck by vertical shock fronts (Mach reflection region) conducted by the ARF in connection with other Air Force sponsored work.

The gage was so placed as to give information on the buildup of pressure in the interior of buildings which have no windows and whose walls are expected to be destroyed by the blast. From such information improved estimates of blast effects on interior equipment and on columns of such buildings can be made. While a wall may fail in the structural sense in a very short time (frequently of the order of 10 or 20 ms), the debris may not clear from the opening until a relatively long period of time has passed. Such slow movement can be expected to permit only a relatively long rise time pressure wave to enter the interior; the peak forces and the dynamic effects of the peak forces may be expected to be considerably lower than if the wall debris moved away earlier.

The gage was located as shown in Fig. 4.31. Its dimensional location was 2 ft 2 in. toward ground zero from the inside back wall, or about 5 ft behind the brick test wall. The gage was about half way between the floor and roof on the pilaster, and about 6 in. from the front of the pilaster. The gage was positioned to read side-on pressure; this placed it side-on to the flying debris so that damage to the gage and erroneous signals due to impact with debris would be minimized.

A plot of the 3.5ce pressure record is shown in Fig. 4.44. Comments on the credibility of this record are indicated in Table 5.4. The table shows that the record is believed to be meaningful until 88 ms, and, if corrected, until 140 ms. Since certain of the other gage plots are believed to have incorrect pressure scales, it is felt that the pressure scale on the 3.5ce record should be used only with caution. However, an estimate is made later in this section that the scale may be satisfactory. The time scale and the shape of the plot, as far as the time noted above, are believed to be very accurate.

From the behavior of the strain gage records, this wall appeared to fail structurally at 10 ms after shock arrival, or earlier, and ceased to transmit force to its supporting structure after about 60 ms (see Fig. 5.3). No motion pictures were made at this location because visibility was expected to be nearly zero. Therefore, the movement of the debris away from the opening cannot be estimated.

The pressure plot of Fig. 4.44 indicates that the peak pressure was reached at about 100 to 110 ms after shock arrival. The rise to this indicated peak is quite smooth and gradual (if correction is made for effects believed to be erroneous at 88 and 104 ms); the rise is very small until after about 50 ms.

A few remarks can be made with regard to the pressure scale on this plot. It is felt that the peak pressure will approximately equal outside side-on pressure plus dynamic pressure since the rise time is so long and the rise so smooth. This conclusion is a consequence of the relatively small time (compared with rise time of the pressure) for rarefaction waves to move across the interior. This rarefaction travel time is of the order of 5 ms for one transit of the interior; three to five transits probably suffice to lower pressures in the cavity to the current pressure outside and immediately in front of the cavity (side-on plus dynamic pressure). The value of side-on pressure plus dynamic pressure at the time of the peak on this gage plot is about 10 psi. This value would lie about 1 psi below the peak on the gage plot if a

reasonable correction were applied for the baseline shift and oscillation noted in Table 5.4.

The record, therefore, shows that after structural failure may be said to have occurred, the brick wall moved very little (as far as admission of pressure is concerned) for about 50 ms and did not move enough to admit full outside pressure until 100 ms or more. This indicates that for structures with no windows or doors (and with no early roof failures), but with walls which fail rapidly, the buildup of pressure in the interior is so gradual that interior items whose response is influenced principally by peak pressures will tend to sustain considerably less damage than if exposed to the outside shock wave.

The effect of wall debris in slowing the rate of interior pressure buildup has been indicated by this test to be a considerably more important factor for blast loadings on interior equipment, downstream wall, and columns and trusswork than might have been expected heretofore. Testing of this effect is being planned for shock tube experimentation. Depending on the outcome of such laboratory tests, it may be desirable to perform additional field tests of this nature with different wall material and with larger structures.

5.1.2 Determination of Transmitted Forces

The forces transmitted by a panel to the supporting structure are measured directly as strains in the sensor bars (C-gages, Figs. 2.2, 2.4, and 2.6). The axial forces measured in the plane of the panels (A-gages) are discussed in Chapter 6 in connection with the failure theories.

Of interest is the manner in which the forces in the sensor bars are converted into total transmitted force for the panel. Since measurements were obtained at discrete points, it is necessary to know the distribution of the reactions along the edge of the panel in order to determine the total transmitted force. This distribution will differ for the various panels tested. The reinforced concrete and masonry panels behaved as two-way slabs; the lightweight covering exhibited one-way or beam action.

Due to the manner of construction, the wood siding panel (3.5af) probably transmitted load to the top and bottom sensors as concentrated forces at the studs. Since the sensor assembly is essentially a beam on continuous supports, the forces in all of the sensor bars should be approximately equal. Thus, the total load transmitted by the top and bottom edges of the panel is taken to be the measured force in the sensors directly under the center stud multiplied by the number of sensor bars along the edge.

One-way slab action of the panel cannot take place until the studs have failed. The reactions along the sides parallel to the studs are assumed to be distributed uniformly during the entire loading period. In this case, the total force transmitted to the sides is equal to the load per unit length multiplied by the length of the side. The load per unit length is approximately equal to the force measured in the center sensor bar divided by the length of the side contributing

to this bar, i.e., the distance between adjacent bars. The total force transmitted by the panel is then the sum of the transmitted forces along each of the four edges.

The approximate manner of estimating the distribution of reactions probably yields a high value of the total transmitted force. Even so, only a small portion of the applied load was transmitted to the supporting structure since the panel failed completely. Therefore, errors in the present approach are not significant.

The corrugated asbestos board and corrugated sheet steel panels are constructed in the same manner and are considered together. Figure 4.9 is an enlargement of the motion picture film at the instant of break for the corrugated asbestos board panel, 3.5ae. As can be seen, each subpanel acts independently as a beam. Thus, the force transmitted along the top and bottom edges is assumed to be distributed uniformly and is computed as above. The center girt transfers load to the side sensors as a concentrated force. Under this condition of loading the center sensor is assumed to measure all of the transmitted load. This is not strictly correct since portions of the load are transferred to adjacent sensor bars. However, the error introduced is believed to be small, and again these panels transmitted only a small fraction of their load to the supports.

The remaining panels tested all acted as two-way slabs. This is clearly evident from the fact that the reactions on adjacent sides are of the same order of magnitude, and that the failure pattern is characteristic of plate behavior (e.g., cracks emanating from the corners at about 45 deg). After establishing plate action, it is necessary to determine the end fixities in order to find the shear distribution along the edges. Both the ratio of forces measured on adjacent sides and the comparison of measured *versus* computed periods of vibration point to the existence of simply-supported edge conditions.

For an elastic plate supported in this manner, under the action of a static uniformly applied load, it is known that the distribution of shear along the edges is in the form of a half sine wave. It so happens that for a plate with clamped edges and of the proportions tested, the distribution of shear is closely approximated by the sine distribution. Thus, in any case, the sine distribution is felt to be an adequate approximation.

The total force transmitted to the structure along any edge, R is taken to be,

$$R = \frac{2}{\pi} q L$$

where q is the maximum shear per unit length along the edge and L is the length of the edge. This relation is simply the area under one loop of a sine wave of amplitude q and wave length 2L. The quantity q is computed from the measured force as described previously. The total force transmitted by the panel is the sum of the R's for the four sides.

It might be noted that elementary plate theory demands that, for simply-supported edges, concentrated forces act at the corners of the plate in the direction of the applied load. These compensate the shear

resulting from twisting moments acting along the edges and prevent the corners from rising; for clamped plates the corner forces vanish. In the present case, where no provision for corner restraint was provided, and where cracking might have occurred, it is probable that these forces did not develop, or at least they cannot be computed according to conventional theory. In any case it is believed that the shear distribution along the edges of these panels did not differ appreciably from the assumed sine distribution. This view is apparently borne out by the agreement between the average transmitted and predicted applied load for the two brick panels which remained intact (Figs. 5.1 and 5.2).

In connection with the distribution of reactions for masonry panels, it might be noted that the test results do not support the view that there is a "strong" and "weak" direction for these panels, at least under the action of dynamic loads. Rather, the measured reactions are in agreement with what one would expect for a simply-supported homogeneous elastic plate of the dimensions tested.

5.1.3 Comparison with Predicted Blast Forces

5.1.3.1 Introduction

The force transmitted by each test panel to its supporting structure is compared with the predicted blast force on the panel[2/] in the present section. As discussed later, this comparison indicates that when a wall remains intact, the predicted applied force serves as a good estimate of the average transmitted load, whereas when a wall fails the impulse of the transmitted force can be correlated in a simple fashion with the diffraction impulse of the predicted applied force (the reinforced concrete panel is an exception). These tentative conclusions form the basis of the proposed simplified method for the prediction of transmitted forces discussed in Chapter 6.

It should be noted that a direct comparison between predicted and applied load on the exterior of the panel and the measured force transmitted by the panel to its supporting frame affords only an indirect check on the validity of the former values. This is due to the fact that the load prediction method (given in Appendix B) does not account for motion of the panel during passage of the blast wave, whereas the force actually transmitted depends on the physical properties of the panel as well as on the incident blast.

5.1.3.2 Masonry Walls

The comparison between predicted and transmitted forces (reduced to unit forces) is shown in Figs. 5.1 through 5.6 for the masonry wall panels tested. The two brick walls which remained in place (Figs. 5.1 and 5.2) acted essentially as damped single-degree-of-freedom systems.

2/ The distinction between these forces, frequently referred to throughout this report as "predicted applied" and "transmitted" forces, should be kept clearly in mind.

The wall at the higher loading (3.5bf, Fig. 5.2) shows a nonlinear behavior in that the period of the vibration is seen to vary from about 65 ms initially to about 45 ms toward the end of the trace; the other panel has a constant period of about 45 ms. This action is quite interesting and is discussed in connection with the Arching Action theory of masonry walls in Chapter 6.

In any event, the relatively high frequency response of the brick walls, which is probably representative of the action of most masonry panels met with in practice, indicates the predicted blast load to be a good estimate of the average load transmitted to the structure, provided of course the panel remains intact during the entire loading period.

With reference to Figs. 5.1 and 5.2, it is seen that for both walls the transmitted load drops below the predicted value toward the end of the blast pulse, whereas it should of course oscillate about the applied load. As discussed in Appendix B, the predicted load is based on the following analytical approximation for the time variation of the free-stream pressure wave,

$$p_\sigma (t) = e^{\frac{-ct}{t_o}} \left(1 - \frac{t}{t_o}\right)$$

where $c = 1$, and the rest of the quantities are as defined in Appendix B.

Now indications are that values of c greater than unity should have been used in the post-test load prediction computations. The exact shape of the incident pressure wave at the test locations is not known. However, based on the results of Project 1.1b (Air Pressure Versus Time, WT-711) it appears that for 3.5ac (6700 ft ground range) $c = 1.6$, and for 3.5bf (4500 ft ground range) $c = 2.2$. These values are only approximate since they were determined by curve fitting the pressure-time records obtained at ground ranges of 6536 ft (SRI gage 85B) and 4558 ft (SRI gage 9b), and are based on only the first 300 ms of these traces.

The variation of c with yield, height of burst, and ground range has been considered in connection with other work being conducted at the ARF (Project 3.1, Tests on Building and Equipment Shapes), and these results lead to values of $c = 1.3$ for 3.5ac and $c = 2.2$ for 3.5bf, which are in rather good agreement with the above values. However, it was found empirically that using $c = 3.0$ for 3.5ac and $c = 1.6$ for 3.5bf brings the predicted and transmitted forces shown in Figs. 5.1 and 5.2 into the most satisfactory agreement.

Since these values indicate a trend in opposition to the values based on experimental data, it may be that the discrepancy between the predicted and transmitted forces noted above is not due to errors in the load prediction scheme alone. More likely the explanation is to be found in a combination of errors resulting from (a) the location of the baseline of the strain records, (b) the method of averaging the individual strain records, and (c) improper representation of the incident blast wave.

Some estimate as to the validity of the load prediction method (applicable to front walls in the Mach reflection region) can be made from the response of the brick wall which acted as a linear system (3.5ac, Fig. 5.1). The general equation of motion for forced vibration of a linear one-degree-of-freedom "mass-spring" system with damping can be written in the following nondimensional form:

$$\ddot{X} + 2\beta\omega\dot{X} + \omega^2 X = \omega^2 f(t) \qquad (5.1)$$

where the terms are defined as follows:

$X = \frac{kx}{F}$ = nondimensional displacement in multiples of the static displacement of the system due to the peak applied force

x = actual displacement of "spring"

k = stiffness of spring (kx = force in spring)

F = peak applied force (F/k = static displacement of spring due to force F)

β = per cent of critical damping

$\omega = \sqrt{\frac{k}{m}}$ = natural frequency of system

m = mass of system

$f(t)$ = nondimensional time-dependent applied force (maximum value of $f(t) = 1$)

t = time

$\dot{X}$ = nondimensional velocity of system

$\ddot{X}$ = nondimensional acceleration of system.

The natural period of vibration, ω, was found to be 45 ms per cycle (the maximum variation in this value was about $\pm$ 10 per cent from cycle to cycle and record to record). The damping ratio was determined from the logarithmic decrement (i.e., the logarithm of the ratio of two successive amplitudes of the vibration) and was found to vary between 4 and 8 per cent, depending on the record considered. These values are in excellent agreement with the damping values for brick quoted in the literature.

The first maximum value of X corresponds to the ratio of peak transmitted force (kx) to peak applied force (F), and in the present case depends only on the rate of decay of the linear portion of the applied load, $f(t)$, in addition to ω and β. For the wall under consideration this ratio is computed to be about 1.35 whereas the measured value is about 1.5. If undamped motion ($\beta = 0$) is assumed up to the first peak, this ratio is computed to be 1.5, which is in excellent agreement with the measured value. It may be, therefore, that the damping forces were first introduced after the first peak had occurred; this action might be explained by the fact that some cracking occurred in the

wall about the time the maximum displacement was reached. However, no definite conclusions can be drawn since the differences in these quantities are now probably of the order of errors in the analysis itself.

Equation 5.1 was solved for the predicted loading (the decay rate during the drag phase was corrected as discussed previously) and is compared in Fig. 5.11 with the measured transmitted force. The agreement with the measured values is seen to be quite good, and these simple response computations tend to confirm the general character of the predicted loading within the Mach region as well as the over-all accuracy of the strain measuring system.

The other panels of masonry construction (i.e., 3.5bd, be, cc, and ce) were all destroyed during the test. The strain records for these panels indicate that initial failure occurred in about the first 20 ms after shock arrival (that is, within about the first half period of vibration for these panels), and that the transmitted load vanished between about 50 and 100 ms. These break times compare rather favorably with the values given in Table 4.1, which were obtained from the motion picture films.

Table 5.1 shows a comparison of wall behavior based on the total impulse of the transmitted force (per unit area) expressed as a percentage of the diffraction impulse of the applied force.3/ It is seen that the masonry walls transmitted between about 50 and 150 per cent of the applied diffraction impulse prior to complete failure. Also, inspection of Figs. 5.3 through 5.6 indicates that much of this impulse was transmitted in a time of the order of the duration of the diffraction loading.

The extent to which the results of Table 5.1 are applicable to masonry wall behavior in general is not known. The impulse transmitted prior to failure probably must be assumed to depend on the load causing failure. Thus, the results of Table 5.1 should not be taken to imply that the magnitude of the transmitted impulse will necessarily increase with increasing overpressure -- a result which is certainly not supported by the test, since only one wall of each type was destroyed. However, if it is assumed that a masonry panel will always fail in about the first half period of its vibration, as indicated by the test (and this seems reasonable enough), then the results of Table 5.1 are probably indicative of masonry wall behavior over a reasonable range of loads causing failure and, in fact, may well serve to bracket the impulse a masonry panel is capable of transmitting prior to failure.

This tentative conclusion is based on the observation that the composite wall, 3.5cc, which failed at 12 psi and transmitted the greatest percentage impulse (about 150 per cent), probably would have remained

3/ The term diffraction impulse as used here refers to the impulse (area under the net force-time diagram) of the applied force up to the time pseudo-steady state pressures are reached (see Appendix B). It should be noted that the uncertainty in the shape of the incident pressure wave discussed previously has only a negligible effect on the diffraction impulse.

TABLE 5.1 - Comparison of Predicted Applied and Transmitted Impulses for Wall Panel Which Failed

Panel	Overpressure (psi)	Predicted Applied		Measured Transmitted	$\frac{I_{Tt}}{I_{Dp}}(100)$
		I_{Tp} (psi-sec)	I_{Dp} (psi-sec)	I_{Tt} (psi-sec)	
3.5bd, 8 in. Cinder Block	7.1	2.73	0.34	0.18	53
3.5ce, 8 in. Brick	12	3.68	0.49	0.34	70
3.5be, 12 in. Cinder Block	7.1	2.73	0.34	0.34	100
3.5cc, 4 in. Brick, 8 in. Cinder Block	12	3.68	0.49	0.72	147
3.5cd, 6 in. Reinforced Concrete	12	3.68	0.49	1.58	323
3.5ad Corrugated Steel	4.2	1.69	0.19	0.04	21
3.5ae, Corrugated Asbestos	4.2	1.69	0.19	0.04	21
3.5af, Wood Siding	4.2	1.69	0.19	0.16	84

I_{Tp} = Impulse of total predicted blast loading

I_{Dp} = Impulse of diffraction portion of predicted blast loading

I_{Tt} = Impulse of total transmitted force

intact as 11 psi as discussed in Chapter 6. Thus, a masonry wall which fails may not be capable of transmitting an impulse substantially in excess of 150 per cent of the applied diffraction impulse associated with the critical overpressure.[4] At the other extreme, the 8 in. cinder block wall, 3.5bd, which probably would have failed at about 2.5 psi, was actually subjected to 4 psi and still transmitted about 50 per cent of the applied diffraction impulse -- or about 150 per cent of the diffraction impulse associated with the estimated critical overpressure (i.e., 2.5 psi). Thus, it might be inferred that a masonry panel will generally transmit an impulse of the order of 150 per cent of the diffraction impulse associated with the critical overpressure prior to failure.

Naturally the results of a single test cannot be carried too far. But in view of the present status of knowledge, even extreme generalization of these results is considered justified at this time. An additional point should be noted. The test results are also dependent on the fact that the panels were restrained (i.e., supported between columns) on all four edges. The strain gages which measured reactions in the plane of the panel indicate these forces to be of a magnitude comparable to the normal reactions which have been considered so far. As discussed in subsection 6.2.1.1, the walls would probably have failed in simple bending, and at a much lesser pressure had they not been restrained on at least two opposite edges. In fact, the 8 in. brick wall, which was not destroyed in a 7 psi region, would probably have failed in bending at about 2 psi had it not been restrained along the sides. Thus, the present results must be restricted to panels restrained on at least two opposite edges, i.e., supported between or continuous over columns. The expected difference in response between a panel restrained on all four sides and one restrained on only two opposite sides is considered in section 6.2.1.2.

5.1.3.3 Reinforced Concrete Wall

The comparison between transmitted and predicted blast force for the reinforced concrete wall is shown in Fig. 5.7 and Table 5.1. This panel transmitted about 43 per cent of the predicted total applied impulse[5] (better than three times the predicted diffraction impulse). It continued to transmit force for about 150 ms after failure was initiated and actually remained in place for about 250 ms. Figure 4.17 shows that the panel was removed almost bodily from the test cell, and whatever bond existed between the reinforcing steel and the sensor-supporting system was probably instrumental in keeping the panel in place for this length of time. It can be imagined that if the steel had been attached more securely to the structure (e.g., monolithic construction) the panel, while suffering extreme cracking, might have

4/ The term critical overpressure refers to the blast loading at which wall failure will just occur; determination of these pressures is considered in Chapter 6.

5/ There is some uncertainty in this value due to the error in the predicted value of the total impulse discussed in connection with the masonry walls.

remained in place and transmitted a good deal more of the applied load. In other words, due to the relatively wide variation in design and construction practice found for reinforced concrete walls, the results of this test may not have wide applicability.

5.1.3.4 Lightweight Covering

The comparison between transmitted and predicted blast force for the corrugated sheet steel panel (3.5ad), the corrugated asbestos board panel (3.5ae), and the wood siding panel (all being referred to as lightweight covering) is shown in Figs. 5.8, 5.9, and 5.10 and in Table 5.1. The first two mentioned panels were both fully removed from their test cells in the first 20 ms or so of the loading, and transmitted only about 20 per cent of the applied diffraction impulse during this time.

While the over-all action of these two walls were nearly identical and the transmitted impulses are probably representative of most walls of this type, several possible exceptions should be noted. For example, in certain instances the end connections of the center girt might fail at loads which the panel as a whole could withstand. Thus, the wall would be blown out of the structure essentially intact and the transmitted impulse would not depend entirely on the strength of the covering.

Another exceptional case is that in which the girt and its connections are substantially stronger than under the test conditions. The girt might then remain in place even though the siding failed. In this event the steel siding wall might transmit a much greater impulse than a similar asbestos board wall since an appreciable amount of the steel covering would probably remain attached to the girt. (Fig. 4.8 this to be the case when the girt fails.) In each of the above cases the transmitted impulse would be expected to differ from the test results.

The wood siding panel remained in place for about 50 or 60 ms and transmitted 84 per cent of the applied diffraction impulse during this time. From static considerations the studding of this wall is expected to fail at a somewhat lesser load than the siding between studs. Thus, gross failure of this panel probably occurred after some of the center studs failed. The mode of failure apparent from the motion picture films, section 4.1.6, tends to confirm this action.

5.2 ROOF ACTION

5.2.1 Predicted Loads on Roofs

The post-test predictions of blast loadings on the roof panels are discussed in Appendix B. These predictions use the pretest method with observed pressure values for the incident blast wave. The angle of incidence of the blast wave as seen in the horizontal plane differed from the planned head-on incidence because of the bomb dropping error on Shot 9. This error in angle varied from 21 deg at 3.5c to 7 deg at

3.5a (see Fig. 2.10). The angle effect was not incorporated into the predictions given in Appendix B; it is not known what errors this uncertainty leads to.6/

A comparison of the post-test predicted applied loads with the transmitted loads for the roofs as determined from strain gage measurements is given in Figs. 5.12 through 5.17, and discussed in section 5.2.3.

5.2.2 Analysis of the Pressure Records

5.2.2.1 Test Conditions

All roof test cells had horizontal bracing located about 2 ft below the lower chord of the trusses (or below the roof surface) which conceivably could influence the interior flow. On the 3.5a and 3.5b roofs this bracing consisted of 10 x 10 in. timber beams oriented transversely to the flow; on the 3.5c roofs 16 x 22 in. reinforced concrete beams were oriented in both the longitudinal and transverse directions. In all cases three transverse beams were present, spaced to divide the length of the building into four approximately equal sections. These members can be seen in a number of the photographs in Chapter 4, and in the construction drawings of Appendix C. Gage mountings and dimensional locations are described in section 2.2.5, Table 5.2, and in Appendix C.

The layout of the structures with respect to Shot 9 ground zero is shown in Fig. 2.10. Distances and pertinent information concerning the incident blast wave are tabulated in Table B.2. These data were obtained from the Summary Report of the Technical Director, WT-782. Free stream pressure records were taken by Stanford Research Institute (SRI) at ground ranges approximately equal to the distances of the 3.5 structures (Project 1.1b, Air Pressure Versus Time, WT-711). SRI blast line gages numbered 0B, 9B, and 85B, were at ground level; gages 0B10, 9B10, and 85B10 were located 10 ft above ground. All were at ground ranges differing from the 3.5 distances by only about 1 per cent or less.

Damage to the roof units must be considered as a part of the test conditions under which the pressure records were taken. The final damage is described in section 4.1. Timewise damage as observed from motion picture photography is described briefly in Table 5.3 for roofs which were gaged. In addition to the comments of this table, it was

6/ Shock tube tests have recently been performed at the ARF on hollow blocks at various angles of incidence simulating simple structures with openings in opposite walls. Tentatively it appears that interior and exterior loads may not change too seriously for changes in angle not larger than those which occurred on the 3.5 structures. However, since net loads on roofs are obtained by subtracting interior and exterior loads (which are not too different during much of the loading period) the net forces may be greatly different; hence, no estimate of the inaccuracies involved here can be made at this time.

TABLE 5.2 - Pressure Gage Locations on Roofs

Structure	Gage	Remarks on Location (see notes below table)
3.5ab Pitched Roof	P1	Front slope about 10 in. behind purlin (4 ft 4 in. spacing)
	P2	Front slope about 34 in. behind purlin (4 ft 4 in. spacing)
	P3	Rear slope, same as P1
	P4	Rear slope, same as P2
	P5	Rear slope, same as P2; 8 in. to side of P4
3.5ba Curved Roof	P1	Rear slope, 4 ft from peak (outside)
	P2	Front slope, 4 ft from peak (outside)
	P3	Rear slope, 5 ft from peak, about 8 in. off truss line; no purlins
	P4	Peak, otherwise as P3
	P5	Front slope, same as P3
3.5bb Flat Roof	P1	About 8 ft from front wall, approximately 6 in. behind purlin (6 ft 7-1/2 in. spacing) in "web" of slab.
	P2	Same as P1 except about 4 ft 1 in. behind purlin
3.5bc Flat Roof	P1	11 ft 9 in. from front wall
	P2	18 ft 5 in. from front wall
3.5ca Flat Roof	P1	About 4 ft from front wall
	P2	About 11 ft 6 in. from front wall
	P3	About 15 ft 6 in. from front wall
	P4	About 18 ft 8 in. from front wall
	P5	About 18 ft 8 in. from front wall (on floor)
3.5cb Flat Roof	P1	Same as 3.5bb P2

Notes:

1. "Front" means toward ground zero; "rear" and "behind" means away from ground zero.
2. The interior length of all structures was approximately 27 ft 4 in.
3. All gages were mounted to read inside pressures except 3.5ba P1 and P2. All gages were mounted on the roof except 3.5ca P5, which was on the floor.
4. Pretest gage nomenclature was the same as that used throughout this report except on structure 3.5ba; P1 and P2 positions have been interchanged and P3 and P5 have been interchanged.
5. Locations are shown schematically (without dimensions) in Figs. 2.1, 2.3, and 2.5.

TABLE 5.3 - Failure Observations from Motion Picture Photography for Pressure Gaged Roofs

Roof	Description of Roof		Significant Times Observed from Film
	Geometry	Material	
3.5ab	Pitched roof with purlins	Corrugaged steel on wood truss	Could not be determined
3.5ba	Curved bow-string truss roof	Wood truss, wood decking	Front slope moved several feet by 30-50 ms after shock arrival; tarpaper in air by 50-100 ms; front slope boards in air by 140-170 ms; debris still coming off roof at 1000 ms
3.5bb	Flat roof with purlins	Precase concrete channels	Could not be determined
3.5bc	Flat roof	Laminated 2 x 4 in. wood	Front edge of roof up a few feet and rising at 230-270 ms, up about 8 feet at about 500 ms
3.5ca	Flat roof	Reinforced concrete	No photographs
3.5cb	Flat roof with purlins	Steel channels with gypsum fill	No photographs

inferred from strain gage records that initial structural failures probably occurred to most roofs betweeen about 10 and 15 ms after shock arrival (about the time for the shock front to move halfway down the length of the structure). Heavy structural damage is believed to occur where the transmitted load curve departs greatly in both magnitude and shape from the predicted applied loads, as can be seen for some roofs in Figs. 5.12 to 5.17. That this method of inferring damage is not entirely reliable can be understood from the remarks given in section 5.2.2 concerning the comparison of transmitted and predicted applied loads of roof 3.5aa

5.2.2.2 General Discussion of Records

Plots of representative linearized pressure records obtained on the test roofs are given in Figs. 4.45 through 4.50. Most gage records were plotted to two different time scales: a "fast" or extended time scale and a "slow" or compressed time scale. The first of these shows features of the record from shock arrival to about 200 ms later; the second generally shows features out to the end of the positive pressure phase (about 1 sec) or more.

Table 5.4 lists comments on the conditions of each pair of gage plots on the basis of a fairly exhaustive examination of prints of the original playbacks, tabulations of linearized data read from the original playbacks, and the linearized plots. This table has already been discussed at some length in section 4.2.4. Additional comments, more appropriate to the present section, are given in the following paragraphs.

Column 1 of Table 5.4 shows that a number of the plots are believed to have pressure scales in error by factors of 20 per cent and more. One of these, 3.5ba P2, was located to read pressure on the outside of the roof, halfway up the front slope. It is known from other tests and from "semi-theoretical" considerations that during most of the record the pressure at that point must be approximately equal to or slightly greater than free stream pressure. Peak free stream pressure was about 7 psi, decaying to about 3.8 psi at 200 ms, whereas at 20 ms this record shows a pressure of about 4 psi, decaying to 1.5 psi at 200 ms.

All other gages listed as in error in column 1 were located to read pressures on the underside of various roof surfaces. Later in this section it is deduced that, ultimately, all gages on the undersides of these roofs should follow approximately the outside free stream pressure decay curve or should be less than this pressure by not more than about one dynamic pressure.1/ Further, it is deduced that this equality must hold at all times greater than about 80 to 100 ms (for some gages, it must occur by 50 to 60 ms) after the first pressure signal arrives at the particular gage. These ranges of pressure are given at two instants of time in Table 5.5 for each of the three test locations. In each entry the lower pressure is free stream pressure minus dynamic pressure; the higher pressure is free stream pressure (best available estimate). These ranges were drawn on "fast" plots and the values at 0 and 200 ms were connected by curves bowed downwards slightly (not too much deviation from a straight line). The 11 gages listed in column 1, Table 5.4, as "OK" lie in or close to these plotted ranges (after 50

1/ Dynamic pressure, frequently denoted by "q," equals one half the air density times the square of the air velocity.

to 100 ms, depending on the gage). The plots of inside gages[8] which are stated in column 1 to be in error required the corrections noted in column 1 to bring them midway within these ranges.

The deduction that inside pressures must ultimately lie in the ranges given in Table 5.5 is made as follows: For blast waves which are as long compared with building length as was the case here, it has been observed in the past that ultimately the pressure at every point of a structure approximately reaches and follows some curve which is related simply to the decaying free stream pressure curve. This related curve can be approximated fairly closely by adding or subtracting from free stream pressure the dynamic pressure curve multiplied by some constant (usually between 0 and 2).

Intuitive arguments support this observation, which has been made in other field tests, other UPSHOT-KNOTHOLE results, and in shock tube tests. This, of course, simply means that some "pseudo steady state" has been reached at all points of the structure. For the test structures, this pseudo steady state will result in a stable but gradually decreasing flow through the interior (front and back wall openings equal to about 17 per cent of the gross wall area were present on all roof test cells). No mechanism could be deduced for raising the pressure of this flow appreciably above outside free stream pressure. On the other hand, several possible mechanisms can be advanced which could lead to a moderate lowering of pressure below outside free stream conditions.[9] A "moderate" lowering of pressure in this case cannot be more than approximately 1 dynamic pressure, judging from steady state wind tunnel tests and from tests with shock initiated flow.

In support of the arguments given above is the evidence from the records themselves: 11 of the 17 relevant pressure plots lie within this range. The six plots which lie outside the range are from three structures which seem to have no features which would give rise to different pressures than those observed on the 11 "correct" gages. One of these structures had other gages which read "correctly." Finally, the six inside gages noted had pressure scales which were both too high and too low, averaging out to approximate agreement with the 11 "correct" gages. If it is assumed that random effects were at work in creating

---

8/ All gages in the table are inside roof gages except 3.5ba P1 and P2, 3.5ca P5, and 3.5ce P1. However, much of what is said about inside roof gages applies to 3.5ca P5, which was located on the floor in the interior of the structure 3.5ca.

9/ Among these mechanisms are the following:
(1) The creation of a low pressure wake in the interior by flow around the edges of the front wall openings.
(2) The lowering of interior pressure by suction from the low pressure wake outside the rear wall openings (i.e., the outside rear wall is heavily affected by a wake caused by the flow around the outside of the structure).

TABLE 5.4 - Summary of Analysis of Pressure Records

Structure	Gage	(1)* Remarks Concerning Pressure Scales	(2) Condition of Baseline Prior to Shock Arrival	(3) Plot is Meaningful Until:	(4) Major Features of Plots which were Ignored	(5) Other Comments
3.5ab	P1	High (0.5-0.7)	OK	End	Pips: f at 25 s at 500	None
	P2	OK	osc. up to 10%	End	None	None
	P3	Low(about 1.2)	OK	300	None	None
	P4	OK	OK	240	None	None
	P5	Low(about 1.3)	OK	240	Dip: f at 190-195	Peak on s 10% higher than peak on f
3.5ba	P1	---	---	---	---	Record discarded (see note below table)
	P2	Low (2-3)	Bas. of 200% h. about 20%	230	See column (5)	f 25-60 smoothed heavily from hashy record; s plot not made
	P3	OK	p. up to 20% h. about 10%	End	Dips: f at 60, 68, 94; "hash": s at 600-850, 1100-1200, 1750-1900, 2800	None
	P4	OK	Bas. up to 15% p. up to 30%	800	Rapid oscillation at 400	None
	P5	OK	Same as P4	End	Baseline shifts 200-600, 1000-1500, 3300-3500	None
3.5bb	P1	OK	Osc. up to 10% p. up to 20%	400	Dip: f and s at 90	None
	P2	---	---	---	---	No record obtained
3.5bc	P1	Probably low, see column(6)	Bas. of 10%	End	Oscillation at 300, shifts at 600-700	Baseline should probably be moved down 1/2 psi
	P2	Probably high (0.65-0.8)	Bas. up to 10%, large p. 30%	See Col. (6)	See column (6)	Original record seems questionable in many respects
3.5ca	P1	OK	OK	End	None	Peak on s 10% lower than on f, f and s disagree 150-170
	P2	OK	OK	End	Dip at 900	None
	P3	OK	OK	End	None	140-200 f is 10% lower than s
	P4	Low(about 1.2)	OK	94	None	None
	P5	OK	OK	88	None	None

TABLE 5.4 - Summary of Analysis of Pressure Records (cont'd)

Structure	Gage	(1) Remarks Concerning Pressure Scales	(2) Condition of Baseline Prior to Shock Arrival	(3) Plot is Believed Meaningful Until:	(4) Major Features of Plots which were Ignored	(5) Other Comments
3.5cb	P1	OK	OK	210	Dips at 101, 128 on f	None
3.5ce (wall)	P1	See Section 5.1.2	OK	See note below	Baseline shift at 88, oscillation at 104	None

Notes:

Column (1): "High" means the pressures as read from the plots are too high.
Numbers in parentheses are approximate correction factors to bring records within bonds construed from Table 5.5 pressure values; pressures read from the plots should be multiplied by these values.
"OK" means that correction factors were closer to 1.0 than about 0.8 and 1.2.

Column (2): "OK" means the baseline appeared clean and flat to within about 5 per cent.
Abbreviations are: Osc. = oscillations, Bas. = baseline shifts, h. = "hash", p. = pip(s).
All percentages are in terms of the maximum meaningful signal recorded.

Column (3) to (5): Numbers without units are ms as given on the gage plots.
"f" denotes the plot with expanded time scale (from "fast" playback).
"s" refers to the plot with compressed time scale (from "slow" playback).

Column (4): Only features appearing prior to the time listed in column (3) are noted.

Gage 3.5ba P1: The first 30 ms of the original playback from the gage may yield useful data. However, no plot was made with the expanded time scale. Otherwise, this gage record simply departs from meaningful pressure values by showing no tendency to follow a decay curve approximately parallel to side-on pressure (as an outside roof gage must for a relatively long blast wave).

Gage 3.5ce P1: In column (3) the record is meaningful until 88 ms if uncorrected. If corrected for items noted in column (4) it is felt to be meaningful until 140 ms.

pressure scale errors, this result would be likely to follow. Admittedly, effects of roof breakage and local effects of purlins might affect the correctness of the above reasoning. However, it appears that both these effects are probably negligible (section 5.2.2.4).

TABLE 5.5 - Pressure Ranges Used in Analysis of Inside Gage Records

Test Cells	Pressure (psi)	
	At time of shock arrival at gage	200 ms later
3.5a	3.6 to 4.2	2.3 to 2.5
3.5b	5.4 to 7.1	3.3 to 3.8
3.5c	10.4 to 12	6.3 to 7

Note: In each column the higher value is free stream pressure and the lower value is free stream pressure minus dynamic pressure at the time indicated.

Throughout the analysis of the records, the various uncertainties as to their accuracy and credibility made it difficult to proceed logically with the deduction of the various conclusions stated in this report. This situation implies, of course, that few, if any, of the conclusions arrived at here are established with great certainty.

5.2.2.3 Effects of Roof Breakage

The effects of roof breakage on the pressure records is believed to be so small as to be negligible for the analysis of the records as described here. This rather surprising conclusion was reached after futile attempts were made to find indications in the records of acceleration effects due to movement of the mount, effects due to striking the gage with debris, and effects resulting from reorientation of the gage face as it moved out of its intended position. Yet ultimately, substantial damage was inflicted on most of the roofs near many of the gage locations as has been described in Chapter 4 and in Table 5.3. The only way in which these results can be explained is by assuming that [10]

1. Acceleration and debris effects were mild compared with the gage sensitivity to these effects.

[10] The text and a footnote in section 4.2.4 discuss an alternative assumption, namely, that some signals on the gages which were rejected may be due to roof failures. There it is concluded that this is probably not the case.

2. Movement of the gage which reoriented it with respect to the flow occurred so long after shock arrival that reorientation effects were very small.[11]

3. Openings in the roof which ultimately occurred on five of the six pressure gaged roofs were probably not large by 200 ms, and were possibly not large until free stream pressure had dropped to around the 2 psi level[12] (when dynamic pressure effects could no longer be distinguished).

This tentative conclusion concerning the effects of roof motion during failure is of considerable importance to field testing and to the prediction of loadings on structures with roofs which ultimately fail.

5.2.2.4 Local Effects

The effects of the purlins (on roofs 3.5ab, bb, and cb) and of longitudinal trusses appear to be minor. On two of the structures with purlins, gages had been placed a short distance behind and a short distance in front of purlins in order to determine whether any long term effects such as low pressure behind and high pressure in front of each purlin might occur. Due to a gage failure, such a direct comparison could be made only on 3.5ab (but all five gages here were useful for the comparison). On the other two structures some indications could be deduced since, as has already been described, most gages have been found to read the same pressures after the pseudo steady state time. This fact implies that no appreciable purlin effect was present since this equality of pressure held for gages on each side of purlins and on roofs which had no purlins. The checks on the 3.5ab roof also showed this result. Thus the fairly definite conclusion can be reached that purlin effects on pressure are confined to areas of the roof not wider than a few purlin heights on either side.

11/ As free stream pressure decreases, dynamic pressure becomes a smaller and smaller percentage of free stream pressure (for the Mach reflection region the ratio of "q" to free stream pressure can be shown to equal approximately $p^2/40$, where p is free stream pressure in psi; in the regular reflection region where 3.5c is located, q is always less than about $p^2/80$. Reorientation effects can be expected to merely change the dynamic pressure effects on the gage; these are extremely small compared with p, when p is below, say, 2 psi.

12/ Or about 300 to 600 ms; these values of time are not to be taken at face value since choice of the 2 psi level above is subject to debate.

Also implied by the general agreement of pseudo steady state pressures is that roof shapes such as the sloped roof, 3.5ab, and the arched roof, 3.5ba, do not seem severe enough to create appreciable differences from pressures which would be felt on the underside of a flat roof. This tentative conclusion does not apply to pressures prior to the pseudo steady state time. Also it does not apply to the outside surfaces of these roofs: the only two outside gages, 3.5ba P1 and P2, are seen from Table 5.4 to have yielded few or no useful data in this regard.

A comparison of pressures on the inside of the roof with pressures on the floor directly below can be made between gages 3.5ca P4 and P5. In Table 5.4 it is noted that the P4 pressure scale may be low; thus it is uncertain whether the record is accurate or not. Plots of P4 and P5 agree (up to about 90 ms when both are rejected) if the correction of Table 5.4 is made. Otherwise, P4 runs low by about 15 per cent. The only conclusion that can be made is that no large differences occurred at the roof and floor for these locations.

5.2.3 Comparison with Predicted Loadings

The time for the interior roof pressures to reach pseudo steady state (i.e., some curve related to the outside free stream pressure decay curve) has been mentioned already in section 5.2.2.2 in connection with the pressure scales on the gage records. This interval of time between shock arrival and pseudo steady state is an important quantity in the prediction of loadings on roofs. In the predictions described in Appendix B this interval of time is denoted by t* and was predicted to be close to 100 ms ($\pm$ 10 ms) after shock arrival at the front wall of the building for all the 3.5 roofs. This prediction is based on formulas developed in the pretest report. The roof interior pressure records check this predicted value satisfactorily, giving about 80 ms to 120 ms for all the roofs. In obtaining these times from the pressure records, the time for the shock to travel from the front wall to each gage had to be added to the observed time. This time to be added varies from about 10 ms to 25 ms depending on the distance of the gage from the front wall openings.

Another important check can be made of the methods of load prediction used in Appendix B. The methods predict inside roof forces prior to the pseudo steady state time, t*, in terms of two principal interior shock waves: (1) the initial interior shock wave which expands from the front wall openings immediately after shock arrival and (2) the interior reflected shock which is simply the initial shock after reflection from the inside rear wall, weakened or strengthened by the presence of openings in that wall; this latter shock moves back towards the front wall. Other shock waves which may move through the interior of the structure are discussed in a later paragraph. It is estimated that all interior shocks move along the length of the interior at speeds of from about 0.9 to 1.35 ft/ms or an average of about 1.1 ft/ms (this holds approximately even for shocks moving upstream,against the air flow). Using these speeds, one can compute the time intervals during which each

particular gage is recording information about each of the two shock waves described above. In all cases, these two time intervals together cover about the first 50 ms of each pressure record. The average pressure read on each gage during each of those intervals was compared with the average pressure predicted according to Appendix B.

Since recorded pressure was often changing rapidly during these intervals, rise time limitations of the gage and minor data reductions errors limited the accuracy with which this comparison could be made. On the other hand, only fairly rough checks could be expected in comparing predicted averages over the entire undersurface of the roof with pressures recorded at the few particular gage locations.

On the 3.5a and 3.5b roofs the measured averages ranged from the predicted values up to about 50 per cent higher (up to 80 per cent higher for the initial wave in 3.5ba). On the 3.5c roofs, measured values were from 3 to 5 times as large as predicted values.[13]

After the end of the interior reflected wave has passed each gage (about 50 ms on all gage plots), the predictions imply that the pressure at most gage locations should move gradually and approximately linearly towards the pseudo steady state curve, reaching this curve at time t^*, after shock arrival at the front wall. In studying the records to check the linearity prediction it is difficult to know exactly when the interior reflected wave can be said to have ended and when other effects begin (the exact time could easily be anywhere between 45 ms and 55 ms). However, it seems that the records indicate a trend somewhat different than the predicted linear change of pressure with time until pseudo steady state. Indications are that the pressure rises above the linear trend predicted, by a moderate but measurable amount, and that this effect is caused by later reflections of shocks from the front and, perhaps, the back wall of the structure. This effect may be peculiar to the geometry of the test structures. The relatively low position of the wall openings in the test cells (they are considerably closer to the floor than to the roof level or lower chord of the truss) and the presence of cross bracing across the interior and of a supporting ledge to carry the roof support bars may have contributed to this overshoot through an entrapment of the interior reflected shock which might not occur in many industrial-type structures.[14] This effect may, therefore, illustrate the effects that unusual geometries can create.

At least three shock waves which do not appear explicitly in the predictions seem to be present in some of the records. The probability of other interior shocks, in addition to the two main ones noted earlier (initial and reflected interior shocks), was recognized in the development

---

13/ Structures 3.5c were in the regular reflection region. A special prediction method which is more conjectural was used for these buildings. These predicted loads are also especially sensitive to slight changes and wall openings.

14/ On the other hand, the comparison of floor and roof gages on 3.5ca, described later, indicates that until 90 ms, inside roof and floor pressures were about the same.

of the predictions but their effect is felt to be minor on the roof loadings. The presence of a re-reflected wave can be seen on a number of the records at about 50 ms. This wave is the reflected-reflected interior wave and moves from the front to the rear wall. Between the reflected wave and this re-reflected wave there appear some indications of still another shock on records 3.5ca P4 and P5, 3.5bc P2, and 3.5ab P4 and P5. This wave is most prominent on gages near the rear wall and may result from the outside shock wave sweeping across the outside rear wall from three sides, reflecting near the center of the wall, and creating shocks around the rear wall openings a short time after the interior shock has reflected from the inside of this wall.

One other wave appears in some records, particularly those of gages near the front wall. This shock appears between the initial shock and the reflected shock and may be due to parts of the initial shock which reflect between roof and floor, or between the side walls as has been observed in shock tube tests in the past. Orientations other than head-on will also tend to create additional secondary reflections of this type through the interior, particularly for the orientation of the test structures.

In conclusion, the comparison of measured inside pressures at a few positions on several of the roof structures with the predicted average loading over the entire inside surfaces of these roofs indicates that the predictions are fair to good in most respects for the Mach reflection region, but are poor in certain respects for the regular reflection region. In this latter region it appears that, prior to pseudo steady state time, the net roof forces (outside minus inside) are lower, in some cases by a factor of about two, than those computed according to the methods in Appendix B (and plotted for one roof in Fig. 5.17). It was felt that no purpose would be served by quoting detailed breakdowns of the comparison between measurements and predictions, since the ultimate use to be made of such comparisons is in the revision of load prediction methods -- which is beyond the scope of this program. It is further believed that such revision can be completed only after still more detailed consideration of the gage records, and after the implications of the comparison with respect to net forces on the roofs have been fully considered.

5.2.4 Transmission of Force

5.2.4.1 Determination of Transmitted Force

The forces transmitted by a roof panel to its supporting structure are measured directly as strains in the sensor bars (V-gages, Figs. 2.1, 2.3, and 2.5). The forces in the gaged sensor bars were converted to total transmitted force for the roofs in a manner similar to that discussed in connection with the wall panels, section 5.1.2. The truss roofs (3.5aa and 3.5ab) were assumed to transmit concentrated forces to the sensor system bars; the channel slab roofs (3.5bb and 3.5cb) were assumed to transmit their reactions uniformly to the sensors through purlins along the two supported sides, as was the laminated wood roof (3.5bc). No usable strain measurements were obtained for the reinforced concrete slab roof, 3.5c (see Table 4.2).

5.2.4.2 Discussion of Roof Behavior

The comparison between predicted and transmitted forces (reduced to unit forces) is shown in Figs. 5.12 through 5.17 for all but one of the test roofs (no comparison is possible for the reinforced concrete roof). As pointed out with respect to a similar comparison for the wall panels, there is no reason to expect close agreement between the predicted applied and measured transmitted forces since the former do not account for motion or failure of the panel during the loading period.

The comparison for the corrugated asbestos covered roof (Fig. 5.12) appears to indicate excellent agreement between the predicted and transmitted loads for as long as 230 ms after shock arrival. However, this apparent agreement is probably in part coincidental and not meaningful since the roof covering failed well before this time. Motion picture photography indicates that the forward portion of the front slope was probably gone by somewhere between 15 to 30 ms, the covering around the peak by 60 to 80 ms, and the rear slope by 120 to 140 ms. Since observation of exactly where the debris came from was uncertain, and since the roof was often obscured by dust, these items are not well defined. However, it is clear that much of the roof covering was in the air by 100 ms.

Figure 5.13 shows that the comparison between predicted and transmitted force for the corrugated sheet steel roof is also remarkably good for the first 50 or 60 ms, whereas the motion picture photography again indicates that failure of the roof covering started prior to this time. It will be noted that the loads transmitted by the corrugated asbestos board roof and the corrugated sheet steel roof compare favorably with each other, although the damage sustained by the trusses of each differed appreciably (see Figs. 4.18 and 4.20). This is no doubt due to the fact that the asbestos board, being the more brittle material, shattered and was torn away from the trusses leaving them intact; the steel siding, on the other hand, most likely adhered to the purlins for a longer period of time (similar behavior was noted for the corrugated steel wall) and caused considerably more damage to the trusses. In view of this behavior it is not at all clear why either of the transmitted forces should agree so well with the predicted applied load or with each other. In any event, if the strain measurements are to be accepted, it must be concluded that the force transmitted by this type of roof (under test conditions) follows the predicted loading rather closely for about 100 ms or more (i.e., duration of the positive or downward loading).

The wood bowstring truss roof (Fig. 5.14) was completely destroyed and transmitted about 15 per cent of the predicted positive impulse prior to failure. It is not possible to draw any firm conclusions regarding the response of the prototype roof from the response of this geometrically scaled model; certainly the inference of a 1:1 correspondence between the two is unwarranted at this time. In fact, as mentioned earlier (section 3.1) the scaling was principally with respect to the truss members and was not exact in all details. For example, the decking used on the test roof was about as heavy as might be found on

prototype structures. Thus, it is not unlikely that the relatively greater strength of the decking caused an excessive load to be transmitted to the truss members. It is possible, therefore, that in the prototype roof the same decking being supported by heavier trusses over larger spans, would have failed before the trusses themselves were destroyed.

The precast concrete channel roof (Fig. 5.15) appears to have responded as an essentially elastic system prior to failure of the front half. The peak transmitted force was somewhat less than twice the predicted peak applied force, as would be expected for a sufficiently high frequency system. The strain records are not meaningful for comparison purposes after about 200 ms since the front portion of the roof had lifted upward by this time (see section 4.1.15 and Table 5.3).

The laminated 2 x 4 in. wood deck roof (Fig. 5.16) transmitted some force for about 50 ms after shock arrival, although structural failure appears to have been initiated considerably earlier; about 60 per cent of the predicted positive impulse was transmitted prior tc complete structural failure. The behavior of this roof (as read from the strain records) is somewhat similar to that of the wood siding wall panel (Fig. 5.10).

The holorib steel channel roof, Fig. 5.17, seems to have failed initially around 20 to 40 ms after shock arrival; and about half of the predicted positive impulse was transmitted prior to complete structural failure.

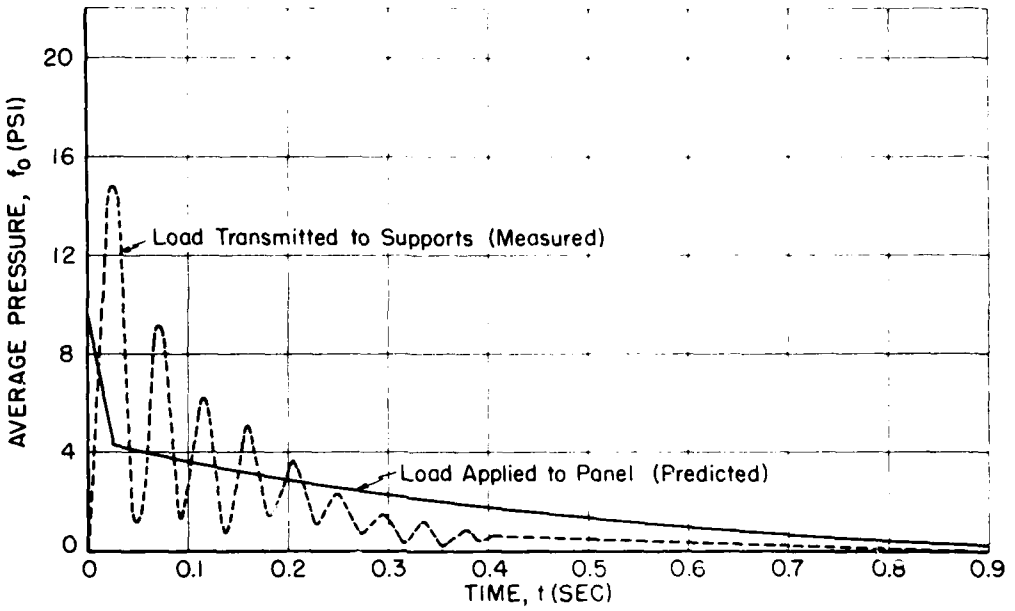

Fig. 5.1 Comparison of Predicted Applied and Measured Transmitted Forces Wall Panel 3.5 ac (8 in. brick)

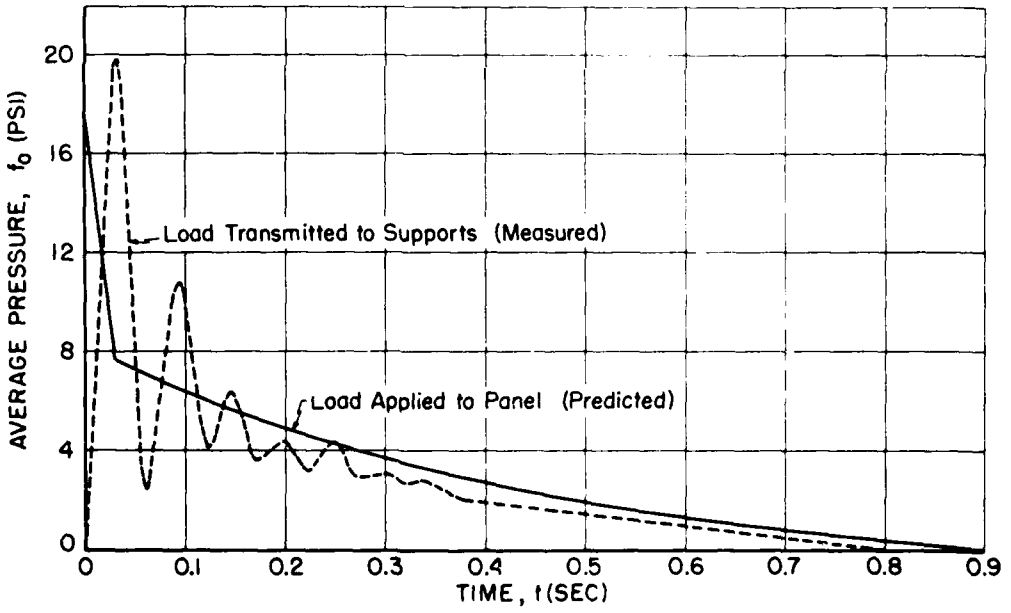

Fig. 5.2 Comparison of Predicted Applied and Measured Transmitted Forces Wall Panel 3.5 bf (8 in. brick)

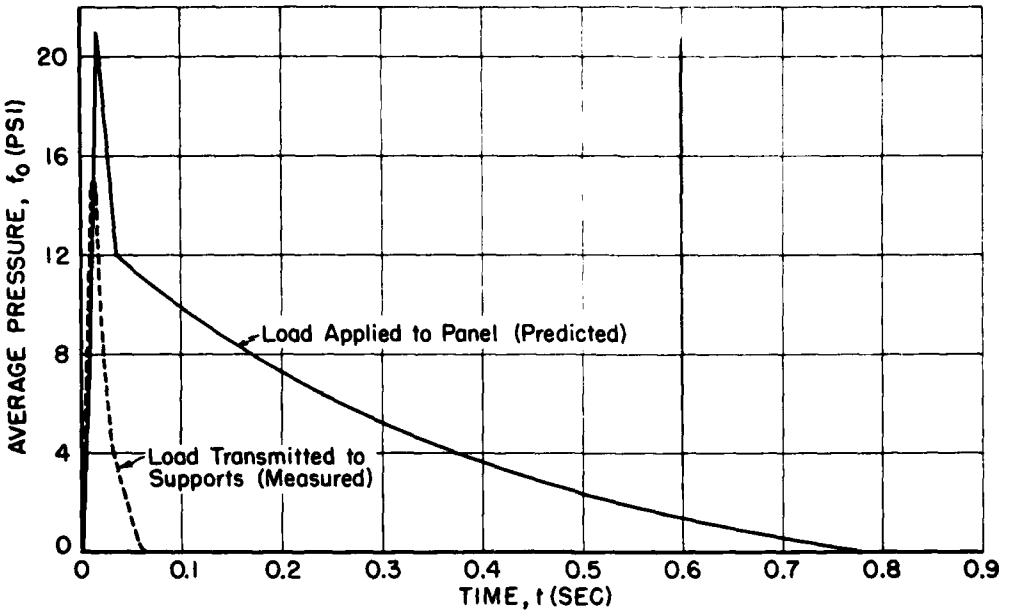

Fig. 5.3 Comparison of Predicted Applied and Measured Transmitted Forces Wall Panel 3.5 ce (8 in. brick)

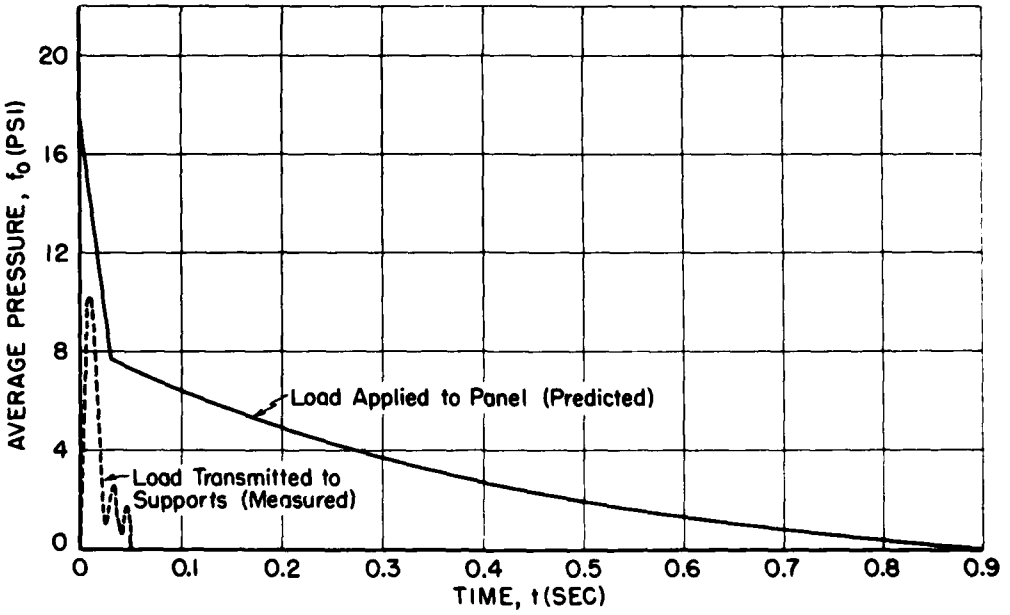

Fig. 5.4 Comparison of Predicted Applied and Measured Transmitted Forces Wall Panel 3.5 bd (8 in. cinder block)

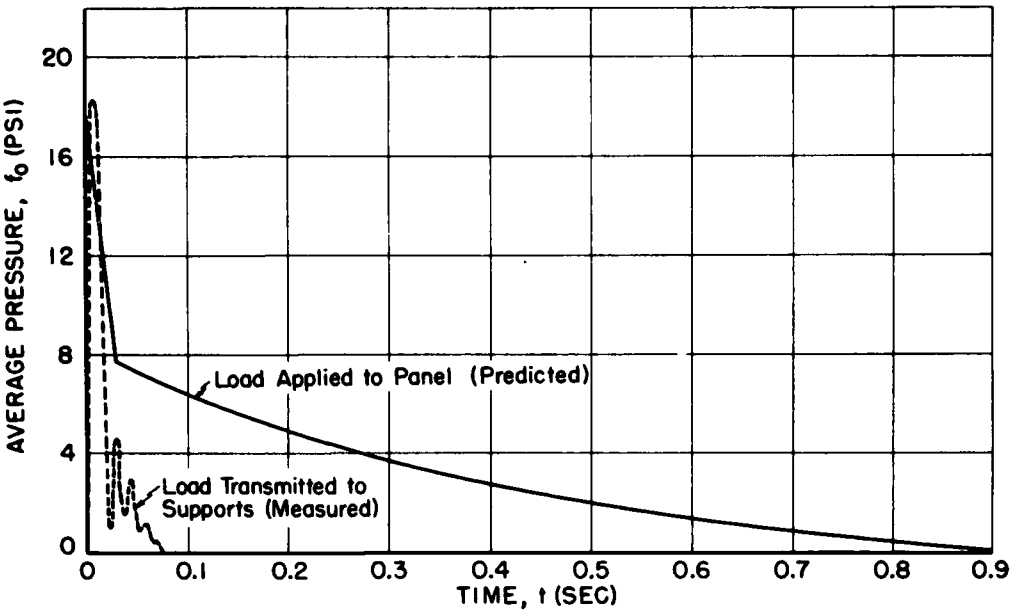

Fig. 5.5 Comparison of Predicted Applied and Measured Transmitted Forces Wall Panel 3.5 be (12 in. cinder block)

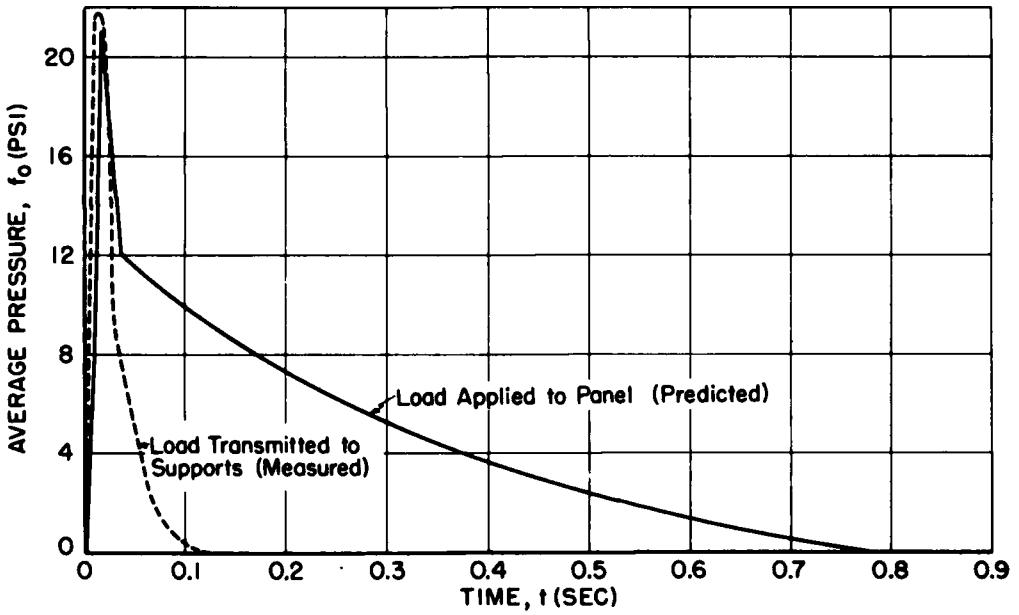

Fig. 5.6 Comparison of Predicted Applied and Measured Transmitted Forces Wall Panel 3.5 cc (8 in. cinder block with 4 in. brick facing)

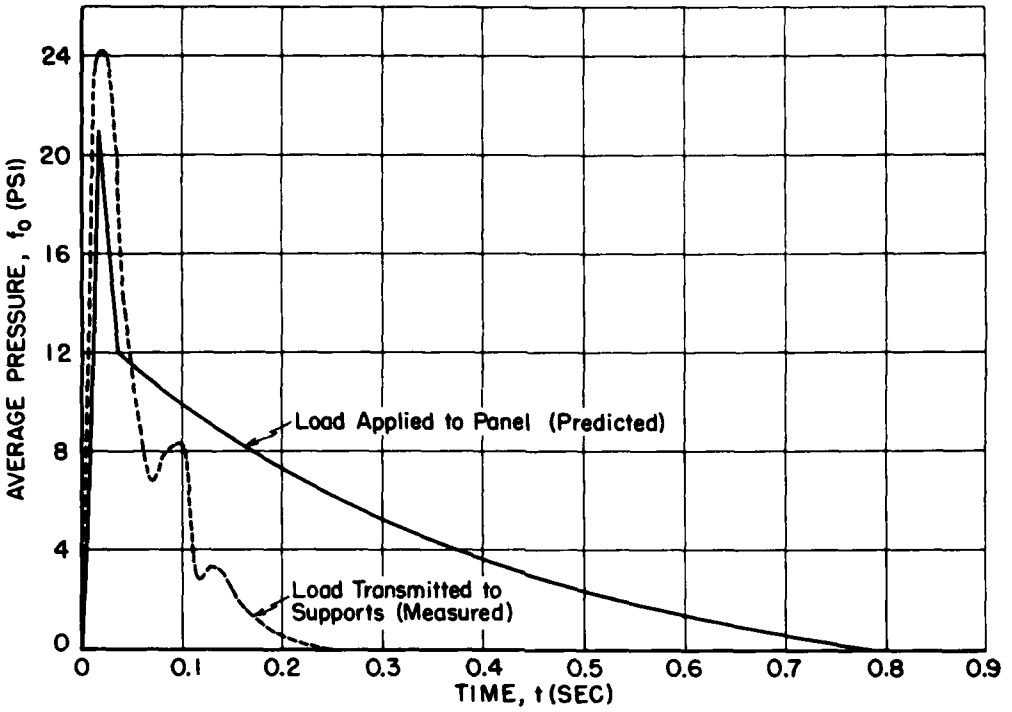

Fig. 5.7 Comparison of Predicted Applied and Measured Transmitted Forces Wall Panel 3.5 cd (6in. reinforced concrete slab, 0.25 per cent steel)

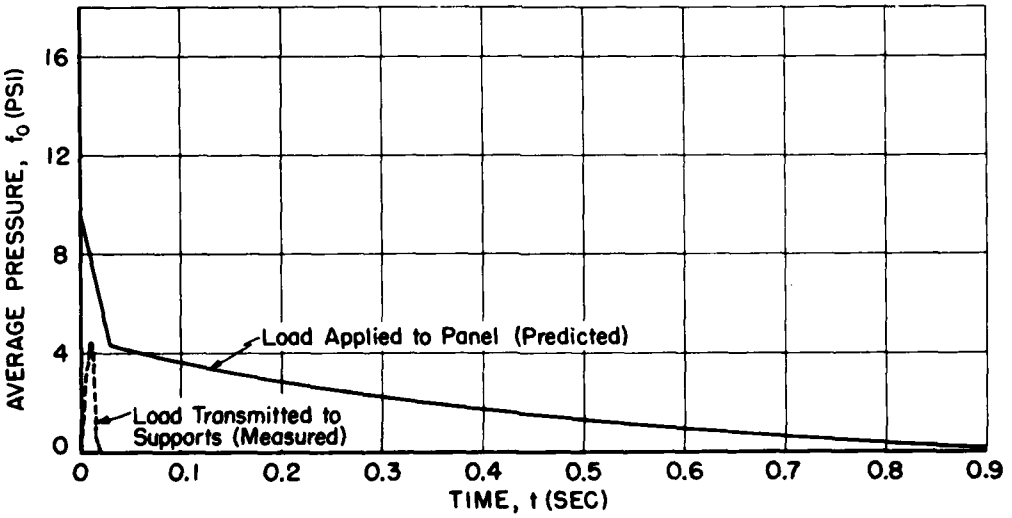

Fig. 5.8 Comparison of Predicted Applied and Measured Transmitted Forces Wall Panel 3.5 ad (Corrugated steel siding over steel girt)

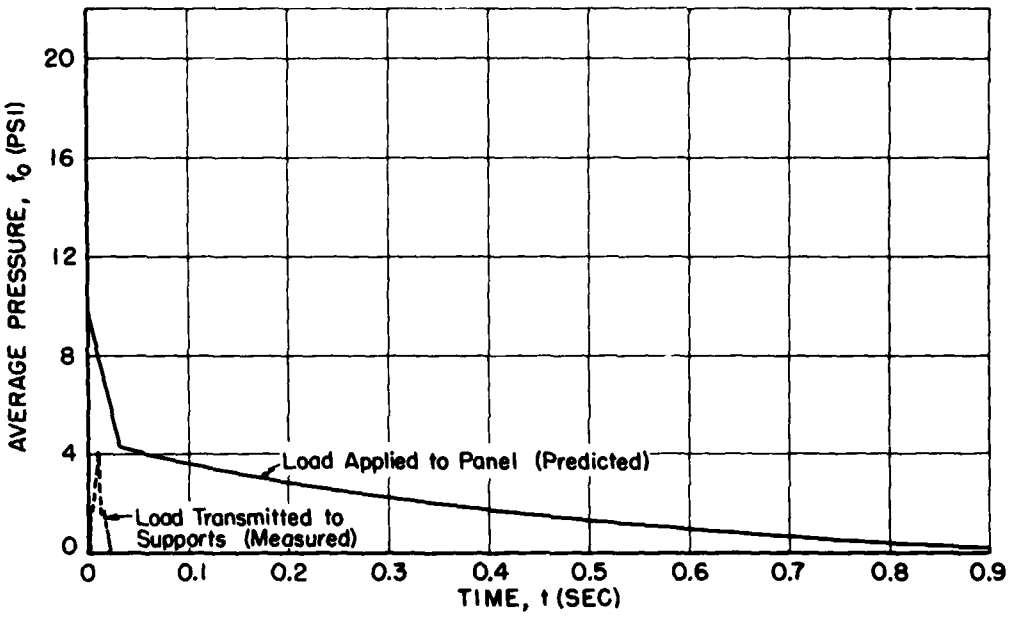

Fig. 5.9 Comparison of Predicted Applied and Measured Transmitted Forces Wall Panel 3.5 ae (Corrugated asbestos board over wood girt)

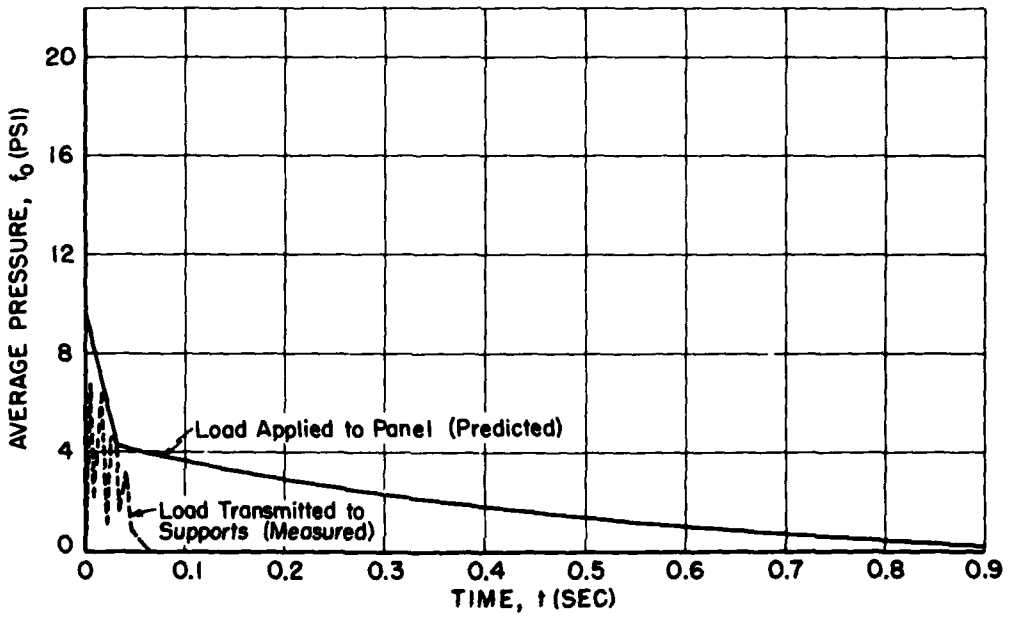

Fig. 5.10 Comparison of Predicted Applied and Measured Transmitted Forces Wall Panel 3.5 af (Wood siding)

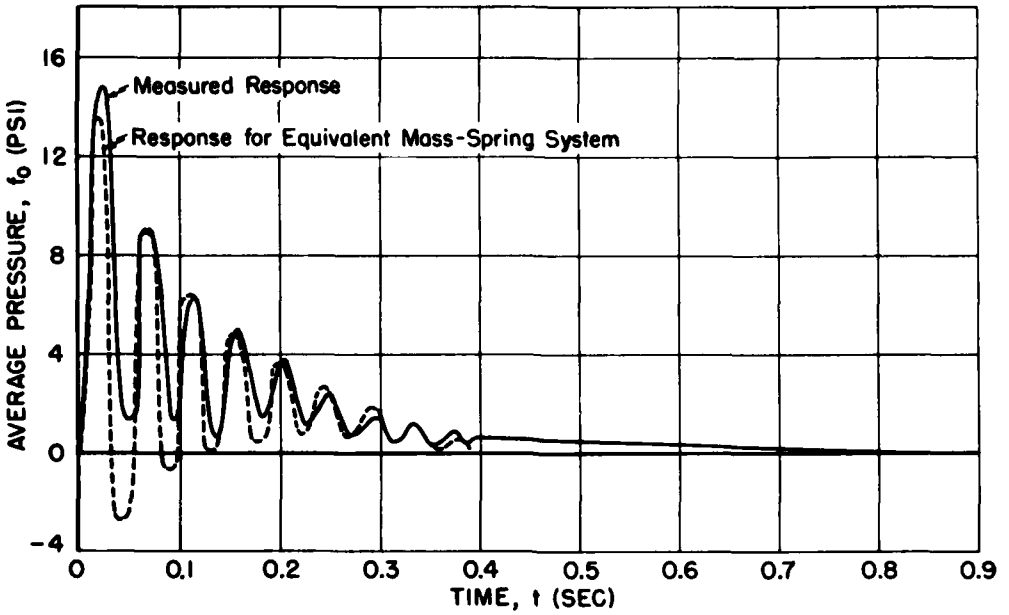

Fig. 5.11 Comparison of Computed and Measured Response
Wall Panel 3.5 ac (8 in. brick)

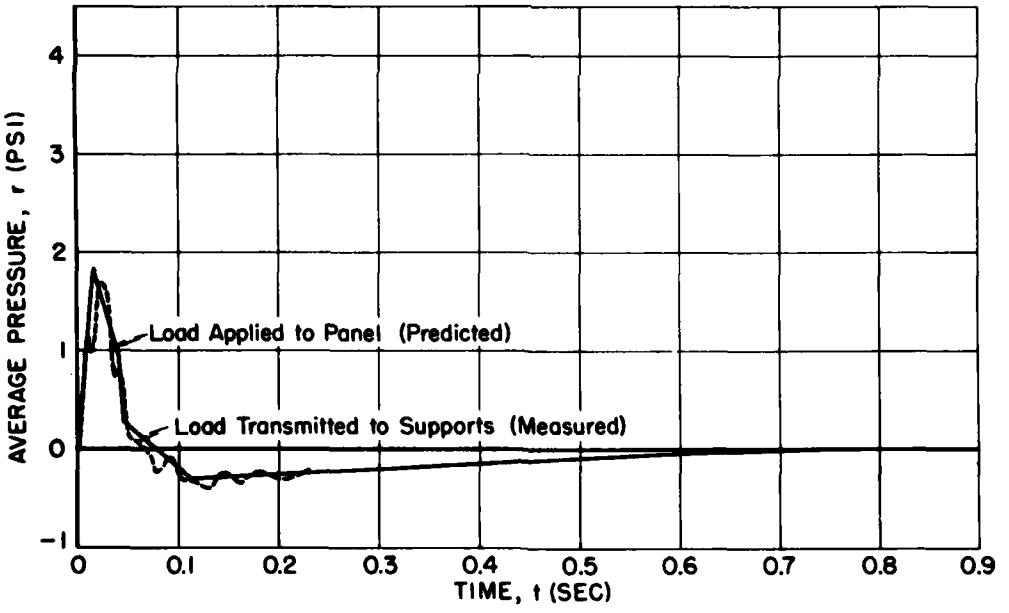

Fig. 5.12 Comparison of Predicted Applied and Measured Transmitted Forces
Roof Panel 3.5 aa (Corrugated asbestos board on wood trusses)

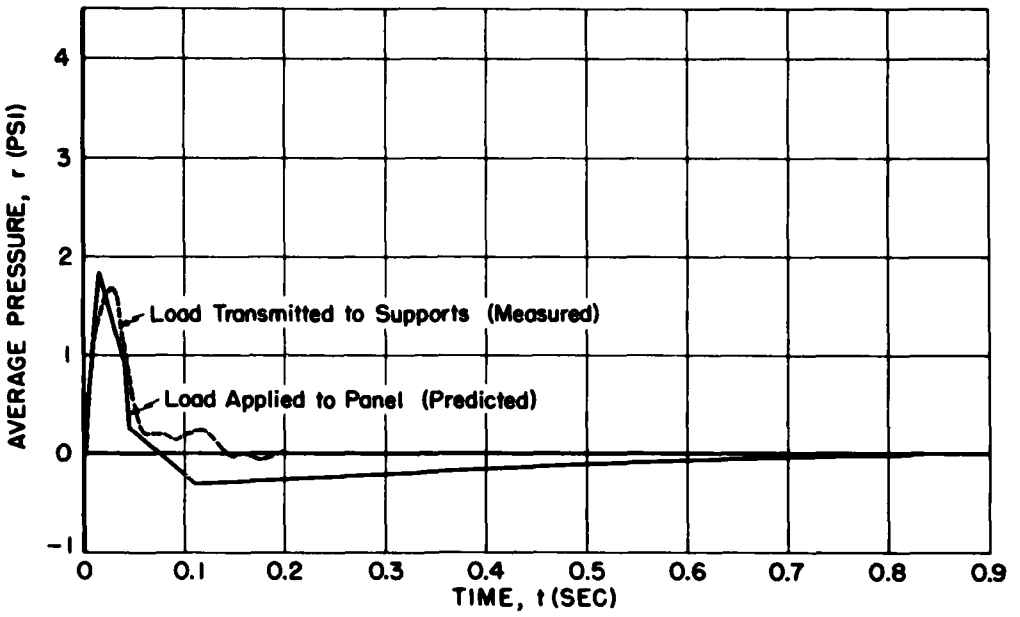

Fig. 5.13 Comparison of Predicted Applied and Measured Transmitted Forces Roof Panel 3.5 ab (Corrugated steel on wood trusses)

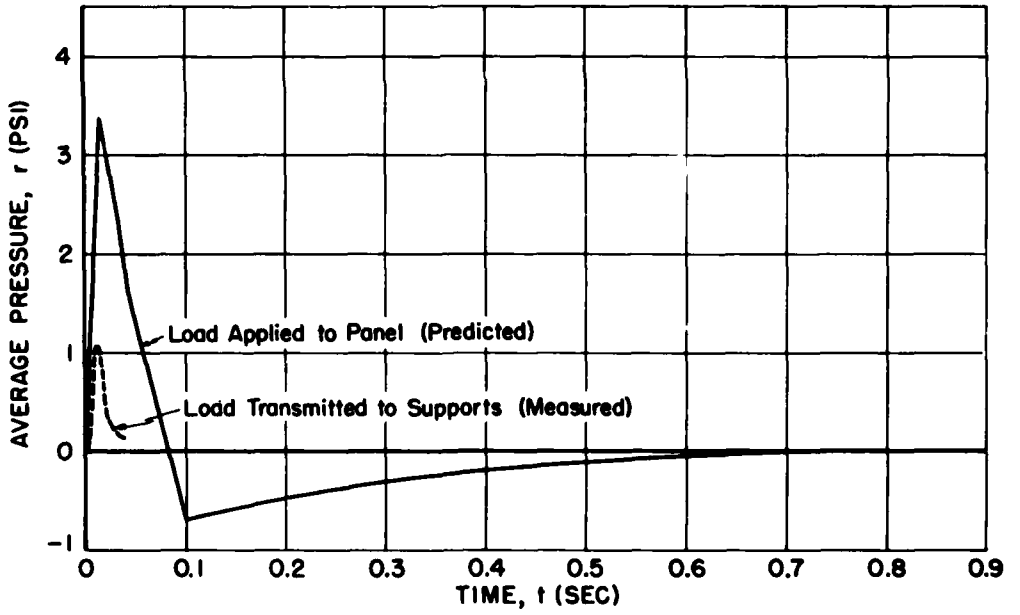

Fig. 5.14 Comparison of Predicted Applied and Measured Transmitted Forces Roof Panel 3.5 ba (Scaled wood bowstring trusses, wood decking)

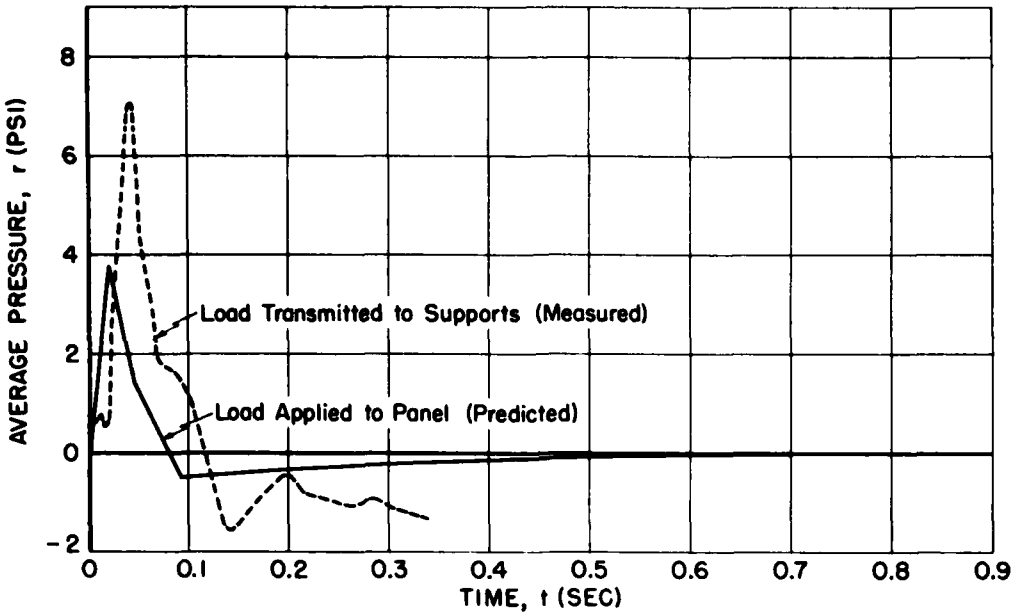

Fig. 5.15 Comparison of Predicted Applied and Measured Transmitted Forces Roof Panel 3.5 bb (3 ½ in. precast concrete channels on steel purlins)

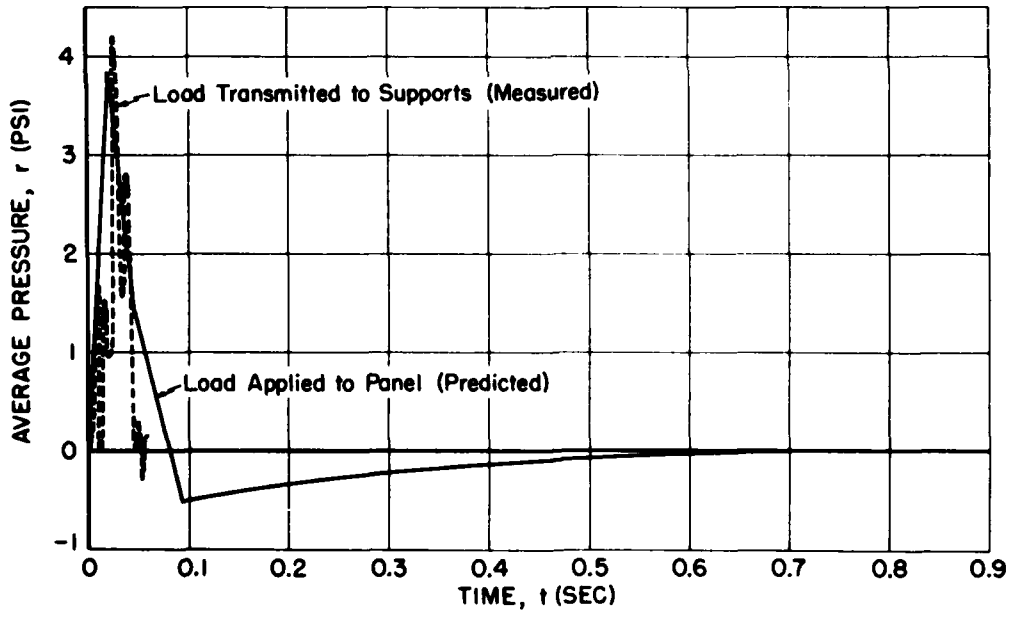

Fig. 5.16 Comparison of Predicted Applied and Measured Transmitted Forces Roof Panel 3.5 bc (Laminated 4 in. wood deck)

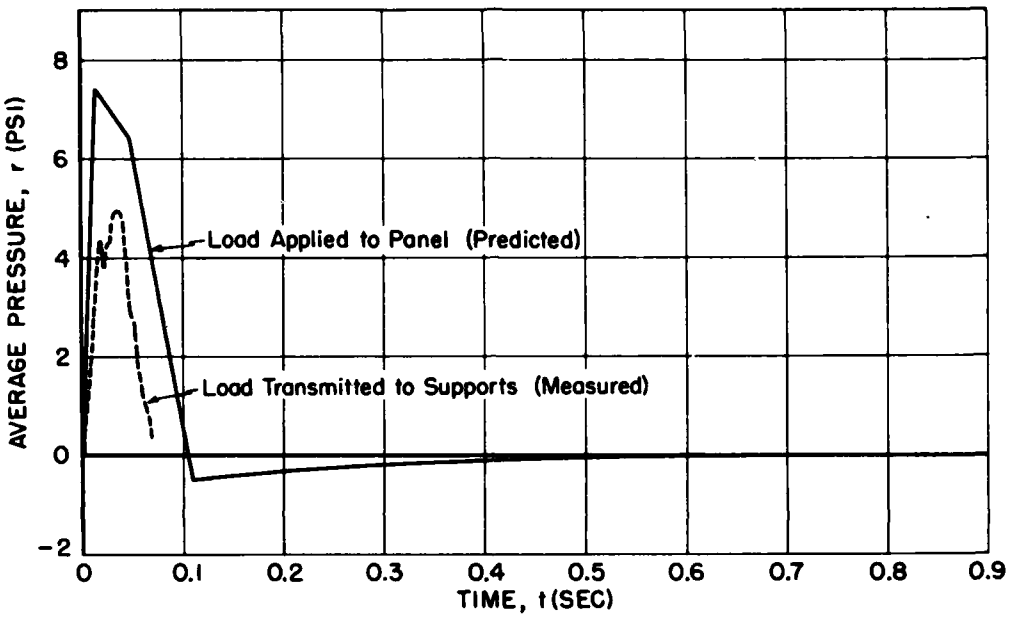

Fig. 5.17 Comparison of Predicted Applied and Measured Transmitted Forces Roof Panel 3.5 cb (Holorib steel channels with gypsum fill)

CHAPTER 6

PREDICTION OF WALL AND ROOF FAILURE

6.1 INTRODUCTION

The test results serve to establish overpressure levels at which failure[1] of wall and roof panels of the types and geometries tested is insured. These overpressure levels are somewhat greater than the "critical overpressure" for each of the panels (i.e., the overpressure at which the panel just fails), and only in the case of the 8 in. brick wall has a lower bound to the critical overpressure been determined. Thus, these results, while of considerable interest in themselves, can have only limited application when one considers the wide variation in panel geometry likely to be encountered in problems of practical interest. This situation was of course realized during the pretest planning phase and it was hoped that in addition to other objectives, the test results would serve as the basis for general failure prediction methods.

Methods for determining critical overpressures for wall and roof panels of the types tested are discussed in this chapter. These methods are basically a "go-no-go" approach in which the aim is to predict only critical overpressures, with no consideration being given to the forces transmitted to the structure prior to failure. Methods for handling the transmitted forces with application to building response analyses are considered in Chapter 7.

It should be made clear at the outset that the methods of approach suggested here are not necessarily "established" by this test, and are therefore not the only ones which might be formulated. However, it is the author's feeling that, in view of the test results, the approach is reasonable enough. It is not expected that one will stray too far from

1/ Failure is used in the sense that the panels are no longer capable of transmitting force to the supporting structure. This implies complete destruction of the wall panels tested, but may indicate only partial destruction of some of the roof construction. Since no strain data were obtained for the reinforced concrete slab roof, there is some doubt as to whether this panel "failed."

reality in applying the suggested methods to situations not radically different from those specifically considered in the test.

6.2 WALLS

6.2.1 Masonry Wall[2/]

Prediction of the behavior of a masonry wall under blast loading is without doubt an extremely complex problem. Considering the degree of uncertainty involved in even defining the physical properties of these materials, it could be argued that one should simply accept the empirical data obtained at face value and let it go at that. While all this is acknowledged, it does not represent the point of view adopted in this report. Accordingly, it may seem to some critical readers that the arguments presented and the tentative conclusions reached are often arbitrary and not fully justified by the test data. It may also appear that too great an effort was expended in forcing the data, limited as it was, into a preconceived theory, and that not enough attempt was made to investigate alternate and possibly more simple approaches.

One cannot effectively argue against criticisms of this nature, and justification for the point of view adopted ultimately rests on the fact that the failure prediction scheme developed yields reasonable results when applied to each of the test panels. In addition, the method has been applied where applicable to the masonry walls included in Project 3.29 (FCDA structure program) with equal success. The general applicability of this method can be determined only as additional data become available.

6.2.1.1 Arching Action Theory of Masonry Wall Behavior

If one were given the task of computing the failure load for the 8 in. brick panels (without prior knowledge of the test results) a logical first approach to the problem might be an assumption of beam (or plate) action. Depending on the choice of end fixity and (primarily) the tensile strength of brick construction, failure pressures of from 1 to 2 psi might be found in this fashion. But one such panel (3.5bf) withstood a peak applied load of 17 psi (an overpressure of about 7 psi) and actually transmitted a peak pressure of almost 20 psi. A simple bending theory also would not explain why the fundamental period of vibration of two presumably identical brick walls which remained intact differed by 30 per cent or more[3/] -- relative behavior that cannot easily be explained in terms of variations in physical properties or workmanship.

2/ Masonry walls are considered to include all walls consisting of separate units set in mortar. Unreinforced concrete might also be considered a masonry material.

3/ As mentioned in section 5.1.3.2, the 3.5ac wall in a 4 psi region had a constant period of about 45 ms/cycle, whereas the 3.5bf wall in a 7 psi region had a period which was initially about 65 ms/cycle and decreased to about 45 ms/cycle by 350 ms after shock arrival.

One might set up some sort of failure theory of panels based on shear action alone, or in combination with bending. If, for example, it is assumed that simple shear failure will occur along a vertical line which is half brick and half mortar and along a mortar bond in the horizontal direction, failure overpressures of from about 4 to 8 psi are found, depending on the shearing strength assumed for the brick and mortar.

While these values are not necessarily unreasonable (they are probably low), this theory would fail to explain why the 8 in. cinder block wall transmitted only about half of the peak force transmitted by the 12 in. cinder block wall, inasmuch as these two walls had very nearly the same cross-sectional area subjected to shear. Nor would a shear theory, which is probably at best applicable only to failure predictions, appear to explain satisfactorily the previously noted effects, or the fact that all of the masonry panels transmitted reactions to the sensor bars located in the plane of the panel (A-gages, Fig. 2.7) which were of the same order of magnitude as the normal reactions. While a detailed investigation of bending or shear behavior of masonry walls has not been undertaken, even this cursory examination would tend to indicate that masonry wall behavior might better be explained in terms of some other theory.

Each of the effects noted above can be explained by (or, possibly better, do not stand in contradiction to) a so-called theory of arching action of masonry walls first proposed in connection with the ARF GREENHOUSE Reports, WT-87. This theory describes the response of the masonry walls tested in the following manner:

Masonry material can withstand only very small tensile stresses and, as transverse loads are applied, cracks develop first at the supporting edges. The maximum bending moment is then located at the center of the span where cracking next occurs. If it were not for the supporting structure which restrains the edges, the panel would now fall apart. What is assumed to happen, however, is that portions of the panel begin to rotate about an edge as a rigid body under the action of the transverse (blast) loads. This motion is resisted by a thrust force couple set up as a result of crushing of the material at the ends and center of the span; hence, the reference to arching action. (This action could also be likened to a prestressed member where the amount of prestressing is proportional to the deflection.) The motion continues until the wall either comes to rest or fails completely.

The test provides several items of direct evidence that tend to support this mode of response. Chief among these is the fact that substantial thrust forces were indeed measured in the plane of the panel. Further, the large crack which occurred at the center of the rear side of the 3.5bf wall (Fig. 4.6) and edges of the front side of the 3.5ce wall, as well as the characteristic crushing failure of the edge blocks of all the masonry walls which failed (see Figs. 4.13 and 4.15) is consistent with this type of response.

While the author feels quite strongly that the test results point definitely to an arching mode of failure for masonry walls, there is no great conviction that such behavior can be characterized quantitatively in a simple or straightforward fashion at this time -- if at all.

However, the theory to be described, while rather grossly idealizing this action, seems to account reasonably well for the test results and also provides a relatively simple means of computing critical overpressures.

The original GREENHOUSE analysis assumed that the tension cracks would occur almost immediately upon loading, and that only the arching action need be considered. While this seems reasonable and has been maintained in the present analysis, other assumptions concerning the kinematics of the motion and the stress-strain relationship for masonry materials have been modified. The complete development of the present theory is contained in Appendix A of this report. The analysis is carried out for a beam (i.e., a panel restrained on two opposite edges only) and then an equivalent length of beam for a panel restrained on all four sides is derived in an approximate manner.

The resisting moment due to crushing of the edge material is shown in Appendix A to be nearly linear for sufficiently small displacements. Within this range the theory would therefore predict a linear response of the wall. In order to yield the measured period for the 3.5ac panel (i.e., 45 ms/cycle) a Young's Modulus (E) of about 700 ksi would be required which is possible but somewhat low for brick.4/ A value of about E = 500 ksi is required to yield this period if the panel is assumed to respond as a simply-supported elastic plate.

As the displacement increases, the resistance function becomes markedly nonlinear and eventually becomes negative (Fig. A.9), at which time the panel is presumed to have failed. There is, however, a range of displacements over which the panel responds with a frequency which increases with increasing time, the initial frequency being a function of the intensity of the applied load. But this is precisely the behavior observed for the brick walls which remained in place.

The equation of motion developed in Appendix A was solved numerically for brick walls based on the predicted blast loads in the 4.2 and 7.1 psi regions. The results of these computations are shown in Fig. 6.1 where the initial period of the motion is plotted against crushing strength. It is seen that at a crushing strength of about 1100 psi, the analysis indicates periods which compare favorably with the measured values in these two pressure regions. The numerical results of Fig. 6.1, of course, are not to be taken at face value, since none of the wall parameters are known with any certainty; perhaps with other parameter values the agreement would be better -- or worse. Rather, the point to be made is that the present theory does embody certain nonlinear features which are consistent with the experimental results.

4/ This value is not to be taken at face value since it depends on an effective panel length. Since the period varies inversely as the square root of E and inversely as the square of the effective panel length (Eq. A.11), the former can be increased substantially and still maintain the 45 ms/cycle period without requiring an unrealistic change in the effective panel length.

The present theory does not account for damping of the wall and is not well suited for the computation of transmitted forces. Thus no purpose is served in attempting a direct comparison between the measured transmitted forces and predictions based on this theory. However, an interesting check on the theory can be made on the basis of some static tests conducted on 8 in. brick beams at the Massachusetts Institute of Technology (Behavior of Wall Panels Under Static and Dynamic Loads, AFSWP113). Fixed-ended beams of 3, 6, 8, and 12 ft span were loaded at the third-points until failure occurred. The results of these tests are shown in Figs. 6.3 and 6.4 (reproduced from Figs. 4.4 and 4.5 of the MIT report) for the 8 and 12 ft beams where the midspan deflection is plotted against an equivalent uniformly distributed load.

The arching analysis presented in Appendix A for dynamic loads can easily be reduced to the static case by omitting the acceleration term ($\ddot{u}$) and by considering the applied load (F(t)) to be constant in Eq. A.6. The resulting algebraic equation was solved using average values of the crushing strength of the mortar (s_y) and the beam dimensions given in the MIT report. The comparison of these results with the experimental data is shown in Figs. 6.3 and 6.4; pertinent data is given in the figures.

The initial portion of the experimental curves is apparently indicative of elastic behavior of the beams, which is not considered in the arching theory. This effect is much less notable for the shorter spans tested, and during this initial range agreement with the computed curve is considerably better. For larger displacements the computed curves are seen to be in very satisfactory agreement, at least up to the peak load. The rapid dropoff in load for several beams after the peak is reached is not understood; possibly the load could not be applied rapidly enough during the latter stages of the test.

6.2.1.2 Computation of Critical Overpressure

The arching action analysis permits the determination of the maximum impulsive loading that a wall can sustain and still remain intact. This so-called critical impulse, i_c, is given by,

$$i_c = \frac{Ak}{2d^2} \left[\rho d\, s_y\, e_y \frac{A(R)}{R} \right]^{1/2} \quad \text{(psi-sec)} \qquad (6.1)$$

d = half depth of wall cross section

A = area of cross section per unit width ($in^2/in.$)

k = radius of gyration of cross-sectional area with respect to the neutral axis (in.)

ρ = mass density of wall material per unit length of span, per unit width (lb $sec^2/in^2/in.$)

s_y = crushing strength of masonry material or mortar, whichever is less (psi)

e_y = strain corresponding to crushing strength (in/in.)

$$R = \frac{e_y}{16}(L_e/d)^2, \text{ dimensionless parameter} \qquad (6.2)$$

L_e = span of equivalent one-way panel obtained from Fig. 6.2 in terms of the ratio of true panel dimensions L_1/L_2 (in.)

$\frac{A(R)}{R}$ = dimensionless parameter obtained from Fig. 6.5..

The critical impulse is derived in Appendix A for a beam of unit width and solid cross section restrained on two opposite edges only. The analysis is then extended in an approximate manner to include panels restrained on all four sides, and for masonry units of other than solid cross section.

The method of determining equivalent one-way panel length, Le, is somewhat arbitrary, but in view of the measured distribution of reactions around the sides of the test panels (the distribution was similar to that for simply-supported plates under a uniformly distributed static load) it seems to be a reasonable enough approach. However, no realistic judgement of the error introduced by use of this equivalent length can be made.

The modification of the critical impulse to include masonry units of arbitrary cross section is even more uncertain. The cross-sectional area influences the resistance function A(R). While this function could conceivably be evaluated for each individual type of masonry unit, as was done for the solid cross section, the additional complexity introduced is not felt to be justified at this time in view of the rather uncertain nature of the entire arching theory. As discussed later, the present approach appears to be in reasonable agreement with the test results.

The critical impulse can be determined from knowledge of the physical parameters of the wall panel alone. The physical constants e_y and s_y (which together determine Young's Modulus, E) for masonry walls are not well defined. A value of $e_y = 0.001$ used for Portland cement seems to be generally acceptable. Values of s_y range anywhere from 500 to 3500 psi (E ranging from less than 500 to about 4000 ksi). If specific values are not available it is recommended that $s_y = 1000$ psi be used. This is convenient since $e_y s_y = 1$ psi for these values. In fact, it might be better to use this value independently of individual values of e_y and s_y.

The critical impulse is related to the blast loading in the following approximate manner. From the discussion of wall behavior in Chapter 5, it seems reasonable to assume that a masonry panel will always fail (at least initially) in a time of the order of the clearing time for the panel and, hence, that the critical impulse can be associated in some way with the diffraction impulse of the applied load. The critical impulse for the 8 in. brick wall is found from Eq. 6.1 to be $i_c = 0.46$ psi-sec, based on values of $s_y = 3000$ psi (construction specifications) and $e_y = 0.001$ in/in. (i.e., E = 3000 ksi). A diffraction impulse of this value is found to correspond to an overpressure

of about 9.5 psi based on the test conditions. If the yield stress is taken to be 2000 psi, i_c is reduced to 0.38 psi-sec, which corresponds to the diffraction impulse associated with an overpressure of about 8 psi.

Since one of the brick walls remained intact at 7 psi, and another was destroyed at 12 psi, a critical pressure ranging from about 8 to 9.5 psi is not at all unreasonable. Therefore, it will be assumed that at the critical failure pressure for masonry walls, the critical impulse, i_c from Eq. 6.1, is equal to the diffraction impulse associated with this overpressure.

For front walls[5] in the Mach reflection region, the diffraction impulse is given approximately by

$$i_s = \frac{3\bar{h}}{2U} (p_r + p_\sigma + p_d), \text{ psi-sec} \tag{6.3}$$

where h is the clearing distance for the panel (ft); U is the velocity of the shock front (ft/sec) ($3\bar{h}/U$ is the clearing time for the panel); p_r is the peak reflected pressure on the wall; and p_σ and p_d are the initial values of the side-on and drag pressures, respectively (p_r and p_d are given in terms of p_σ in Appendix B). Equation 6.3 is based on a drag coefficient of 1,[6] and the approximation that neither the drag nor the side-on pressures at the time $3h/U$ differ appreciably from their initial values. A particularly simple expression for i_s, i.e.,

$$\frac{i_s}{\bar{h}} = \frac{p_\sigma}{250}, \text{ psi-sec/ft} \tag{6.4}$$

can be shown to be a satisfactory approximation to Eq. 6.3 for all reasonable pressures within the Mach reflection region (e.g., within 2 per cent for pressures up to 50 psi). Therefore, the computation of critical overpressure is considerably simplified by using the relation

$$\frac{i_c}{\bar{h}} = \frac{i_s}{\bar{h}} = \frac{p_\sigma}{250}, \text{ psi-sec/ft.} \tag{6.5}$$

Equation 6.5 is based on an ambient atmospheric pressure of $P_o = 14.7$ psi (under test conditions $P_o = 13.2$ psi) and is valid only for the region of Mach reflections. An expression for the diffraction

---

5/ The case of a wall shielded directly from the blast (e.g., a rear wall) is discussed in section 6.2.4.

6/ The drag coefficient for the front of a wall is not well defined for transient flow; some data indicate a value as high as 2. However, at the relatively low pressures of interest, this uncertainty will probably not be of consequence.

impulse on a front wall in the regular reflection region could also be determined, but the functional relationship with overpressure is considerably more complicated. In addition, the angle of shock incidence enters as still another parameter. For any particular case, this impulse can be determined by the methods of Appendix B.

An additional restriction to the use of Eq. 6.5 should be noted. The association of i_c with i_s was based on the observation that the walls failed (at least initially) in a time of the order of the clearing time, $3\bar{h}/U$. In the event that a wall panel has a much larger clearing distance than under the test conditions (e.g., if the panel under consideration were in the center of much larger area), a more realistic approach might be to equate i_c to the impulse of the predicted applied force up to the first 20 or 30 ms only.

As an aid in applying the present method to panel geometries not specifically considered in the test, the critical impulse, i_c, is plotted against the equivalent panel length, L_e, in Fig. 6.6 for the various types of masonry construction tested. A plot of L_e 1/ as a function of the true panel dimensions L_1 and L_2 is given in Fig. 6.2. The dependence of i_c on the yield stress and strain of the masonry material is indicated by the band for the 8 in. brick wall shown in Fig. 6.6; nominal values of i_c based on s_y = 1000 psi and E = 1000 ksi (and average block dimensions) are shown for the other types of walls. For any given values of these parameters, the proper value of i_c can be computed from Eq. 6.1.

The calculation of the critical pressure will be illustrated for the 8 in. cinder block wall, 3.5bd. This wall measured 13.75 ft by 8.75 ft, so that L_1 = 13.75 ft and L_2 = 8.75 ft. The equivalent panel length, L_e, is then found from Fig. 6.2 to be about 8 ft. For this value of L_e, the critical impulse, is found to be i_c = 0.12 psi-sec from Fig. 6.6. The clearing length, h, (see Appendix B) is taken to be the over-all height of the test cell, which was about 12 ft. Thus, $i_c/\bar{h}$ = 0.12/12 = 0.01 psi-sec/ft, and the corresponding critical pressure is found to be 2.5 psi from Eq. 6.5.

The effective dimensions of the test panels (i.e., $L_e \cong 8$ ft, and $\bar{h} \cong 12$ ft) are smaller than generally found in most conventional construction. Therefore, the critical overpressures for the test panels probably represent maximum failure pressures for such construction. Based on the results of Fig. 6.6, walls of both solid 8 in. brick and 8 in. cinder block with 4 in. brick facing are expected to be destroyed at overpressures of about 9 psi or less; conventional 12 in. cinder block construction should fail at about 4 psi or less, and 8 in. cinder block at about 3 psi or less. In view of the wide range of panel sizes which might be encountered, it is not practical to assign a lower bound to these failure pressures.

1/ When the panel is supported on only two opposite edges, L_e is equal to the panel length between supports.

The overpressure values quoted above refer to the region of Mach reflection and it is understood that whenever overpressure damage criteria are employed, the duration of the blast wave is not shorter than, say, about 200 ms. Some difference is to be expected if the same overpressure level occurs in the regular reflection region since both the peak force and diffraction impulse will be less. For example, the predicted diffraction impulse for the 3.5c walls, at 12 psi in the regular reflection region, corresponds to only a 10 psi shock in the Mach region. However it is expected that in most instances the failure pressures, being relatively low, will occur in the Mach region. Otherwise the critical impulse, i_c, can be related to the diffraction impulse of the loading in the regular reflection region according to the methods of Appendix B.

6.2.2 Lightweight Covering

The test results do not permit the detailed treatment of failure prediction for lightweight covering afforded the masonry construction. In the present case it is probably best to accept the empirical data at face value. Dynamic tests on corrugated asbestos board and corrugated sheet steel have been conducted at Massachusetts Institute of Technology (AFSWP113). It was found that for panels of both materials having spans used in normal construction, failure occurred at peak loads slightly less than 2 psi (or about 1 psi overpressure). The test panels were situated in a 4 psi region, where complete destruction occurred. Therefore the above values, while possibly low, are not necessarily unreasonable even under field conditions. It can be tentatively concluded, therefore, that walls of corrugated asbestos board and corrugated sheet steel of the types and spans met with in practice will most likely be destroyed at overpressures of from 1 to 2 psi, and will definitely be destroyed at overpressures of about 4 psi.

The wood siding panel (3.5af) is representative of most construction of this type and it can probably be concluded, therefore, that destruction of these walls is assured for 4 psi. In order to determine the critical pressure for this type of wall (the test panel would no doubt have failed at a lesser pressure) it would be necessary to consider the response of the supporting members (e.g., studding) since wood siding, as it is generally supported can withstand a higher loading than the studs. The response of the studs, and after their failure, the subsequent behavior of the unsupported section of the wall, can be estimated in the following simplified manner.

A good deal of work has been done by the ARF and others on the response of simple elastic-plastic[8] systems to forcing functions of an analytical nature which approximate the blast pulse. In particular,

8/ An elastic-plastic system refers to a single-degree-of-freedom system whose resistance to motion increases linearly with displacement to a limiting value, and then remains constant with increasing displacement.

Brooks and Newmark (Development of Procedures for Rapid Computation of Dynamic Structural Response) have deduced an empirical relationship for the maximum displacement of an elastic-plastic system subjected to an initially peaked triangular shaped pulse. This relationship is given in Eq. 6.6,

$$\frac{F}{R} = \frac{I}{\pi t_1}(2\mu - 1)^{1/2} + \frac{2\mu - 1}{2\mu}\,\frac{1}{1 + 0.7\,\frac{T}{t_1}} \qquad (6.6)$$

where

F = peak force of triangular pulse

R = maximum static (yield) resistance

T = natural period of vibration of system, sec/cycle

t_1 = duration of triangular pulse, sec

$\mu = x_m/x_y$ = ratio of maximum displacement, x_m, to elastic yield displacement, x_y. (The yield displacement is the displacement associated with the maximum resistance R.)

Equation 6.6 can be applied to the present case as follows: Consider first the response of the studs. The studs were standard 2 x 4 in. lumber, 8 ft 9 in. long and spaced 16 in. on center (see Fig. 4.10). Assuming these members to act as simply-supported beams receiving load over a 16 in. width, a static load of about 0.6 psi (86 psf) is found to produce a maximum stress of 3600 psi (an average value of yield stress for the type of lumber tested) in the stud. This seems to be a reasonable static failure load and the maximum static resistance of the panel is taken to be $R = 0.6$ psi. Since wood is not too ductile a material, the studs are estimated to fail at a maximum displacement of about five elastic yield displacements, or $\mu = 5$.

The natural period of vibration of the individual studs is computed to be about 44 ms/cycle. The wood siding and plaster board attached to the studs prevent precise determination of the true period; the strain records (Fig. 5.10) show the wall as a whole to be responding in a period of about 15 ms/cycle. However, in the present case the value of F from Eq. 6.6 is not too sensitive to the value of T chosen within the range indicated here. Accordingly, T is taken to be 44 ms/cycle. If the triangular pulse on which Eq. 6.6 is based is taken to represent the diffraction portion of the applied load (a reasonable assumption since the panel failed during the diffraction loading), the duration t_1 is estimated from Fig. 5.10 to be about 60 ms.

Substituting these values in Eq. 6.6, one finds $F/R = 1.3$, or $F = 0.78$ psi. (For $T = 15$ ms/cycle, $F = 0.62$ psi; for $T = 44$ ms/cycle and $\mu = 10$, $F = 0.98$ psi.) Since F represents the peak reflected pressure on the panel, the overpressure causing failure ranges between

about 0.3 and 0.5 psi; in any event, failure of some of the studs is expected at overpressures of 1 psi or less.

The subsequent behavior of the wood siding is uncertain since it is not known over what span the siding is now supported (the resistance of the plaster board can be neglected). For example, a nominal 3/4 in. board supported over 16 in. is expected to fail at about 4 psi overpressure, while the same board spanning the entire width of the test cell would probably fail at about 0.1 psi. While it would be difficult to determine the most probable value between these two extremes, it does seem reasonable to conclude that this type of panel is not substantially stronger than the other lightweight cover tested, and that failure of all panels of this type is to be expected at from 1 to 2 psi overpressure.

6.2.3 Reinforced Concrete Walls

Inasmuch as only one reinforced concrete wall panel was included among the test structures, it is not to be expected that a general failure prediction scheme can be deduced for this type of construction from the data obtained. It is clear, however, that any such scheme would be substantially different from the methods of analysis considered previously in this report.

While concrete itself could be classified as a masonry material, the presence of reinforcing steel would seem to invalidate the arching action theory proposed for unreinforced masonry. Since the steel can develop appreciable tensile stresses, an adequate theory would have to account for bending and shear in addition to the arching action. The situation is further complicated in that the response of the panel depends on the degree of end-fixity present. Under the test conditions the steel bars extended into the supporting channels but were not welded or otherwise fastened to these members. As can be seen from Fig. 4.17, little if any end restraint developed since the steel pulled completely free of the channels. Had monolithic construction been employed, however, both the mode of failure and the load causing failure would have differed considerably, due to the increased resistance provided by continuity of the reinforcing steel.

Thus it would seem that the application of the test results must be restricted at the outset to reinforced concrete panels having essentially zero end restraint, i.e., analogous to simply-supported panels.

If the panel is assumed to develop only bending resistance, the method of the previous section can be employed. For a reasonable range of the parameters T, t_1, and μ, the value of F/R from Eq. 6.6 is found to vary between about 1 and 2. If the maximum resistance, R, is taken to be the static loading at which a plastic limiting moment is reached at the center of the span, the peak loading causing failure, F, varies between 4 and 8 psi, the critical overpressure being between about 2 to 4 psi within the Mach region, and somewhat higher in the regular reflection region. (The finite rise time of the loading in the regular reflection region complicates the situation additionally since Eq. 6.6 is based on an initially peaked triangular pulse.)

While the test results do not rule out the possibility that this panel would have failed at pressures of around 4 psi or less, these values seem somewhat low in view of the large percentage of load transmitted by the panel prior to failure at 12 psi. The fact that the reinforced brick walls withstood a 4 psi overpressure loading also indicates that these are low. In fact, if the test panel had had no steel reinforcing, failure according to the arching theory would be expected at about 5 psi.

The arching theory does not account for the increased resistance of the steel, and hence is not applicable in the present case. An extension of this theory to account for both bending and arching action, while apparently feasible, would be necessarily involved and well beyond the scope of this report. Even if a critical impulse could be determined in this way, it is questionable whether this impulse could be related to overpressures in as simple a fashion as was possible for the masonry walls since the concrete panel remained in place for times well beyond the duration of the diffraction loading period. In an attempt to account for the added resistance of the steel, the full depth of the section might be considered in computing the quantity R in Eq. 6.2. In the present case this leads to a predicted failure load of about 11 psi; this approach, however, while yielding what might be a reasonable result, is arbitrary and cannot be defended on a rational basis.

6.2.4 Rear Walls

The discussion so far has dealt with failure prediction for a front wall (i.e., a wall struck head-on by the blast (orientations other than head-on are beyond the scope of this report). In the computation of building response problems it is necessary to know the net force on the structure; hence, failure prediction methods are desired for rear walls (and in some cases side walls) also.

In a structure with no open area in the front wall, the loadings on the back side of the rear wall builds up rather slowly (actually in about $5\bar{h}/U$ time units or less after the shock traverses the length of the building) to about peak free stream pressure. Hence the peak load on the rear wall is substantially less than the peak load on the front wall, at least if the front wall remains intact. Thus, in the event the front wall is not destroyed, the rear wall of the same type will most certainly be unaffected.

At pressures capable of destroying the front wall, the response of the rear wall is rather uncertain. As discussed in section 5.1.1.2, the front wall debris may attenuate the incoming shock to a marked degree. Thus, at loads just causing failure on the front wall, the interior shock (or compression wave) may be too weak to destroy the rear walls. In the event that the debris does not affect the interior shock significantly, the presence of interior equipment of other protuberances may accomplish the same effect.

The effects of wall debris and interior equipment considerably complicate the determination of the incident loading on the rear wall, and hence the prediction of the critical failure pressure. While the

test results are not related directly to this problem, it would not seem unreasonable at apply the previous methods if the incident loading were known. From this point of view one could place bounds on the failure pressures desired, the minimum pressure causing failure of the rear wall being the critical pressure for the front wall, and the maximum failure pressure being determined by means of the loading on the back side of the rear wall only. Since the determination of the upper bound pressure in this fashion does not account for the presence of the interior wave (the front wall surely having failed at this load), the mode of response might not be as implied here (i.e., the rear wall would be blown inward due to the back side loading alone). However, within the Mach region, for example, the upper bound pressure will be greater than twice the critical overpressure for the front wall, and hence, this approach would seem to offer a conservative upper bound. This discussion is, of course, not intended as a complete study of rear wall behavior, and much additional information is required before such a study could be expanded.

6.3 ROOFS

6.3.1 INTRODUCTION

The discussion of failure prediction methods for roofs of the types tested is again limited to the determination of critical overpressure levels. Now while it is clearly desirable to establish critical pressures which are applicable to a given type of roof construction (as was done for the walls), it is neither obvious nor at all certain that this can be legitimately done. First, there is always the uncertainty in discounting the influence of the shape and duration of the blast wave on the response of the structure. But again, as for the walls, the relatively early failure times observed for the roofs, together with the general lack of knowledge concerning roof response, seem to justify this approach, at least for the present.

The major uncertainty in the widespread application of the test results stems from the fact that both local and average roof loads depend on the building and roof geometry as well as on the blast wave itself. In other words, a given roof covering will experience different loads for the same blast wave, depending on such parameters as the percentage of front and rear wall opening, length of the building (in the direction of flow), and pitch and orientation of the roof relative to the blast. Thus, even if it is reasonable to establish critical overpressures for the test roofs, the question remains as to whether these values are applicable to other roofs of similar construction where the building geometry is radically different than under test conditions. Such extrapolation can, it seems, be justified only on the basis of application of these results to the building response problem where all that is required is some estimate of the forces transmitted by the roof to the frame and, possibly, the subsequent blast loading on the building once roof failure occurs.

The most significant building parameter affecting the net average roof load appears to be the percentage of open wall area. All other

things being equal, the net roof load is a maximum when there are no openings in the wall and it is generally taken to be zero when the wall opening is effectively complete.

Buildings with a smaller area of wall openings than the test structures (i.e., less than about 17 per cent), but otherwise essentially similar, will sustain higher roof loads than in the test and failure of these roofs seems assured at critical overpressures deduced from the test results. In the event that wall openings in such buildings are substantially greater than under test conditions, the net roof loads are expected to be less and, hence, the forces transmitted by the roofs may not significantly influence the response of the building even in the event that the roofs do not fail at these critical overpressures.

Following this point of view the problem can be further simplified. It may be that roof response need be investigated only when it appears that the walls of the building under consideration remain intact. Otherwise failure of the walls will result in rapid equalization of the roof loading (and, to a certain extent, vice versa) so that the force transmitted by the roof becomes negligibly small -- or at least this assumption appears justified in view of the approximate nature of most response analyses. Furthermore, whenever roof behavior must be considered, it is probably sufficient to determine only if the covering material remains intact without any undue attention being given to the response of the supporting structure (e.g., trusswork and purlins).

Now while simplification is generally desirable, one can carry even a good thing too far, and the above argument may well be a case in point. For example, it is not hard to imagine buildings in which the response of the roof structure influences the general behavior of the entire building. Also, the present approach does not satisfactorily account for the influence of the degree or extent of local roof damage on either the transmitted roof load or the subsequent blast loading on the building. In fact, it is not certain that even the concept of roof failure is well defined. Nevertheless, when one considers the current lack of experimental evidence and general knowledge concerning the blast response of structures, even a somewhat questionable application of available data may be justified.

6.3.2 Critical Overpressures

The corrugated asbestos board and corrugated sheet steel covering on the two gabled roofs (3.5aa and 3.5ab, respectively) were both destroyed in a 4 psi region. The peak average net load over the front portion of the roof was somewhat less than 2 psi (see Fig. B.7). As discussed in Appendix B, the geometry of the roof causes the peak loads on various portions of the roof to differ considerably; the peak average pressure on the outside of the front half of the roof, for example, was predicted to be about 5.4 psi. A peak failure pressure of around 2 psi, determined for front walls of these materials, is believed to be applicable for roofs of the same covering. In terms of a critical overpressure, however, this value should be somewhat higher since the roof does not sustain as high a reflected pressure over its entire surface for a given overpressure as does a front wall.

It is estimated, therefore, that roof covering of corrugated asbestos board and corrugated steel will most likely be destroyed at overpressures of from 2 to 3 psi, and will definitely be destroyed at overpressures of 4 psi or more. It might also be noted that greater damage to the trusses and purlins is effected for a roof covered with corrugated steel than one covered with the asbestos board.

The precast concrete channel roof, 3.5bb, and the laminated wood roof, 3.5bc, were both partially destroyed in a 7 psi region. The holorib steel channel roof, 3.5cb, was totally destroyed in a 12 psi (regular reflection) region. While these roofs differ widely in material and construction details, each would be expected to fail under uniform static loads of between 1 and 2 psi. Based on a reasonable range of the parameters in Eq. 6.6, one would not expect the peak dynamic force causing failure to exceed 3 or 4 psi at the most. According to the load prediction method, the roofs in the 7 psi region sustained a peak average force over the entire roof surface of somewhat less than 4 psi; the peak force toward the front of these roofs was about 6.5 psi; the loads on the steel channel roof in the 12 psi region were correspondingly higher. It is estimated therefore, that the critical overpressure for each of these roofs is about 7 psi, but it is also considered likely that significant damage might be sustained at even 3 or 4 psi overpressure.

The prediction of failure loads for the reinforced concrete slab roof and the scaled bowstring truss roof is not felt to be warranted on the basis of the test results inasmuch as these roofs are not representative of the majority of such construction and no rational means are available for the purpose of computing the dynamic response of even the particular structures tested. The discussion of reinforced concrete wall panels in subsection 6.2.3 is generally applicable to roofs of this construction.

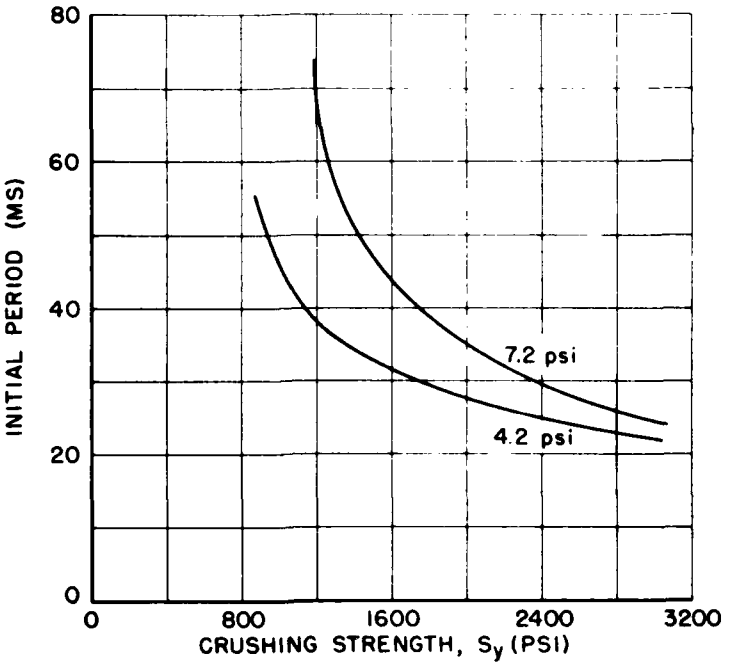

Fig. 6.1 Variation of Period with Crushing Strength

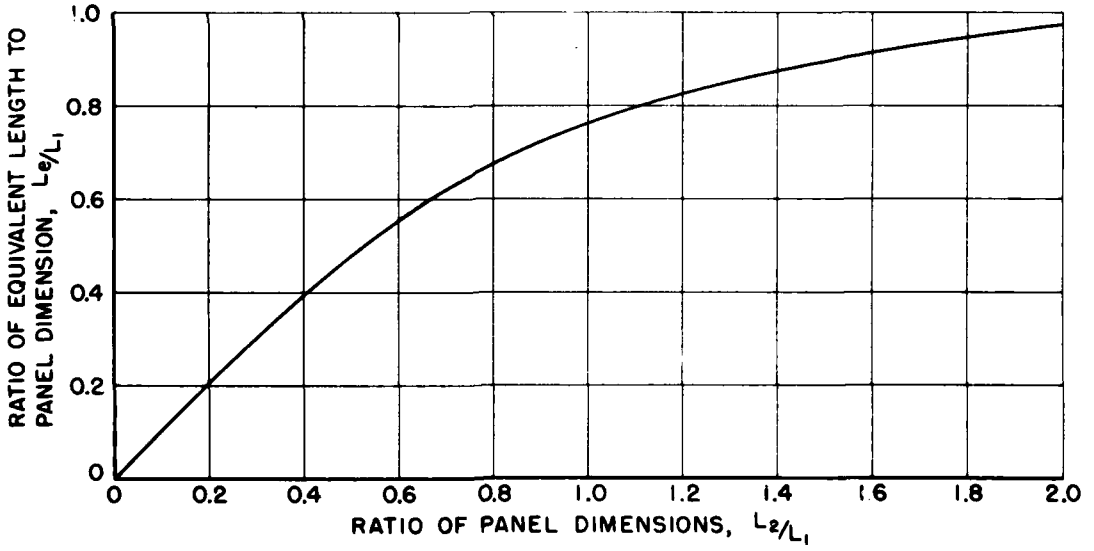

Fig. 6.2 Equivalent One-Way Span

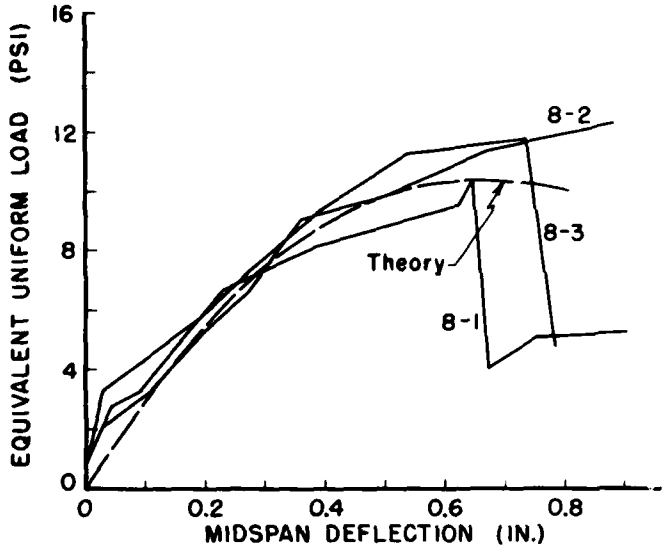

PERTINENT DATA

BEAM	WIDTH (IN.)	AVERAGE COMPRESSIVE STRENGTH OF MORTAR (PSI)
Fig. 6.3		
8-1	10.25	648
8-2	18.00	881
8-3	10.25	1162
Theory		900
Fig. 6.4		
12-1	18	796
12-2	18	581
12-3	18	675
Theory		690

Fig. 6.3 Comparison of Arching Theory with MIT Static Test Results on 8 in. Brick Beams, 8 ft Fixed-end Span

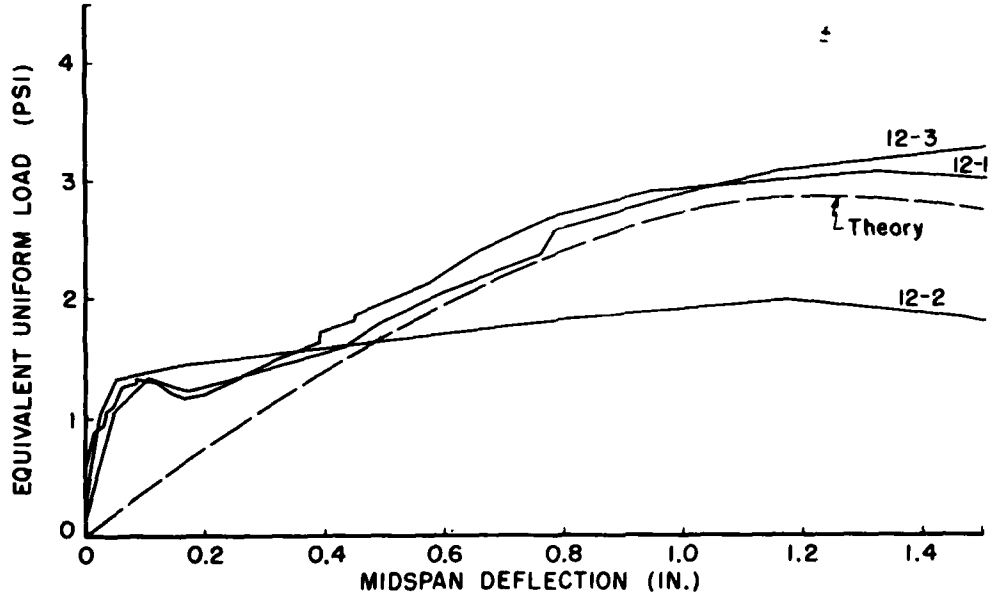

Fig. 6.4 Comparison of Arching Theory with MIT Static Test Results on 8 in. Brick Beams, 12 ft Fixed-end Span

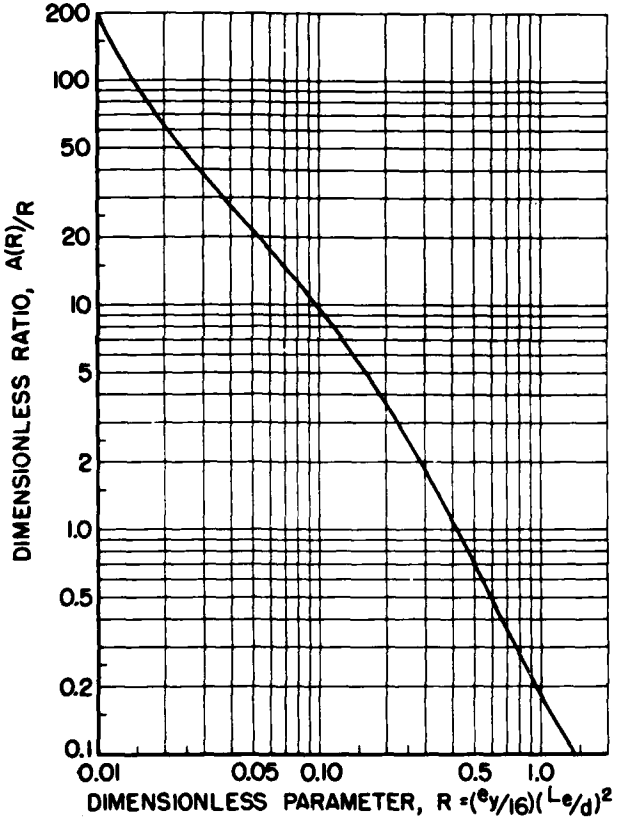

Fig. 6.5 Plot of Dimensionless Ratio $A(R)/R$ versus R, Masonry Wall Analysis

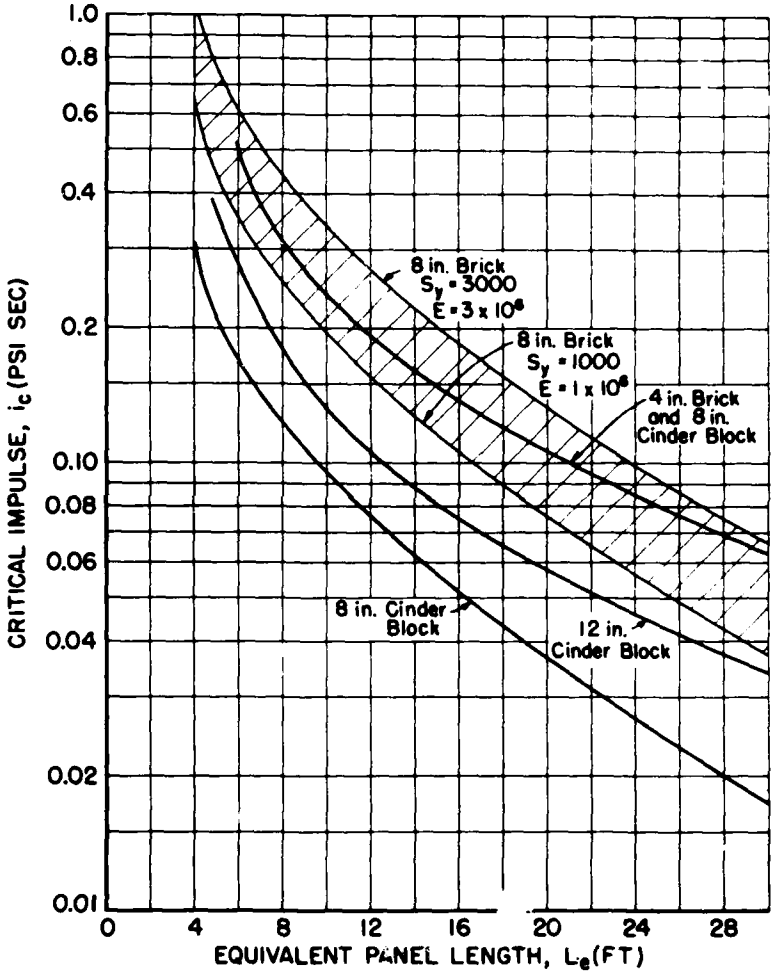

Fig. 6.6 Critical Impulse Variations with Length

CHAPTER 7

PREDICTION OF TRANSMITTED FORCE

7.1 INTRODUCTION

An attempt is made in the present chapter to indicate the application of the test data to the problem of predicting the blast forces which actually act on the structural frame of a building, i.e., the forces transmitted to the frame by the wall and roof covering. When one considers the wide assortment of special cases met with in problems of practical interest, it should be evident that the recommended methods of approach and tentative conclusions reached on the basis of but one test cannot be accepted as being final; their application can be determined only from the nature of the particular problem at hand. Still, it is believed that the information provided here will prove to be of general value to those confronted with the problem of computing the dynamic response of actual structures.

7.2 FORCES TRANSMITTED BY WALLS

To date most dynamic structural analyses have assumed that either the wall covering remains in place during the entire loading period, or that the covering is completely destroyed early in the loading period. In the first case, the walls are often assumed to act as an integral part of the building and the force acting on the structural frame is taken to be timewise identical to the predicted net exterior loading (front wall minus rear wall loading); in the second case the loading is generally determined as if the building were initially without walls. In computing the response of buildings when the loading is presumed known, it is also common practice to assume that the diffraction portion of the load is applied as an initial impulse to the dynamic system, the time details of the subsequent drag loading being accounted for in the formal solution of the equations of motion. The hope of incorporating the actual forces transmitted by a failing wall into the response analysis in just such a manner explains the emphasis placed on considering these forces in terms of a percentage of the applied diffraction impulse.

The force transmitted by the two brick walls which remained intact generally tends to support the first assumption of wall action, insofar as the average transmitted force is concerned. Certain obvious discrepancies (e.g., an initial peak force occurs on the outside of front walls in the Mach region, whereas initially the transmitted force must be zero) probably do not introduce serious errors into the response computations since most walls are relatively stiff and the peak transmitted force is reached quite early in the loading period. When the covering fails during the loading period it is clearly not permissible to discount the presence of the walls in many instances. Reinforced concrete panels may be blown out and still transmit a substantial portion of the applied load; the masonry walls transmitted an impulse of the order of the applied diffraction impulse prior to failure, which may be significant in certain cases. Even when the transmitted forces can be neglected, indications are that the presence of wall debris may materially influence the subsequent loading on the building.

Based on the discussion of section 5.1.3 it seems reasonable to conclude that (with the exception of the reinforced concrete panel) all of the wall types tested will fail and cease to transmit load in a time of the order of the duration of the diffraction loading period for the panel. During this time masonry walls will transmit an impulse approximately equal to 150 per cent of the entire diffraction impulse associated with the critical loading for the panel; lightweight covering (e.g., corrugated asbestos board and corrugated sheet steel panels) will transmit 20 to 40 per cent of this impulse. (The wood siding panel, usually considered as lightweight cover, transmitted in excess of the entire diffraction impulse of the critical loading, so that this type of wall may represent an exception to the last statement.)

While the percentages quoted above are admittedly based on rather tenuous evidence, they probably do represent the proper order of magnitude of the transmitted impulse. In any event, the impulses associated with the critical loading for these types of walls are liable to be only of negligible importance when compared with the total impulse of the loading required to damage many, if not most, structures of military interest.

No general statement can be made concerning the load transmission of reinforced concrete slabs on the basis of the test results. Unless the loading under consideration is substantially in excess of the critical load, it may be best to assume simply that the predicted load is transmitted for as long as 200 ms or more after shock arrival. In any case it is likely that this type of wall will transmit in excess of twice the diffraction impulse of the critical loading, especially if monolithic construction is being considered.

7.3 FORCES TRANSMITTED BY ROOF

Vertical loads are believed to affect structural response in two ways: (1) the loading produces a gross overturning moment that is proportional to column displacement, and (2) the load is transferred to the columns as an axial compressive stress which affects the bending resistance of the columns. Buckling of the columns, in a dynamic sense, may also result.

With respect to effect (1), the influence of the vertical loads increases with increasing displacement. During the initial loading period the overturning moment of the vertical forces is in many cases negligible compared to the overturning moment of the horizontal forces and, if vertical loads are transmitted for only the first 50 ms or so, it would be reasonable to neglect them in the response analysis. The situation is more complicated with respect to effect (2). During the initial loading period, both the horizontal and vertical forces attain their maximum values. Thus, the vertical forces could conceivably cause the resistance of the building to be decreased to a minimum value at the time the maximum horizontal forces act.

It should also be kept in mind that the loading is not uniformly distributed over the roof, as is approximately the case for wall loading. For long spans the problem is equivalent to that of a moving load, whereas for buildings with openings in the wall, the forward section of the roof sustains a substantially higher loading than the rear portion. A great deal remains to be learned about the combined action of time-dependent horizontal and vertical forces, and associated problems of dynamic buckling. This test serves to establish the fact that under certain circumstances substantial vertical loads can be transferred to the structural frame by roofs of representative construction prior to failure.

With the exception of the scaled bowstring truss roof and the reinforced concrete slab roof, the test results indicate the average force transmitted by the roofs prior to failure to be in substantial agreement with the predicted values of the blast loading during about the first 50 to 100 ms, at least for pressures of the order of the critical loads. Generalization of these results is compromised by the fact that the test concerned only one wall geometry (i.e., 17 per cent opening in the front and rear walls) and the agreement with the predicted values may be mostly coincidental for certain of the roofs (e.g., the corrugated steel and asbestos panels) where the failure of the covering occurred considerably earlier than the times for which the agreement was still quite good.

It can only be recommended, therefore, that in the event the walls remain intact, the total transmitted roof load be taken as the predicted applied load during the positive (downward) period of the loading. (Note that current load prediction methods have been indicated to be in error during the initial period.) For loadings substantially in excess of those under test conditions, it may be more reasonable to simply accept the measured transmitted force as representing maximum conditions rather than use the predicted forces associated with these higher overpressures. This approach would at least serve to bound the transmitted force on the low side.

No data were obtained on the force transmitted by the reinforced concrete roof. The behavior of this type of construction was discussed in connection with the reinforced concrete wall in section 6.2.3. No conclusions can be reached with respect to the forces transmitted by a wood bowstring truss roof of prototype dimensions.

Another point might be mentioned with reference to current building response analyses. Many of these analyses, especially those

pertaining to single-story structures, are based on the assumption that the building responds as a single-degree-of-freedom system. That is, the displacement of a single point on the structure is taken to characterize the building configuration as a whole, and damage criteria are formulated from this point of view. The dynamic model is then considered to be simply a rigid roof system set atop a series of columns which constitute the structural frame of the building (additional resistance elements such as shear walls need not be considered for this brief discussion). The key assumption here is the "rigid" roof, since otherwise the columns could act as independent elements and the single-degree-of-freedom approach becomes meaningless. The test results, however, point up the fact that roofs of actual structures may well be destroyed or damaged locally to the point where the above approach is no longer realistic.

7.4 APPLICATION

The following approach is recommended in order to obtain net horizontal and vertical blast loads on simple building shapes (for which load prediction methods are currently available) for the purpose of response computations. The first step is to determine the overpressure at which failure of the front wall, rear wall, and roof is expected. Based on the results of these computations, the following possibilities exist:

1. All panels remain intact: In this case the walls and roof can be assumed to act as rigid componets. Therefore, all of the loading is transferred to the structural frame, and the force transmitted by both the roof and walls is taken to be identical to the predicted applied force.

2. The walls remain intact but the roof covering fails: The horizontal transmitted loads are treated as in (1) above. However, the load predictions should account for the fact that the roof has failed, if this proves feasible. If the response analysis considers a resistance function which depends on axial forces (e.g., column action), the predicted vertical load should be included for the duration of positive loading. Insofar as the gross overturning effect of the vertical forces is concerned, it may be neglected in the analysis.

3. The walls fail; the roof covering may or may not remain intact: When the walls fail completely a percentage of the net diffraction loading computed on the basis that the walls remain intact should be incorporated into the analysis as an initial impulse. This percentage will depend on the type of wall under consideration as indicated in section 5.1.3.

After the walls break out the interior blast wave may be attenuated to a marked degree as discussed in section 5.1.1.2. The subsequent loading may therefore be less than had the walls been absent at the start. While it is not possible at present to account for this

effect in a quantitative manner, it would seem that a consistently high estimate of the subsequent drag loading could be obtained by computing the loading on the basis of a building initially without walls. The error in this method of approach is probably a function of the type of wall. For example, walls with a certain amount of open area (e.g., windows) will permit the blast to pass into the building prior to wall failure. Thus at least the initial interior flow characteristics will not be affected by wall failure. Also there will be less debris per unit wall area if openings are present. The debris effect is also likely to be less severe for lightweight covering (e.g., corrugated asbestos board), which will shatter and break out earlier than masonry materials. The vertical forces are handled as in (2) above.

Special cases occur when the loading under consideration is near the critical failure load for the walls. For example, a rear wall may remain intact in a pressure region where the front wall just fails. The prediction of load in these cases should depend on the particular objectives of the response analysis.

CHAPTER 8

CONCLUSIONS AND RECOMMENDATIONS

8.1 CONCLUSIONS

The following conclusions have been reached as a result of the test data and analysis presented in this report:

1. For spans encountered in normal practice, 8 in. brick walls with no open area, supported between or continuous over columns, are expected to fail at overpressures of about 9 psi or less; 1/ composite masonry construction of the type tested (i.e., 8 in. cinder block with 4 in. brick facing) has comparable strength. Conventional cinder block construction (12 in. or 8 in.) will fail at 4 psi or less; lightweight covering, such as corrugated asbestos board and corrugated sheet steel siding and wood siding, will fail at less than 2 psi. The upper bound pressures pertain to the test panels which are probably of smaller size (and hence greater strength) than most such construction met with in practice. In view of the wide range of panel dimensions which might be encountered, it is not practical to assign lower bound failure pressures. Failure pressures cannot be generally stated for reinforced concrete panels since their behavior depends on such variable quantities as per cent and strength of steel and end fixity.

1/ Whenever failure pressures are quoted, the panels referred to were destroyed so early in the loading period that peak pressure damage criteria are believed to be justified provided that the duration of the blast wave is in excess of, say 200 ms. The failure pressures refer to panels located in the region of conventional Mach reflection and some difference is to be expected whenever the same overpressure level occurs in the regular reflection region. However, the failure pressures are sufficiently low so that the latter case is not expected to occur in most real situations.

2. Lightweight roof covering of the type tested will most likely be destroyed at overpressures of 4 psi or more, and will probably be damaged at overpressures of from 2 to 3 psi. Greater damage is expected to the trusses and purlins of a corrugated sheet steel roof than one covered with corrugated asbestos board. Flat roofs of precast concrete channels, holorib steel channels, and laminated wood of the types tested are expected to fail, at least partially, at overpressures of about 7 psi, and will probably be damaged at pressures as low as 3 or 4 psi. In connection with these failure pressures it might be noted that walls and roofs of most lightweight covering and some masonry construction can be expected to be destroyed for loadings commonly associated with structural damage to representative buildings of military importance.

3. Based on the behavior of the two brick walls which remained intact, it appears that the predicted applied load on a wall panel without openings represents reasonably well the average load transmitted by the panel to the supporting structure, provided the panel remains intact throughout the entire loading period.

4. The masonry walls tested transmitted an impulse prior to failure which varied from about 50 to 150 per cent of the diffraction impulse of the predicted applied loading. It is estimated that masonry walls will transmit on the average about 150 per cent of the predicted applied diffraction impulse associated with the critical loading (i.e., the loading which just causes failure) regardless of the actual loading causing the panel to fail. Lightweight covering is estimated to transmit from 20 to 40 per cent of this impulse prior to failure. The wood siding panel, while not appreciably stronger than the other lightweight materials, appears to transmit an impulse equal to the entire diffraction impulse prior to failure. Each of the test panels which were destroyed (with the exception of the reinforced concrete slab) ceased to transmit load in from 20 to 100 ms after shock arrival. The initial failure times (i.e., the time at which a marked decrease in transmitted load was observed) correspond to the first half period of the panel motion and are of the order of the duration of the diffraction loading on the isolated panel.

5. The average force transmitted by the test roofs prior to failure (with the exception of the reinforced concrete slab and the scaled bowstring truss roofs) appears to be in substantial agreement with the predicted applied loading during the positive (downward) phase of this loading (about 100 ms for the test roofs), at least for the building geometries considered and pressures of the order of the critical loads. Whether or not this can stand as a general conclusion is not certain since portions of the covering on several of the test roofs were observed to fail at times for which the agreement was still good, and the reasons for the continuing agreement are not understood. Also, current net load prediction methods for roofs are indicated by the test data to be in error (see conclusion 10).

6. The masonry and reinforced concrete panels appeared to fail as two-way slabs. The test results seem to support a so-called arching action theory of masonry walls which was first proposed in the ARF GREENHOUSE report. This theory has been extended (see Appendix A) and, while no doubt grossly idealizing the actual situation, it permits the computation of critical loadings for the test panels which appear quite reasonable. It might also be noted in support of this theory that the measured distribution of transmitted force around the edges of the masonry panels give no indication of a strong or weak direction for this type of construction. The lightweight wall and roof covering appeared to fail in bending as one-way slabs (the mode of failure of the corrugated asbestos board wall is strikingly illustrated in Fig. 4.9.

7. Even though a wall fails structurally quite early in the loading period, the debris may not clear from the opening until a relatively long period of time has passed. In such cases the peak forces and the dynamic effects of the peak forces in the interior of the building are expected to be considerably lower than if the wall debris had cleared away more rapidly. The effect of wall debris may therefore be of considerably greater importance than had been previously anticipated in reducing the loading on interior equipment, downstream walls, columns, and trusswork.

8. Early structural failure of the roof does not necessarily imply that interior pressures are altered quickly from what would occur with no roof failure, at least for the geometries considered. In fact, for the six pressure-gaged roof panels it appears that roofing was removed

by the blast too slowly to have a large effect at any time on the interior pressures. Furthermore, the pressure gages used appear to be relatively insensitive to acceleration effects which are created during roof failures; this fact is of interest for any future field tests with this type of gage on failing structures.

9. The effects of purlins on pressures on the undersides of roofs are probably confined to areas closer to the purlins than about one purlin height. The effects of longitudinal trusswork on pressures is also indicated to be small. In fact, the later (pseudo steady state) pressures on the undersides of all roof shapes which were tested appear to be unaffected by the geometric differences between these roofs, including pitched and arched shapes.

10. Comparison of measured pressures with predicted loadings on the roofs tested indicates that the predictions are fair to good in most respects for the Mach reflection region, but are poor in certain respects for the regular reflection region. In the latter region it appears that prior to pseudo steady state time, the net roof forces (outside minus inside) are lower, in some cases by a factor of about 2, than those computed according to the methods in Appendix B. Comparison of transmitted loads (from strain records) with predicted applied loads for the wall panels generally substantiates current prediction methods for these units.

11. The force measurement system proved quite satisfactory and appears to offer a reliable method for measuring the load transmission properties for wall and roof structures comparable to those tested.

The test results have been considered in relation to the ultimate problem of building response analysis. Inasmuch as the following statements summarizing this work are not in every case directly supported by the test, they are not intended as general conclusions.

1. The average force transmitted by walls and roofs which remain intact may be assumed to have the same time distribution as the predicted applied loading on these components.

2. When walls are destroyed in about 100 ms or less after shock arrival, the load transmitted prior to failure may be approximated by considering a fixed percentage of the diffraction portion of the predicted applied loading as being imparted to the structure as an initial

impulse. The subsequent drag loading on the building is not well defined since, in the case of a failing brick wall, the debris appears to influence the interior loading significantly. One method of approach would be to compute the loading after wall failure as if the building were originally without wall covering. This will probably lead to a high estimate of load, but should become more accurate for buildings with walls of lightweight covering or walls with relatively large initial openings (e.g., window or door area).

3. When either the walls or the roof fail, net vertical loads will be transmitted for approximately the predicted duration of the positive (downward) loading period. If the response analysis considers a resistance function which depends on vertical forces, these forces as predicted should be included for this length of time. If only the gross overturning effect of the vertical forces is considered, they may be neglected entirely.

It should be noted that the quantitative effects of the alternate approaches indicated above are not known. It is not improbable that a detailed investigation of building response in these cases will point to additional simplifications. For example, consideration of the horizontal diffraction impulse when the walls fail may prove to be a second-order refinement, and the walls may be considered to transmit no load to the structure once wall failure is assumed.

In summation the following can be said with regard to the specific objectives of this test listed in Chapter 1.

1. The objective dealing with the determination of the percentage of applied load that walls and roofs of the types tested transmit to the supporting frame has been fulfilled with the exception of the reinforced concrete roof and of prototype wood bowstring truss roofs. In the former case no usable data were obtained from the test structure, and in the latter case it was not possible to correlate the response of the scaled roof tested with the behavior of actual size structures. Similarly, the load transmission properties determined for the reinforced concrete wall panel probably do not have wide applicability.

2. The objective dealing with the modes of failure of walls and roofs of the types tested has been fulfilled, again with the possible exception of the two types of construction indicated above.

3. The objective dealing with the determination of loading changes inside of buildings due to failure of the walls and roofs has been fulfilled to the extent that the test design would permit.

4. The objective dealing with the determination of pressures which insure damage to typical roof and wall panels has been fulfilled for all of the test structures with the exception of the reinforced concrete construction and prototype wood bowstring truss roofs.

8.2 RECOMMENDATIONS

With a view toward increasing the applicability of the results of this test to the more general problem of building response, it is recommended that:

1. Laboratory and, if necessary, field tests be conducted to obtain additional information as to the net loading on buildings whose wall and roof covering breaks out when struck by the blast. This appears to be especially crucial with respect to wall failure.

2. Theoretical and experimental work be conducted in determining the primary effect of vertical forces on structural response.

3. Theoretical and experimental work be conducted on the behavior of reinforced concrete panels under blast loading.

4. Additional study be made of the roof loading prediction methods and the pressure records to determine what changes should be made in the prediction methods.

APPENDIX A

MASONRY WALL ANALYSIS

by K. E. McKee and E. L. McDowell

A.1 INTRODUCTION

This appendix contains a development of the so-called arching action theory of masonry walls. The method of approach was first discussed in the ARF GREENHOUSE Report. However, the present development is believed to be more realistic both from the point of view of geometric considerations and stress-strain relationships involved in the action of masonry units. Masonry walls are considered to include all walls consisting of individual units set in mortar.

The analysis is presented for a beam of solid cross section, and then modified to include two-way slab action and walls of arbitrary cross section. The response of a wall subjected to pure impulsive loading is considered in detail. This solution is interpreted to yield the minimum impulse necessary to cause failure of a masonry wall.

A.2 GEOMETRIC CONSIDERATIONS

A.2.1 Basic Relationships

For the purpose of analysis a masonry beam of unit width is considered to be supported at both ends, Fig. A.1. It will be assumed that masonry material can sustain no tensile stress and, upon application of transverse loads, cracks will occur at the supports and mid-span. At the instant of failure the cracks will extend to the half-depth of the beam. The subsequent motion is assumed to be rigid body rotation of each half-span about its support. This motion is resisted by axial or thrust forces set up at the supports due to the crushing action of the material, Fig. A.1. Figure A.2 shows the condition at the support in greater detail and defines the nomenclature used. With reference to this figure,

$2L$ = length of beam

$2d$ = depth of beam

w = deflection at mid-span of beam

θ = angular displacement of half span

αd = length of beam in contact with support; α is a dimensionless number

y = coordinate

δ = shortening of the fibers in contact with support

δ_o = maximum shortening of fibers

a = perpendicular distance from center line of beam to first point in contact with support.

$F(t)$ = net external time-dependent force

$P(t)$ = time-dependent thrust forces

r = moment arm of couple formed by thrust forces

The predominant feature of the resulting motion is that the contact area, αd decreases with increasing deflection, w. The original GREENHOUSE analysis assumed that $\alpha = 1$, i.e., that the contact area was independent of the deflection. The following geometric relationships exist between the above parameters, as can easily be verified:

$$a = \frac{L}{2}\left(\frac{1 - \cos\theta}{\sin\theta}\right) = d(1 - \alpha\cos\theta)$$

$$w = 2L\left(\frac{1 - \cos\theta}{\sin\theta}\right)$$

$$\delta = \frac{\delta_o}{\alpha d\cos\theta}\left(\alpha d\cos\theta - y\right)$$

$$\delta_o = \alpha d\sin\theta\ .$$

From these relations it is seen that

$$a = \frac{W}{4}\ ,$$

which shows clearly the dependence of the contact area on deflection.

It is convenient to introduce the following nondimensional parameters:

$$u = \frac{w}{2d}$$

$$v = \frac{d}{L} .$$

The original variables can now be expressed in terms of u and v. That is,

$$\sin\theta = \frac{2uv}{1 + u^2 v^2}$$

$$\cos\theta = \frac{1 - u^2 v^2}{1 + u^2 v^2} \qquad \text{(A-1)}$$

$$\alpha = \frac{1 + u^2 v^2}{1 - u^2 v^2}\left(1 - \frac{u}{2}\right)$$

$$\delta = \frac{2u\,d^2}{L}\left[\frac{1 - u/2 - y/d}{1 - u^2 v^2}\right]$$

A.2.2 Arching Strains

The quantity δ_o represents the shortening of the lower fiber of the beam in contact with the support. Due to the cracking at mid-span, the fibers at this position are unstressed. It is reasonable to define the average strain along the length at any depth in the beam as

$$e = \frac{\delta}{L} .$$

If the variation of strain along any fiber is assumed to be linear,1/ the strain at the support end will be $e = 2\delta/L$. The strain at any point, y, along the contact area is

$$e = \frac{4u\,d^2}{L^2}\left(\frac{1 - u/2 - y/d}{1 - u^2 v^2}\right) . \qquad \text{(A.2)}$$

Define the dimensionless parameter R as

$$R = \frac{e_y L^2}{4d^2} \qquad \text{(A.3)}$$

where e_y is the yield strain of the masonry material (i.e., the strain associated with the crushing strength of the material). The deflection,

1/ This assumption is admittedly arbitrary.

w, is usually quite small compared to the span length. Therefore, it is reasonable to neglect the quantity

$$(uv)^2 = (\frac{w}{2L})^2$$

as compared to unity. In this case, Eq. A.2 may be written in the form

$$R\frac{e}{e_y} = u(1 - \frac{u}{2} - \frac{y}{d}) \cdot \qquad (A\text{-}4)$$

This relation defines the ratio of arching strain to yield strain for the fibers in contact with the support. The surface represented by this equation as a function of u and y/d is shown in Fig. A.3.

A.2.3 Stress-Strain Relationships

As previously stated, it is assumed that masonry can withstand no tensile stress. The stress-strain relationship for the material based on this assumption is shown schematically in Fig. A.4. The reversal of strain during a loading cycle is shown in Fig. A.5. During the initial application of load the material behaves elastically (AB). As the load is increased the transition to the plastic state is assumed to occur instantaneously, and the strain increases without a corresponding increase in stress (BC). Physically the material may be thought to have crumbled but is confined against the support. Thus, as the load is relaxed, separation occurs at the support and the stress drops instantaneously to zero with no recovery in strain. (CD).

The implication as to the state of stress at the support based on the above behavior, and the geometric distribution of strain given by Eq. A.4 is shown in Fig. A.6. There is a region, depending on the value of R, where the stress always remains elastic, i.e., the surface OCADF. The region under the plane ABC is in the fully plastic state; the remaining regions are those where separation has occurred at the supports after the yield condition was reached, and are now unstressed.

This situation may possibly be made more clear by considering the stress distribution along the contact area for various values of beam deflection, as shown in Fig. A.7. Initially, u = 0; there is no compressive stress along the contact area. As u increases the initial point of contact drops below the center line of the beam and the distribution of stress is elastic. At u = 0.1 the bottom portion of the contact area has reached the crushing strength of the material, and the region of plastic stress increases with increasing displacement. Meanwhile, the contact area is decreasing. At u = 0.4 the strain at some point begins to decrease. However, since the stress at this point has previously reached its maximum value it immediately drops to zero and an unstressed region exists between the area of elastic and plastic stress. This unstressed area continues to increase until around u = 0.7 when all of the area now in contact has at one time been stressed to the

maximum value. This condition increases until at about u = 1.0 the material in contact with the support is completely unstressed. Collapse of the wall, of course, may have previously occurred.

A.2.4 Thrust Forces

The thrust per unit width, P, is obtained by summing the stresses acting over the contact area. As can be seen from Fig. A.7 the form of the summation will depend upon the particular distribution of stress existing which, in turn, depends on the displacement, u, and the parameter, R. For $R \geq 1/2$ (elastic state) the form of the thrust force is given by

$$P(u) = \frac{s_y d}{2R} u \left(1 - \frac{u}{2}\right)^2$$

where s_y is the crushing strength of the masonry material. The quantity $s_y d$ represents the maximum thrust force which can be developed (i.e., for a = 0) and affords a convenient manner in which to non-dimensionalize P(u). The thrust ratio $4P(u)/s_y d$ is plotted as a function of u for various values of R in Fig. A.8.

The couple formed by the thrust forces is defined as the resisting moment, M(u), and is given by

$$M(u) = r(u)\, P(u) . \tag{A.5}$$

This relation may be put into nondimensional form by introducing the maximum moment $s_y d^2$. The dimensionless ratio

$$\Omega(u) = \frac{4M(u)}{s_y d^2} \tag{A.6}$$

is plotted as a function of u for various values of R in Fig. A.9. For the fully elastic condition, $R \geq 1/2$, this ratio is given by

$$\Omega(u) = \frac{4M(u)}{s_y d^2} = \frac{8u}{3R}\left(1 - \frac{u}{2}\right)\left(1 - \frac{5u}{4}\right) . \tag{A.7}$$

A.3 DYNAMIC ANALYSIS

A.3.1 General Loading

Up to now the development has dealt solely with the dependence of the thrust forces and resisting moment on the rotation of the beam element. The present section deals with the influence of the external loads on this rotation.

The equation of motion of each half of the beam taken as a rigid body rotating about a point in contact with the support[2/] is found to be

$$I_o \ddot{\theta}(t) + M'(\theta) = \frac{L^2}{2} F(t) \qquad (A.8)$$

where I_o = mass moment of inertia of beam about axis of rotation

$$I_o = \frac{L^3 \rho}{3}$$

ρ = mass of beam per unit length (for a beam of unit width)

$M'(\theta)$ = resisting moment as a function of the angle of rotation.

In general, the beam element will be considered to start from rest, so that the initial conditions for Eq. A.8 are

$$\theta = 0, \ \dot{\theta} = 0 \text{ at } t = 0 .$$

It is convenient to again replace the angular displacement, θ, by the nondimensional deflection, u. A simple relationship between θ and u can be obtained from Eq. A.1, if the assumption of small displacements compared to span length is made. That is, the sine of the angle is approximated by the angle itself and the quantity (uv) is neglected as compared to unity. Then, from Eq. A.1

$$\theta \approx 2uv = \frac{2du}{L} = \frac{w}{L} .$$

The physical approximation is clear since $L\theta$ is the arc length generated by the radius L rotating through the angle θ. This is tantamount to replacing the arc length by the chord length w. The relation between accelerations is then,

$$\ddot{\theta} = \frac{2d}{L} \ddot{u} .$$

Introducing the function Ω, Eq. A.6, the equation of motion becomes

$$\frac{8 L^2 \rho}{3 s_y d} \ddot{u} + \Omega(u) = \frac{2 L^2}{s_y d^2} F(t) \qquad (A.9)$$

$$u(0) = \dot{u}(0) = 0 .$$

2/ This point is taken on the center line of the beam, and is an approximation in that the axis of rotation actually depends on the beam displacement. The error introduced, however, is not large.

Once the character of the external load, F(t), has been defined this equation may be solved directly for u. However, due to the nonlinear dependency of $\Omega(u)$ on u, closed solutions in terms of simple functions cannot, in general, be obtained. Therefore, either a series form or numerical solution must be employed. As can be seen from Fig. A.9, the quantity $\Omega(u)$ is approximately linear for sufficiently small displacements. Thus an approximate solution to Eq. A.9 could be obtained by neglecting powers of u greater than unity in the expansion for $\Omega(u)$. The difficulty in obtaining a closed form solution then depends on the form of F(t).

For a linear form of $\Omega(u)$, it is possible to compute a natural frequency (or period) of vibration for the beam according to Eq. A.9. In this case choose $\Omega(u) = ku/R$ (see Eq. A.7) where k is a constant depending on R and R is given by Eq. A.3. Then, with $F(t) \equiv 0$, Eq. A.9 can be written,

$$\ddot{u} + \frac{3d\, s_y k}{8L^2 \rho R}\, u = 0 \ . \qquad \text{(A.10)}$$

The frequency of the system, p, is defined as the square root of the coefficient multiplying u in Eq. A.10. Therefore the following proportionality holds,

$$p \sim \sqrt{\frac{s_y d}{L^2 \rho R}} \sim \sqrt{\frac{s_y d^3}{L^4 \rho e_y}} \sim \sqrt{\frac{Ed^3}{\rho L^4}} \qquad \text{(A.11)}$$

where Eq. A.3 has been used for R and Young's modulus for the material E is defined as s_y/e_y. For purposes of comparison it will be noted that the bending frequency of beams (according to conventional theory) is proportional to the same group of physical parameters given in Eq. A.11. Specifically, for $R \geq 1/2$ the constant k in Eq. A.10 has the value 8/3 (see Eq. A.7) and the frequency p has the value,

$$p = 2\sqrt{\frac{Ed^3}{\rho L^4}} \ .$$

For a simply-supported beam of rectangular cross section (unit width) the fundamental bending frequency is

$$p_b = 2.01\sqrt{\frac{Ed^3}{\rho L^4}} \quad \text{(d = half depth; L = half span).}$$

Thus for this range of R the arching analysis indicates (coincidentally) a frequency nearly identical to the fundamental bending frequency for a simply-supported beam.

A solution of physical interest can be obtained directly for the case of impulse loading, i.e., when the deflection of the system

during the period of the loading can be neglected. The loading can then be replaced by imparting an initial velocity to the system. This procedure is as follows:

The first integral or momentum form of Eq. A.9 is

$$\frac{8\,L^2\rho}{3\,s_y d}\,\dot{u}(t)\Big|_o^t + \int_o^t \Omega(u)\,dt = \frac{2L^2}{s_y d^2}\int_o^t F(t)\,dt\,. \qquad (A.12)$$

Let the duration of the impulsive type loading be denoted by t_d, i.e., $F(t \geq t_d) \equiv 0$. Now, by assumption, t_d is sufficiently small so that the quantity $\Omega_m(u)\,t_d$ can be neglected, where $\Omega_m(u)$ is the maximum value $\Omega(u)$ in the interval $0 \leq t \leq t_d$. This is equivalent to neglecting the integral function of $\Omega(u)$ in Eq. A.12 during the interval. Introduce the following notation,

$$\dot{u}(t_d) = \dot{u}_d$$

$$\int_o^t F(t)dt = i\,.$$

Then Eq. A.12 becomes

$$\dot{u}_d = \frac{3i}{4\,\rho d}\,. \qquad (A.13)$$

This is the equivalent initial impulse of the system and can be obtained directly once F(t) is known.

The response of a beam with an initial velocity (equivalent impulse loading) will be considered in detail. The form of the equation of motion, Eq. A.9, and its initial conditions now become

$$\frac{8\,L^2\rho}{3\,s_y d}\,\ddot{u} + \Omega(u) = 0$$

$$u(0) = 0,\ \dot{u}(0) = u_d\,. \qquad (A.14)$$

Another form (energy form) of this equation is

$$\frac{4\,L^2\rho}{3\,s_y d}\,\frac{d(\dot{u}^2)}{du} + \Omega(u) = 0\,.$$

A first integral is

$$\frac{4\,L^2\rho}{3\,s_y d}\left[\dot{u}(t)^2 - \dot{u}_d^2\right] + \int_o^{u(t)} \Omega(u)du = 0\,. \qquad (A.15)$$

The integral expression is seen to represent the area under the curves in Fig. A.9 from the origin to an arbitrary displacement u(t). When the dependency of these functions on time, t, is known, Eq. A.14 may be solved directly for u.

A.3.2 Critical Impulse

The critical impulse is defined to be the minimum impulse loading necessary to cause failure of the wall. Since the impulse is related to the initial velocity by Eq. A.13, it is sufficient to determine the critical initial velocity. From a mathematical viewpoint, failure is guaranteed if the velocity, $\dot{u}(t)$, always remains positive in value. The limiting or critical condition occurs when the system has a zero velocity at the time the failure displacement is reached. The failure displacement, in turn, may be associated with the value of u for which $\Omega(u) = 0$. That is, failure is assured if, at the time for which $\Omega(u) = 0$, the velocity of the system is positive. From Fig. A.9 this value of u, u_c, is seen to be dependent on R.

The critical initial velocity $\dot{u}_c$ can now be determined. This velocity is the one for which

$$\dot{u}_c = \dot{u}_d;$$

then

$$\dot{u}(t_c) = 0; \quad u(t_c) = u_c$$

$$\Omega(u_c) = 0.$$

From Eq. A.15,

$$\dot{u}_c^2 = \frac{3\, s_y d}{4L^2 \rho} \int_0^{u_c} \Omega(u)\, du \,. \tag{A.16}$$

Let

$$A(R) = \int_0^{u_c} \Omega(u)\, du, \tag{A.17}$$

and introduce the parameter R in Eq. A.16. Then using Eq. A.13 for $\dot{u}_d = \dot{u}_c$, the required impulse is,

$$i_c = \left[\frac{1}{3} \rho d\, s_y\, e_y \frac{A(R)}{R} \right]^{1/2}. \tag{A.18}$$

The quantity A(R)/R is plotted as a function of R in Fig. 6.5. The critical impulse is a function of only the physical parameters of the beam. The association of i_c with blast parameters is considered in Chapter 6.

The analysis could be extended, with a corresponding increase in complexity, to materials with other stress-strain relationships or subjected to other types of loadings. The present analysis, however, has been carried out only so far as it need be applied to the problem at hand.

A.4 TWO-WAY PANEL ACTION

The previous analysis would apply to beams or panels supported on two opposite sides only. In order to extend the results to the case of a panel supported on all four sides, the concept of an equivalent beam length is introduced. Two-way panel action can be handled by considering the applied load to be distributed in a certain fashion to beams in either direction crossing at the center of the panel. The distribution condition is that the center deflection of the equivalent beams must agree.

Consider a panel whose edge dimensions are L_1 and L_2. If the load distribution factors are denoted by C_1 and C_2, the center deflection, Δ, can be written as[3]

$$\Delta = \frac{C_1 BpL_1^4}{EI} = \frac{C_2 BpL_2^4}{EI} = \frac{CBpL_e^4}{EI} \qquad (A.19)$$

where

B = constant depending on end fixity of panel

p = applied transverse load per unit length

EI = stiffness of beam element

L_e = length of equivalent one-way panel (= 2L of previous analysis)

C = load distribution factor for equivalent beam.

The factors C_1 and C_2 are obtained from the ACI Building Code. These are related to the equivalent distribution factor C as

$$mC = C_1 + C_2 \qquad (A.20)$$

where m may be thought of as the percentage of total load acting on the equivalent beam which causes the required displacement. The percentage m is a function of the panel dimensions but, according to the ACI code, is independent of end fixity. By eliminating the C's from Eq. A.19 and A.20, the following deining relationship for L_e is obtained:

3/ A basic assumption of this development is that the distribution of loads on a masonry panel is the same as for an elastic plate.

$$\frac{L_e}{L_1} = \left[\frac{m}{1 + \left(\frac{L_2}{L_1}\right)^4}\right]^{1/4}\left[\frac{L_2}{L_1}\right] \qquad (A.21)$$

This relationship is plotted in Chapter 6, Fig. 6.4. For a given panel the value of L_e given by Eq. A.21 is to be used for the length 2L in the previous development. In those cases where the actual panel is supported on only two opposite sides, L_e is taken to be the distance between supports.

A.5 OTHER TYPES OF MASONRY CONSTRUCTION

The previous development pertains to masonry units of solid cross section. The cross-sectional area affects the thrust force, its moment arm and, in turn, the resisting moment M(u). Thus, as can be seen from Eqs. A.17 and A.18, the cross-sectional area influences the critical impulse, i_c, in terms of the quantity A(R). Of course the density per unit length of span, ρ, depends on the type of masonry unit, but this can be computed for each particular case.

The quantity A(R) could be evaluated for each individual type of masonry unit as was done for the solid section. However, the additional complexity introduced is not felt to be justified at this time in view of the uncertain nature of the entire theory. Rather, the value of i_c found previously is modified to include beams of other than solid cross section (e.g., hollow block or composite masonry construction) in an approximate manner. While the following approach is admittedly questionable, numerical results based on the method check reasonably well with the test data as discussed in Chapter 6.

The quantity A(R), being the area under the M(u)-u curve, is taken to be proportional to the product M(u)u. The thrust force is approximately proportional to the displacement u, at least for the initial motions (see Fig. A.8). Therefore it is assumed that

$$A(R) \sim M(u)P(u).$$

Two additional assumptions are now made:

1. The thrust force is proportional to the area of the cross section, A,[4] multiplied by the crushing strength of the masonry material, i.e.,

$$P(u) \sim As_y$$

2. The dependence of the resisting moment on cross-sectional area is of the order of this dependence in the case of elastic bending, i.e.,

---

4/ The area A refers to the minimum cross section of the masonry unit, e.g., a section through the openings in a hollow block unit.

$$M(u) \sim I = Ak^2,$$

where k is the radius of gyration of the cross section with respect to the neutral axis.

Based on these assumptions,

$$i_c \sim \sqrt{A(R)} \sim \sqrt{Ak^2 \cdot A} = Ak.$$

Let the subscripts s and a refer to beams of solid and arbitrary rectangular cross sections, respectively. Then, by definition $i_{cs} = i_c$ and

$$i_{ca} = i_c(i_{ca}/i_{cs}) = i_c(A_a k_a)/(A_s k_s).$$

For a beam of unit width and half depth d, $A_s k_s = 2d^2/\sqrt{3}$ and, omitting the subscript a, the modified impulse using Eq. A.18 becomes

$$i_c = \frac{Ak}{2d^2}\left[\rho d\, s_y\, e_y \frac{A(R)}{R}\right]^{1/2} \qquad (A.22)$$

where the quantities A and k now refer to arbitrary cross sections. For solid cross sections, Eq. A.22 is, of course, identical to Eq. A.18.

It is not possible to judge the accuracy or the reliability of the present approach; as indicated earlier the test results seem to support the type of correction factor introduced here. It is felt that the method is more realistic for symmetrical cross sections such as hollow block constuction and possibly less so for composite constructions.

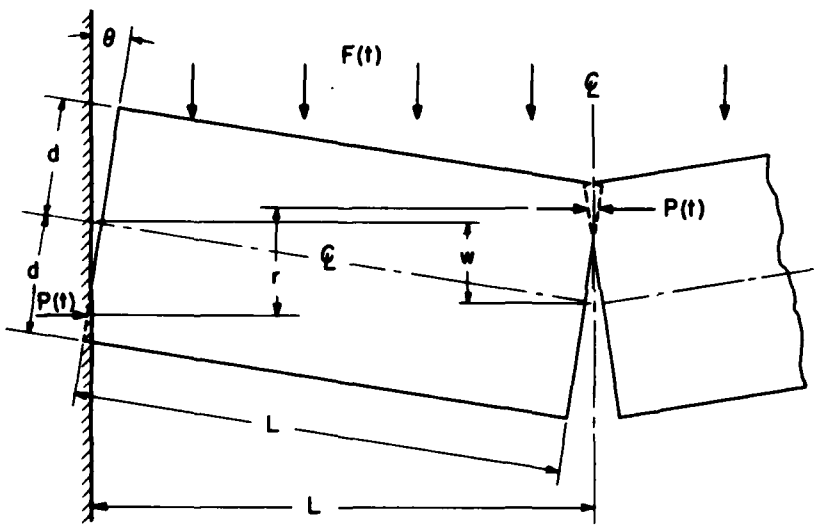

Fig. A.1 Schematic Representation of Arching Action

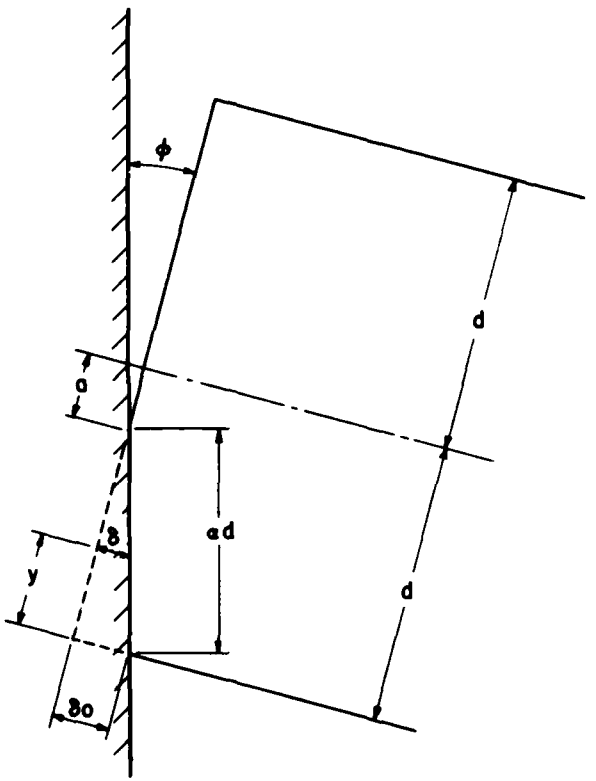

Fig. A.2 Conditions at Beam Support

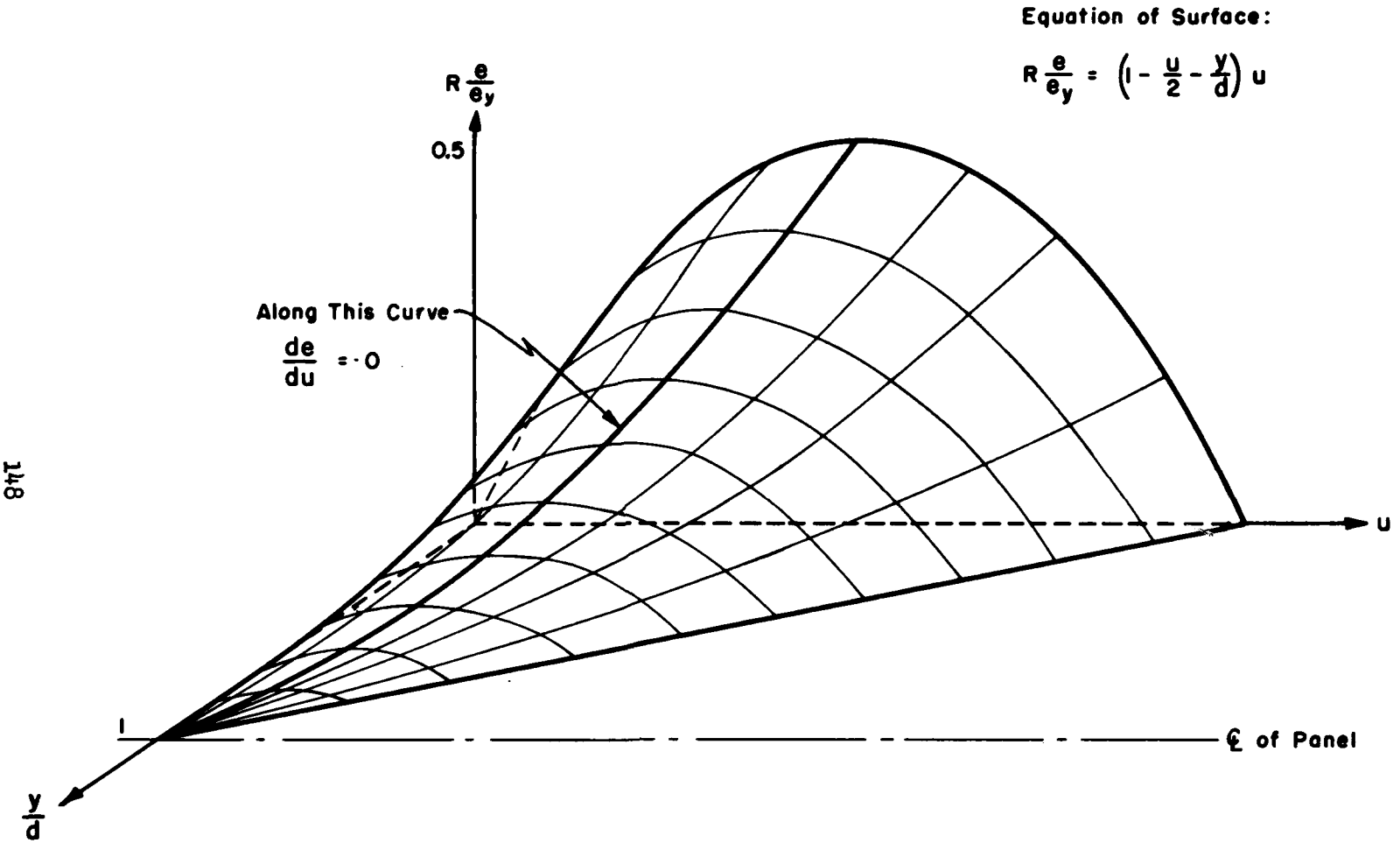

Fig. A.3 Geometric Distribution of Strain Along Contact Area

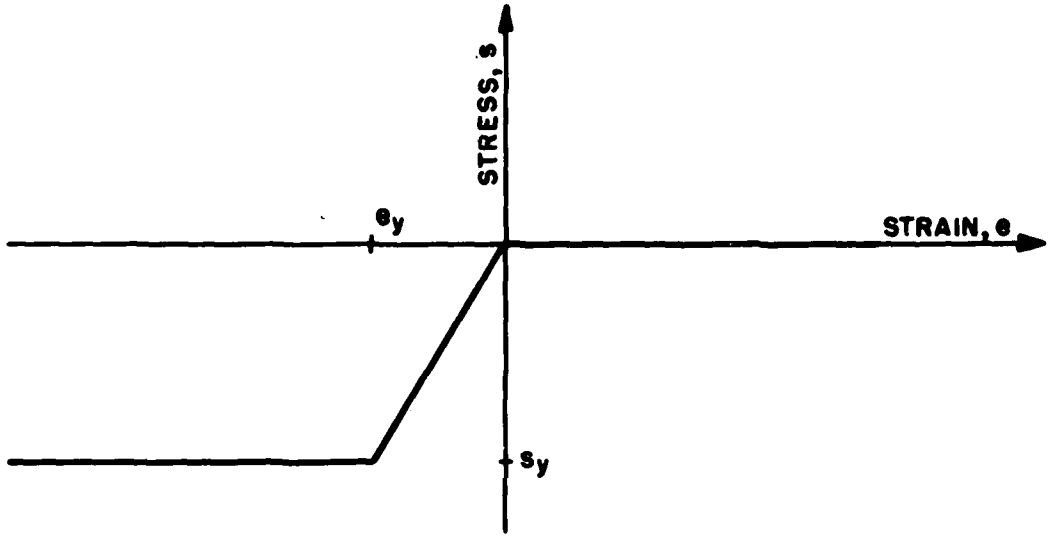

Fig. A.4 Assumed Stress-Strain Relationship for Masonry Materials

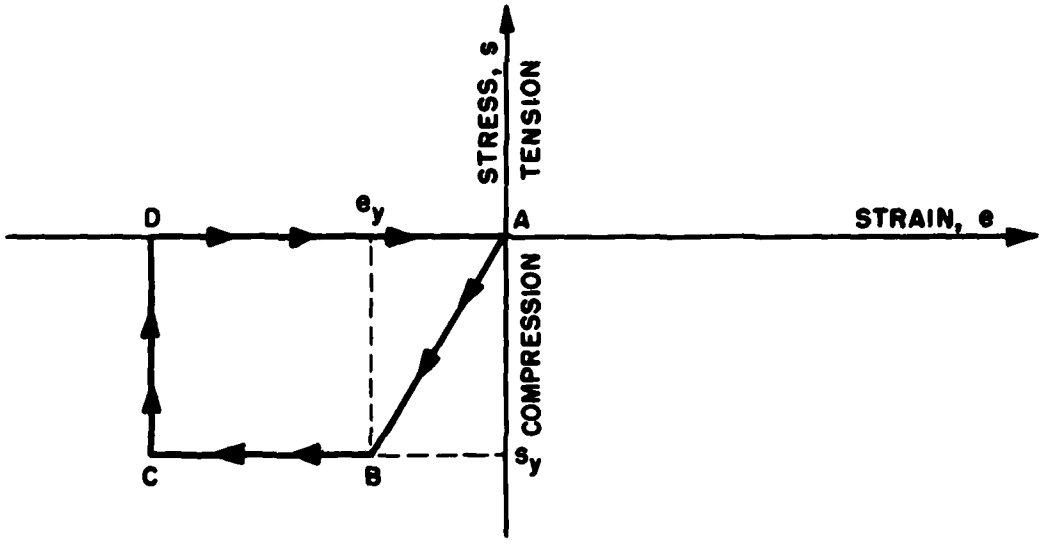

Fig. A.5 Assumed Stress-Strain Behavior During Loading Cycle for Masonry Materials

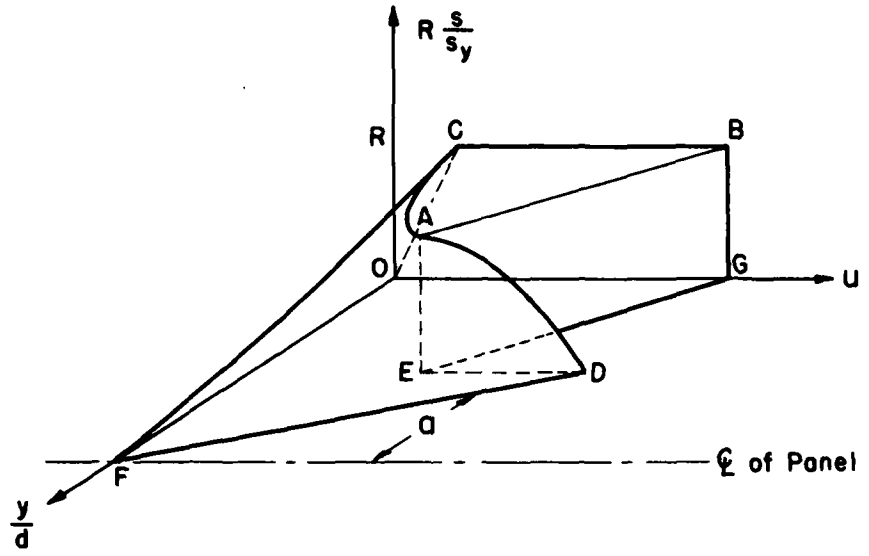

Fig. A.6 Geometric Distribution of Stress Along Contact Area

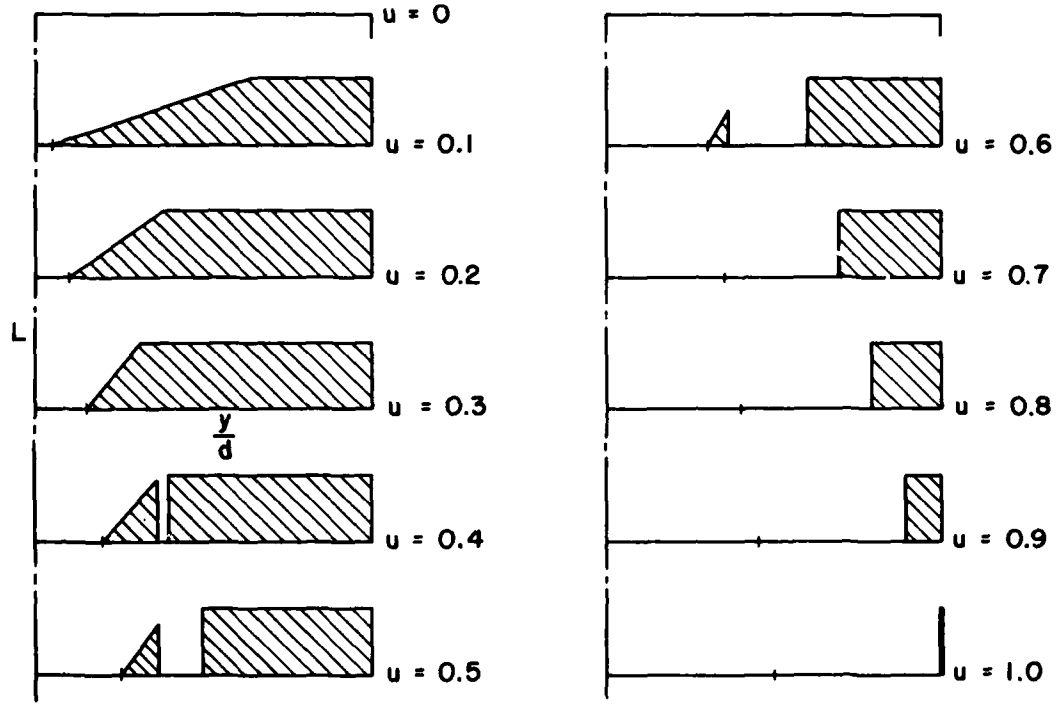

Fig. A.7 Stress Distribution Along Contact as a Function of Mid-Span Deflection

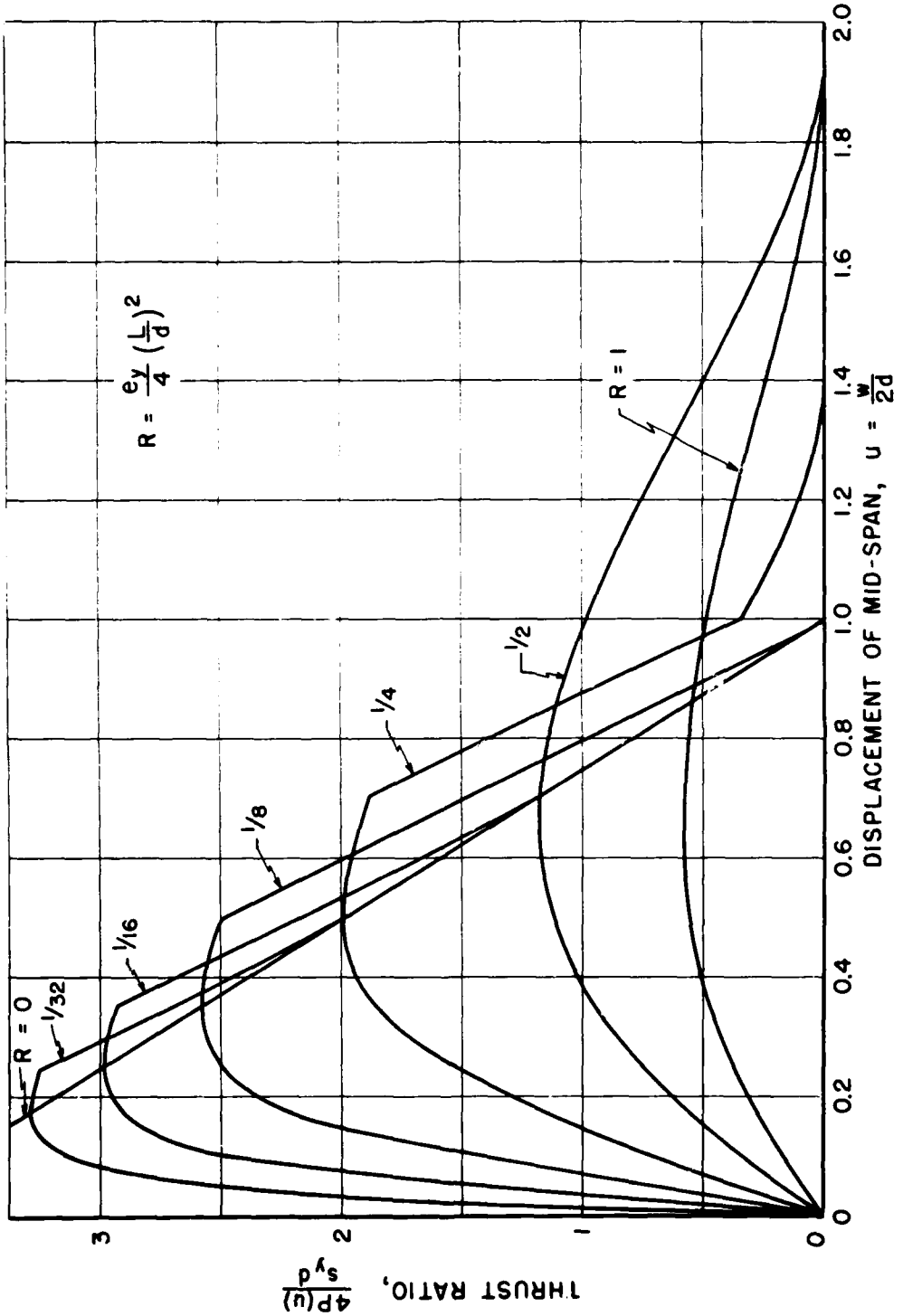

Fig. A.8 Variation of Thrust Force with Beam Deflection

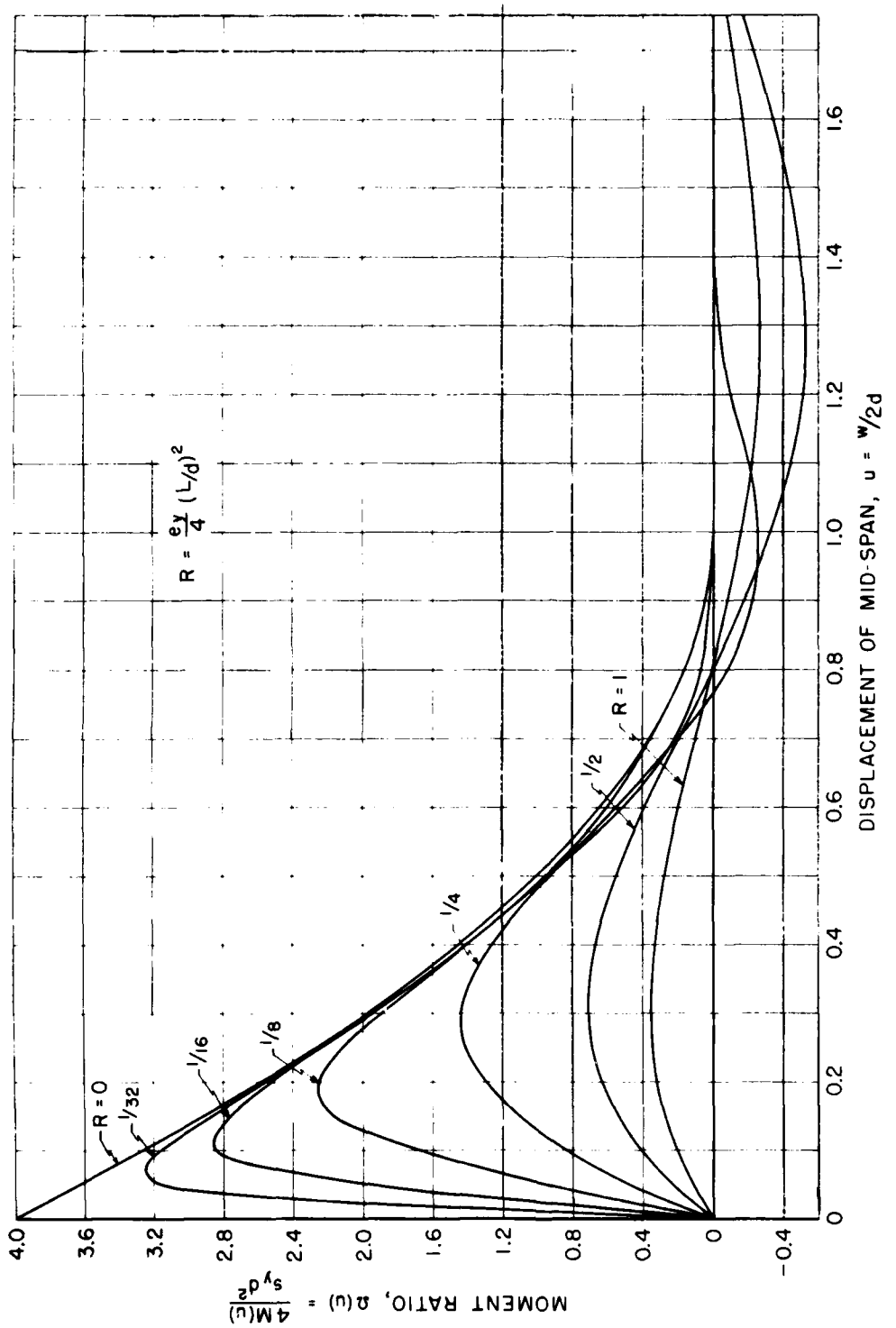

Fig. A.9 Variation of Resisting Moment with Beam Deflection

APPENDIX B

BLAST LOADING ON WALL AND ROOF PANELS

by T. Schiffman

B.1 INTRODUCTION

The prediction methods for loading computations on roof and wall panels of the types tested were developed in the final pretest report, and this appendix contains a summary of the pertinent results of that work. The loading schemes are presented in terms of arbitrary geometry and shock parameters for solid front walls and roofs of flat, curved, and pitched shape atop partially open two-dimensional structures, i.e., "hollow models." Loading conditions for both Mach and regular reflection are considered. The front wall loadings are obtained directly. The net loading on the roofs is obtained by subtracting the loading on the inside surface from that on the outside, and is best done graphically. These procedures are illustrated numerically for certain of the test roofs.

The load prediction methods were, of course, developed prior to the test and have not been revised as a result of the test data obtained, since this work is beyond the scope of the test program. As discussed in Chapter 5, the test results indicate that the predictions for roof loading are fair to good in most respects for Mach reflection, but are poor in certain respects for the regular reflection region. It was realized during the course of this work that certain aspects of the development were of a questionable nature. While no formal error estimate in terms of upper and lower bounds was practical, a relative accuracy for the test structures, starting with what is considered the most reliable prediction and ending with the most uncertain, was believed to be as follows:

(1) Panels in Mach region
(2) Panels in regular reflection region
(3) Flat roofs in Mach region
(4) Pitched and curved roofs in Mach region
(5) Flat roofs in regular reflection region

There are many shock tube data and data from a few large-scale field tests available for panels in the Mach region; hence these head the list of reliability. As far as panels in the regular reflection region are concerned, the peak loadings due to re-entrant corner effects were confirmed in the ARF shock tube, and the theoretical predictions for relief time and drag pressures are considered fairly accurate, too. The loadings on flat roofs in the Mach region are supported by shock tube and large-scale field tests and the predictions would have been considered satisfactory, were it not for the large beams, trusses, purlins, etc. in the 3.5 structures which introduce local extraneous turbulences, and reflected pressures, i.e. phenomena which were not taken into account in the predictions. It is significant to note that the present test data indicate such effects to be minor. Pitched and curved roof load predictions are only minor perturbations of the flat ones (for the 3.5 structures) due to the slight slope in pitched roofs and large radius of curvature of curved ones, combined with only about a 15 per cent change in volume of the buildings. Far removed in accuracy from these cases is the loading on roofs in the regular reflection region, where both incident and reflected shocks enter the structure and interact with the interior surfaces and with each other. Accordingly, load prediction methods for such a complex problem were acknowledged as being highly speculative, and in need of experimental verification.

B.2 NOMENCLATURE

B.2.1 General

The loading cycle is divided logically into two phases, the diffraction phase and the drag phase. The diffraction phase deals with the initial diffraction of a shock front around a structure, during which time pressures on most surfaces change very rapidly. The drag phase deals with established flow, when pressures on all surfaces change relatively slowly. This second phase, in which the loading decreases monotonically at a rate proportional to side-on pressure variation, is also referred to as pseudo steady state. The drag forces are proportional to the product of one-half the density times the square of the flow velocity times the area. The factor of proportionality is defined as the drag coefficient.

Throughout this appendix the term "hollow model" refers to a building having openings symmetrically located in the front and back walls. In addition, the building is assumed to have a minimum amount of obstructions or protuberances on the inside. The front wall is that surface first struck by the shock. For hollow models the loading pertains only to the roof section.

B.2.2 Geometric Parameters

h = height of hollow model or front wall panel (ft)

ℓ = length of hollow model measured in the direction of flow (ft)

w = width of front surface of hollow model or wall panel (ft)

$\Omega_f = \Omega$ = per cent opening in front wall of hollow model, equal to that in back wall = Ω_b

Ω_m = percent opening adjusted for the increased volume of models with pitched or curved roofs

$\Delta \ell = \Omega - \Omega_m$ = difference between actual and adjusted percent openings

α = angle of incidence of shock with ground (deg)

α_{ext} = limiting angle of regular reflection, Fig. B.9

θ = slope angle of roof

B.2.3 Shock Parameters

$p_\sigma(t)$ = side-on pressure (gage psi)

p_σ = initial side-on pressure in Mach region (gage psi)

p_σ' = initial side-on pressure in regular reflection region (gage psi)

$p_d(t)$ = nominal drag pressure (gage psi)

p_d = initial nominal drag pressure (gage psi)

P_o = atmospheric pressure (psi)

c_o = atmospheric sound velocity (ft/sec)

C_{df} = drag coefficient of front surface of wall

C_{dr} = drag coefficient of roof

U = velocity of shock front (ft/sec)

U_m = velocity of shock front in Mach region (ft/sec)

ξ = absolute shock strength, Eq. B.1

ξ'^* = reduced shock strength due to effect of leading edge

$f_o(t)$ = pressure on front surface of wall (gage psi)

$f_{os}(t)$ = pseudo steady state pressure on outside front surface of hollow model (gage psi)

$r_o(t)$ = pressure on outside surface of roof of hollow model (gage psi)

$r_{os}(t)$ = pseudo steady state pressure on outside surface of roof of hollow model (gage psi)

$r_i(t)$ = pressure on inside surface of roof of hollow model (gage psi)

$r_{is}(t)$ = pseudo steady state pressure on inside surface of roof of hollow model (gage psi)

$r(t)$ = net pressure difference on roof of hollow model (gage psi)

$C(\theta, \xi)$ = reflection coefficient for pitched and curved roofs, Fig. B.6

m = numerical constant for the relief time on front half of pitched and curved roofs, Fig. B.6

q = numerical constant for the buildup time on back half of pitched and curved roofs, Fig. B.6

ξ_{if} = inside shock strength near front wall of hollow model

ξ_{ib} = inside shock strength near back wall of hollow model

ξ_{ib3} = inside shock strength near back wall of special model where the ratio of length to height (or to half width) is equal to 3

$p_{\sigma if}$ = overpressure behind inside shock wave near front wall of hollow model (gage psi)

$p_{\sigma ib}$ = overpressure behind inside shock wave before striking back wall of hollow model (gage psi)

p_{irf} = pressure after reflection from inside front wall of hollow model (gage psi)

p_{irb} = pressure after reflection from inside back wall of hollow model (gage psi)

$p_{re}(t)$ = side-on pressure in regular reflection region (analogous to $p_\sigma(t)$ in Mach region) (gage psi)

p_{re} = initial side-on pressure in regular reflection region (gage psi)

$\bar{p}_{\sigma i}$ = overpressure behind inside shock wave in regular reflection region (gage psi) Eq. B.22

$\bar{p}_{ir}$ = pressure after reflection from inside back wall in regular reflection region (gage psi)

p_1 = peak pressure on front face in regular reflection region when incident shock has covered entire face, Eq. B.15 (gage psi)

p_2 = peak pressure on front face in regular reflection region when reflected shock has covered entire face, Eq. B.16 (gage psi)

p_3 = peak pressure on outside roof in regular reflection region when incident shock has covered roof, Eq. B.21 (gage psi)

K = correction factor for drag pressures in regular reflection region

t = time measured for the instant the shock first contacts the front surface of hollow model or wall (sec)

t_o = duration of first positive phase (sec)

t* = time at which pressure inside hollow model reaches a pseudo steady state value (sec)

B.3 SUMMARY OF LOADING FORMULAE

B.3.1 Mach Reflection Region

The shock strength, ξ, is defined as the ratio of absolute pressures across the outside shock front, which is given in terms of the initial overpressure p_σ and the atmospheric pressure $P_o = 14.7$ psi as

$$\xi = 1 + \frac{p_\sigma}{14.7} \quad . \tag{B.1}$$

The overpressure-time variation of the outside blast wave is approximated by the relation,

$$p_\sigma(t) = p_\sigma e^{-t/t_o}\left(1 - \frac{t}{t_o}\right) . \qquad (B.2)^{1/}$$

The nominal drag pressure, $p_d(t)$, is given approximately by

$$p_d(t) = p_d e^{-2t/t_o}\left(1 - \frac{t}{t_o}\right)^2 \qquad (B.3)$$

where

$$p_d = \frac{2.5p_\sigma^2}{7P_o + p_\sigma} \approx \frac{p_\sigma^2}{40} \text{ (psi)} . \qquad (B.4)$$

The shock front velocity, U, is given by

$$U = \frac{c_o}{\sqrt{7}}\sqrt{1 + 6\xi} = 422\sqrt{1 + 6\xi} \text{ (ft/sec)} . \qquad (B.5)$$

B.3.2 Regular Reflection Region

The shock strength, ξ, associated with a shock striking the ground with an incidence angle, α, is defined as the square root of the ratio of absolute pressures across the outside incident shock front, and is given approximately in terms of initial reflected overpressure, p_{re}, and the atmospheric pressure, $P_o = 14.7$ psi, as

$$\xi = \sqrt{1 + \frac{p_{re}}{14.7}} . \qquad (B.6)$$

The reflected overpressure of the outside blast wave is approximated by the relation

$$p_{re}(t) = p_{re} e^{-t/t_o}\left(1 - \frac{t}{t_o}\right) . \qquad (B.7)$$

1/ A somewhat more general form of this pressure-time relationship is

$$p_\sigma(t) = p_\sigma e^{-c(t/t_o)}\left(1 - \frac{t}{t_o}\right) .$$

For the purposes of the pretest computations, the value c = 1 was used. As discussed in Chapter 5, better values appear to be c = 1.6 and c = 2.2 for the 3.5a and 3.5b structures, respectively.

The nominal drag pressure $p_d(t)$ is given approximately by

$$p_d(t) = K\, p_d\, e^{-2t/t_o} \left(1 - \frac{t}{t_o}\right)^2 \qquad (B.8)$$

where

$$p_d = \frac{10P_o(\xi - 1)^2(6\xi + 1)}{(6 + \xi)^2} \sin^2 \alpha \qquad (B.9)$$

and

$$K = 1 + \frac{p_{re}}{10P_o} \quad . \qquad (B.10)$$

The correction factor K has been introduced to preserve the total drag impulse when using the approximate relationship given by Eq. B.8.

It should be noted that p_{re} in the regular reflection region,

$$p_{re} = P_o(\xi^2 - 1), \qquad (B.11)$$

corresponds to p_σ in the Mach region,

$$p_\sigma = P_o(\xi - 1), \qquad (B.12)$$

and should not be confused with p_σ' in the regular reflection region, where

$$p_\sigma' = P_o(\xi - 1) = \frac{p_{re}}{\xi + 1} \quad . \qquad (B.13)$$

The shock front velocity is again given by Eq. B.5, but the velocity vector makes an angle α with the ground, whereas the Mach velocity vector moves parallel to the ground.

B.4 GEOMETRIC AND BLAST PARAMETERS FOR TEST CONDITIONS

The test roof and wall panels are described fully in Chapters 2 and 5 and in Appendix C. For convenience the pertinent dimensions of these structures are repeated in Table B.1. The measured blast parameters at the test locations are given in Table B.2. It is seen that the 3.5c panels were in the regular reflection region, whereas the other items were all in the Mach region.

For the purpose of load predictions, it is assumed that the 3.5a and 3.5b structures are situated in the path of a Mach stem of much greater height than the height of the panels. The front surface is assumed to be struck head-on, i.e., under normal incidence. The 3.5c

TABLE B.1 - Pertinent Dimensions of Test Panels

Panel	Type	Height, H (ft)	Width, W (ft)	Length, L (ft)	Opening, Ω (%)	Adjusted Opening Ω_m, (%)	Slope Angle, θ (deg)
3.5bb	Flat roof	10'2"	16'1"	30'	0.165	---	---
3.5ba	Curved roof	10'2"	16'1"	30'	0.165	0.135	15
3.5ab	Pitched roof	9'8"	16'1"	30'10"	0.18	0.157	19
3.5ca	Flat roof	12'5"	16'9"	27'4"	0.12	---	---
3.5ae	Wall	12'	17'1/2"				
3.5af	Wall	12'	17'1/2"				
3.5cd	Wall	12'	17'1/2"				
3.5bd	Wall	12'	17'1/2"				

Note: The height of the wall panels refers to the over-all height of the test cell.

TABLE B.2 - Blast Parameters for Test Panels

Panel	Ground Range (ft)	Overpressure, p_σ (psi)	Duration (sec)	Incidence Angle with Ground, α, (deg)	Type of Reflection
3.5c	2162	12 $\pm$ 0.8	0.78	42	Regular
3.5b	4500	7.1 $\pm$ 0.3	0.91	62	Mach
3.5a	6693	4.2 $\pm$ 0.1	1.0	70	Mach

Atmospheric pressure, P_o = 13.2 psi.

structures are assumed to be in the regular reflection region, where phase velocity vectors are also normal to the front surfaces.

The actual test conditions were such that the deviations from normal orientation ranged from 7 to 10 deg for the 3.5a and 3.5b structures, and up to 20 deg for the 3.5c structures. The height of the Mach stem impinging on the former panels was from 40 to 60 ft (or higher), and a so-called pseudo Mach stem caused by a thermal layer up to 2 ft in height was probably incident on the 3.5c structures. It is expected that this over-all discrepancy between assumed and actual test conditions does not seriously affect the validity of the load predictions.

B.5 FRONT WALL PANELS IN THE MACH REGION

The loadings on two-dimensional front wall panels located in the Mach region are presented in Table B.3. The pressure rises instantaneously to the reflected pressure, p_r, where

$$p_r = p_\sigma \frac{6 + 8\xi}{6 + \xi} \quad . \tag{B.14}$$

It then drops linearly to the pseudo steady state value in $3\bar{h}/U$ time units ($\bar{h} = H$). From that time on it follows the pseudo steady state value until the end of the first positive phase. The drag coefficient chosen for the front wall surface is $C_{df} = 1$; $p_\sigma(t)$ is given by Eq. B.2 and $p_d(t)$ by Eq. B.3. Table B.3 also illustrates the loading numerically for the 3.5bd panel.

For end panels the three-dimensional effects speed the relief to pseudo steady state pressures. A study of Princeton fringe shift diagrams suggests the relief time of $t = 2.5\bar{h}/U$, instead of $t = 3\bar{h}/U$, the value used for all other panels in the Mach region. This modification has an entirely negligible influence on the magnitude of the net force, if the panel is assumed to remain intact during the loading period.

B.6 LOADING ON FRONT WALLS IN THE REGULAR REFLECTION REGION

The loading on front wall panels in the regular reflection region is presented in Table B.4. The pressure increases linearly from zero to a value p_1, at the time the wave has just swept over the front surface (from top to bottom), i.e., at $t = \bar{h} \cos \alpha/U$. The magnitude of p_1 is given by the following relationship

$$p_1 = \frac{p_{re}}{\xi + 1} \left[1 - \frac{\alpha^\circ}{90} + \left(\frac{6 + 8\xi}{6 + \xi} \right) \left(\frac{\alpha^\circ}{90} \right) \right] . \tag{B.15}$$

TABLE B.3 - Pressure on Front Walls in the Mach Region

Time, t (sec)		Pressure, f (psi)	
Symbolic 3.5bd	Numerical	Symbolic 3.5bd	Numerical
0	0	p_r	17.2
$\frac{3\bar{h}}{U}$	0.0269	$p_\sigma(t) + C_{df}\, p_d(t)$	$p_\sigma(t) + 1\, p_d(t)$
$> \frac{3\bar{h}}{U}$	> 0.0269	$p_\sigma(t) + C_{df}\, p_d(t)$	$p_\sigma(t) + 1\, p_d(t)$
t_o	0.91	0	0

TABLE B.4 - Pressure on Front Walls in the Regular Reflection Region

Time, t (sec)		Pressure, f_o (psi)	
Symbolic	Numerical 3.5cd	Symbolic	Numerical 3.5cd
0	--	0	0
$\frac{\bar{h}\cos\alpha}{U}$	0.007	p_1	8
$\frac{2\bar{h}\cos\alpha}{U}$	0.014	p_2	21
$\frac{5\bar{h}\cos\alpha}{U}$	0.035	$p_{re}(t) + C_{df}\, p_d(t)$	$p_{re}(t) + 1\, p_d(t)$
$> \frac{5\bar{h}\cos\alpha}{U}$	> 0.035	$p_{re}(t) + C_{df}\, p_d(t)$	$p_{re}(t) + 1\, p_d(t)$
t_o	0.78	0	0

The average pressure on the front face continues to increase until it reaches its peak value at $2\bar{h} \cos \alpha / U$ due to the re-entrant corner effects. The peak magnitude is designated by p_2, where

$$p_2 = \frac{p_{re}}{4} \left[\frac{3\xi(\xi \xi'^*)^{3/2} - 3}{\xi^2 - 1} + 1 \right] \qquad \text{(B.16)}$$

and

$$\xi'^* = 1 + \frac{\alpha_o}{90} (\xi - 1) \quad . \qquad \text{(B.17)}$$

The pressure then decreases linearly to its pseudo steady state value in an additional $3\bar{h} \cos \alpha / U$ units. The drag coefficient chosen is taken to be $C_{df} = 1$, the same as for the Mach region. The pressure $p_{re}(t)$ is given by Eq. B.7 and $p_d(t)$ by Eq. B.8. Table B.4 illustrates the loading method for panel 3.5cd. The incidence angle is $\alpha = 42$ deg and the shock strength is $\xi = 1.38$ for this case.

B.7 LOADING ON ROOFS IN THE MACH REGION

B.7.1 Flat Roofs

B.7.1.1 Outside Surface of Roof

Table B.5 exhibits the loading on the outside surface of a flat roof of a hollow model. The pressure builds up linearly to the pseudo steady state value at the time $t = \ell/U$, when the shock front has swept across the roof. From that time on, it follows the pseudo steady value until the end of the first positive phase. The drag coefficient is taken to be $C_{dr} = -0.55$. The numerical values in Table B.5 pertain to the 3.5bb panel. This loading is shown graphically in Fig. B.1.

B.7.1.2 Inside Surface of Roof

Table B.6 exhibits the loading on the inside surface of a flat roof. The loading at $t = \ell/U$, the time when the shock front reaches the back wall, is taken as the average of $p_{\sigma if}$ and $p_{\sigma ib}$. The pressure $p_{\sigma if}$ is obtained from Fig. B.2 and the relation

$$p_{\sigma if} = P_o(\xi_{if} - 1),$$

while $p_{\sigma ib}$ is obtained from Fig. B.4 in terms of $p_{\sigma ib3}$ which applies only to a structure of length to height ratio of 3:1. The numerical value for $p_{\sigma ib3}$ is found from Fig. B.3 and the relation

$$p_{\sigma ib3} = P_o(\xi_{ib3} - 1) \ .$$

TABLE B.5 - Pressure on Outside Surface of Flat Roof in Mach Region

Time, t (sec)		Pressure, r_o (psi)	
Symbolic	Numerical 3.5bb	Symbolic	Numerical 3.5bb
0	0	0	0
ℓ/U	0.0224	$p_\sigma(t) + C_{dr}\, p_d(t)$	$p_\sigma(t) - 0.55\, p_d(t)$
$> \ell/U$	> 0.0224	$p_\sigma(t) + C_{dr}\, p_d(t)$	$p_\sigma(t) - 0.55\, p_d(t)$
t_o	0.91	0	0

TABLE B.6 - Pressure on Inside Surface of Flat Roof in Mach Region

Time, t (sec)		Pressure, r_i (psi)	
Symbolic	Numerical 3.5bb	Symbolic	Numerical 3.5bb
0	0	0	0
ℓ/U	0.0224	$\frac{p_{\sigma if} + p_{\sigma ib}}{2}$	2.2
$2\,\ell/U$	0.0448	$\frac{p_{irf} + p_{irb}}{2}$	4.35
$t^* = (5-4\Omega)\,\ell/U$	0.096	$p_\sigma(t)$	$p_\sigma(t)$
$> t^*$	> 0.096	$p_\sigma(t)$	$p_\sigma(t)$
t_o	0.91	0	0

At the time $t = 2\ell/U$, when the wave reflected from the back wall has reached the front wall, the loading is the average of p_{irf} and p_{irb}, where p_{irb} is obtained from Fig. B.5 and

$$p_{irf} = p_{irb}\left(\frac{p_{\sigma if}}{p_{\sigma ib}}\right) . \qquad (B.18)$$

The loading then varies linearly until the pseudo steady state value is reached, whereupon it follows the pseudo steady state curve until the end of the first positive phase. The numerical values pertain to the 3.5bb roof and are plotted in Fig. B.1.

B.7.2 Pitched Roofs

B.7.2.1 Outside Surface of Pitched Roof

The loading on the outside surface of a pitched roof is presented in Tables B.7 and B.8 in conjunction with Fig. B.6. Table B.7 gives the loading on the front half of the roof, while Table B.8 gives the loading on the rear half. The average load per unit area over the entire roof is obtained by averaging these component loadings. The numerical values shown in the tables and Fig. B.7 pertain to the 3.5ab roof.

Figure B.6 shows both the reflection coefficient (ratio of peak pressure to side-on pressure) as a percentage of side-on pressure at the time when the wave has covered the front half of the sloped roof, and the time when pseudo steady state has been reached on the front half in terms of ℓ/U time units. Experimental data (solid lines) are shown for a shock strength of $\xi = 2$. It will be noted that the theoretical dashed line for the peak pressure does not deviate too far from the solid line. A theoretical expression for the dashed curve, namely,

$$\frac{p}{p_\sigma} = C(\theta,\xi) = \frac{\pi - 2\theta}{\pi} + \left(\frac{6 + 8\xi}{6 + \xi}\right)\left(\frac{2\theta}{\pi}\right) \qquad (B.19)$$

has been extended to shock strengths other than $\xi = 2$. The solid curves for the pseudo steady state time given in Fig. B.6 are assumed to apply for all shock strengths.

The curve showing the time to reach pseudo steady state on the back was derived in a manner similar to that mentioned above. The drag coefficient for the pseudo steady state curves on front and back surfaces is taken as $C_{dr} = -0.8$.

B.7.2.2 Inside Surface of Pitched Roof

As the Mach wave enters a hollow model it undergoes the following changes brought about by the sloped roof.

(a) In general, the wave will be weaker due to the over-all increase in volume.

TABLE B.7 - Pressure on Outside Surface of Front Half of Pitched and Curved Roofs in Mach Region

Time, t (sec)		Pressure, r_o (psi)	
Symbolic	Numerical 3.5ab	Symbolic	Numerical 3.5ab
0	0	0	0
$\frac{\ell}{2U}$	0.0123	$p_\sigma C(\theta,\xi)$	5.35
$\frac{m\ell}{2U}$ a/	0.0369	$p_\sigma(t) - 0.8\, p_d(t)$	$p_\sigma(t) - 0.8\, p_d(t)$
$>\frac{m\ell}{2U}$	>0.0369	$p_\sigma(t) - 0.8\, p_d(t)$	$p_\sigma(t) - 0.8\, p_d(t)$
t_o	1.0	0	0

a/ The value of m is obtained from Fig. B.6 (m = 3 for 3.5ab roof)

TABLE B.8 - Pressure on Outside Surface of Back Half of Pitched and Curved Roofs in Mach Region

Time, t (sec)		Pressure, r_o (psi)	
Symbolic	Numerical 3.5ab	Symbolic	Numerical 3.5ab
0	0	0	0
$\frac{\ell}{2U}$	0.0123	0	0
$\frac{q\ell}{2U}$ a/	0.0369	$p_\sigma(t) - 0.8\, p_d(t)$	$p_\sigma(t) - 0.8\, p_d(t)$
$>\frac{q\ell}{2U}$	>0.0369	$p_\sigma(t) - 0.8\, p_d(t)$	$p_\sigma(t) - 0.8\, p_d(t)$
t_o	1.0	0	0

a/ The value of q is obtained from Fig. B.6 (q = 3 for 3.5ab roof).

(b) The wave is weakened as it covers the front half of the structure due to the increase of volume caused by the pitch of the roof.

(c) The wave then is strengthened as it covers the rear half of the structure due to the relative decrease in volume caused by the back half of the pitched roof.

(d) The wave reflected from the back wall is then weakened as it travels the back half toward the front of the structure. This is due to increase in volume caused by the back half of the pitched roof.

(e) This wave is then strengthened as it covers the front half of the structure due to the relative decrease in volume caused by the front half of the pitched roof.

It is reasonable to account for these changes by introducing an adjusted percent opening, Ω_m, which would be that percent opening for a ficticious flat-roofed structure of the same total volume and opening as the pitched roof structure under consideration. In terms of Ω_m the alternate strengthening and weakening effects are described by evaluating $p_{\sigma if}$, $p_{\sigma ib}$, p_{irf} and p_{irb} for the "apparent" openings Ω_f', Ω_f'', Ω_b' and Ω_b''. The primed quantities refer to the apparent openings during the first transit of the shock from front to back, and the double primed quantities refer to the return of the wave (reflected from the back wall) to the front wall. In terms of the true and adjusted openings these quantities are defined as

$$\Omega_f'' = \Omega_b' = \Omega_m + \Delta\Omega$$
$$\Omega_f' = \Omega_b'' = \Omega_m - \Delta\Omega \quad , \tag{B.20}$$

and $\Delta\Omega$ is the difference between the actual and adjusted openings

$$\Delta\Omega = \Omega - \Omega_m \quad .$$

The symbolic loading scheme for the inside surface of a pitched roof is presented in Table B.9. By the above approach it is possible to evaluate the loading for the entire roof surface directly. It should be noted that the time to reach pseudo steady state is defined in terms of the adjusted percent opening in order to account for the volumetric change due to the pitched roof, i.e., $(5 - 4\Omega_m)\ell/U$ instead of $(5 - 4\Omega)\ell/U$. The numerical example pertains to the 3.5ab roof.

B.7.3 Curved Roofs

The loading on curved roofs is reduced to the previous case by introducing an equivalent slope, namely, the slope of lines drawn from the vortex of the roof at $\ell/2$ to the front and rear edges. For example, the equivalent slope angle for the 3.5ba roof is 15 deg. The exterior loadings for curved roofs are therefore obtained in the same manner as for flat roofs, i.e., from Tables B.7 and B.8 in conjunction with Figs. B.6 and B.10.

The artificial slope is not considered in treating the inside loadings. Rather, the loading scheme is identical to that of the pitched roofs with the exception that Ω_m is the Ω associated with a ficticious flat roof building of the same volume and the same window opening as the curved roof building. The quantities Ω_f', Ω_f'', Ω_b', and Ω_b'' are defined as before, Eq. B.20. In terms of these parameters the inside loading is again given by Table B.9.

B.8 LOADING ON FLAT ROOFS IN THE REGULAR REFLECTION REGION

B.8.1 Outside Surface of Roof

The pressures on the outside surface of the roof are listed in Table B.10. The average pressure on the roof increases linearly from zero to a value p_3 at the time the wave has just swept over the roof, $t = \ell \sin \alpha / U$, where p_3 is given by

$$p_3 = \frac{p_{re}}{\xi + 1}\left[\frac{\alpha^\circ}{90} + \frac{6 + 8\xi}{6 + \xi}\left(1 - \frac{\alpha^\circ}{90}\right)\right] . \qquad \text{(B.21)}$$

The loading then increases linearly to its pseudo steady state value in an additional $4h \cos \alpha / U$ time units, and follows the pseudo steady state curve from this time on. The drag coefficient is taken to be $C_{dr} = -0.55$, the same value as that employed for flat roofs in the Mach region. The numerical values in Table B.10 pertain to the 3.5ca roof. The incidence angle is $\alpha = 42$ deg, and the value of ξ required for Eq. B.21 and for the computation of U is equal to 1.38. The loading for this roof is plotted in Fig. B.8.

B.8.2 Inside Surface of Roof

This loading is exceedingly complicated. Both the incident and reflected shocks enter the opening in the front wall at an angle, expand inside, and reflect alternately off the floor and roof surfaces. In addition, the shocks interact with each other. For such studies in the Mach region, shadowgraphs and interferrograms available in the literature were of material aid in formulating a loading sequence. Unfortunately, no such information is available in the regular reflection region and, thus, intuitive engineering judgement has been used in forming an approximation of the loading inside a hollow model. The methods are essentially a modification of those for the Mach region.

TABLE B.9 - Pressure on Inside Surface of Pitched and Curved Roofs in Mach Region

Time, t (sec)		Pressure, r_i (psi)	
Symbolic	Numerical 3.5ab	Symbolic	Numerical 3.5ab
0	0	0	0
$\frac{\ell}{U}$	0.0247	$\frac{p_{\sigma if}(\Omega_f') + p_{\sigma ib}(\Omega_f'')}{2}$	1.72
$\frac{2\ell}{U}$	0.0494	$\frac{p_{irf}(\Omega_b'') + p_{irb}(\Omega_b')}{2}$	3.30
$t^* = (5 - 4\Omega_m)\frac{\ell}{U}$	0.108	$p_\sigma(t)$	$p_\sigma(t)$
$> t^*$	> 0.108	$p_\sigma(t)$	$p_\sigma(t)$
t_o	1.0	0	0

TABLE B.10 - Pressure on Outside Surface of Flat Roofs of Structures in Regular Reflection Region

Time, t (sec)		Pressure, r_o (psi)	
Symbolic	Numerical 3.5ca	Symbolic	Numerical 3.5ca
0	0	0	0
$\frac{\ell \sin \alpha}{U}$	0.0143	p_3	8.7
$\frac{\ell \sin}{U} + \frac{4h \cos \alpha}{U}$	0.0456	$p_{re}(t) + C_{dr}p_d(t)$	$p_{re}(t) - 0.55p_d(t)$
$> \frac{\ell \sin}{U} + \frac{4h \cos \alpha}{U}$	> 0.0456	$p_{re}(t) + C_{dr}p_d(t)$	$p_{re}(t) - 0.55p_d(t)$
t_o	0.78	0	0

The critical pressure and time values are listed in Table B.11. At the time the shock front reaches the back wall, $t = \ell \sin \alpha / U$, the loading is equal to $\bar{p}_{\sigma i}$, where

$$\bar{p}_{\sigma i} = P_o \frac{\left\{\left[(\xi \xi_r')^{n/2} - 1\right]\left[\left.\frac{\xi_{if} + \xi_{ib}}{2}\right|_{Mach} - 1\right]\right\}}{\xi^2 - 1} \qquad (B.22)$$

where

$$\xi_r' = \frac{1}{\xi}\left[1 - \frac{p_3}{p_{re}}\right] + \xi \frac{p_3}{p_{re}}$$

and p_3/p_{re} is obtained from Eq. B.21. The exponent n is selected as follows:

$$\frac{\ell}{h} \tan \alpha < 3 \qquad n = 2$$

$$\text{if} \quad 3 \leq \frac{\ell}{h} \tan \alpha < 4 \quad \text{choose} \quad n = 3 \ .$$

$$4 \leq \frac{\ell}{h} \tan \alpha \qquad n = 4$$

The quantity $\left.\xi_{if} + \xi_{ib}/2\right|_{Mach}$ is evaluated from Figs. B.2, B.3, and B.4 as if the structure were located in the Mach region with equivalent Mach shock strength, $\xi_{Mach} = \xi^2_{reg\ refl}$.

At the time when the reflected wave from the back wall reaches the front wall, $t = 2\ell \sin \alpha / U$, the loading is taken equal to $\bar{p}_{ir}$, where

$$\frac{\bar{p}_{ir}}{\bar{p}_{\sigma i}} = \frac{p_{irb}}{p_{\sigma ib}}$$

and $p_{irb}/p_{\sigma ib}$ is computed from Fig. B.5 with ξ^2 replacing the parameter ξ in the Mach region.

The pressure then varies linearly to its pseudo steady state value $p_r(t)$ and follows the latter until the end of the first positive phase. The quantity α_{ext} appearing in the pseudo steady state time, t*, of Table B.11 refers to the limiting value of regular reflection and is plotted in Fig. B.9 as a function of ξ.

The loading schemes of Table B.11 are illustrated with the roof of the 3.5ca structure.

TABLE B.11 - Pressure on Inside Surface of Flat Roofs of Structures in Regular Reflection Region

Time, t (sec)		Pressure, r_i (psi)	
Symbolic	Numerical 3.5cm	Symbolic	Numerical 3.5cm
0	0	0	0
$\frac{\ell \sin\alpha}{U}$	0.0143	$\bar{p}_{\sigma i}$	1.2
$\frac{2\ell \sin\alpha}{U}$	0.0286	$\bar{p}_{\sigma ir}$	2.4
$t^* = (5-4\Omega)\left[\left(\frac{3\ell+4h}{2U}\right)\left(\frac{a_{ext}-a}{a_{ext}}\right) + \frac{a}{a_{ext}}\frac{L}{U_m}\right]$	0.108	$p_r(t)$	$p_r(t)$
$> t^*$	> 0.108	$p_r(t)$	$p_r(t)$
t_o	0.78	0	0

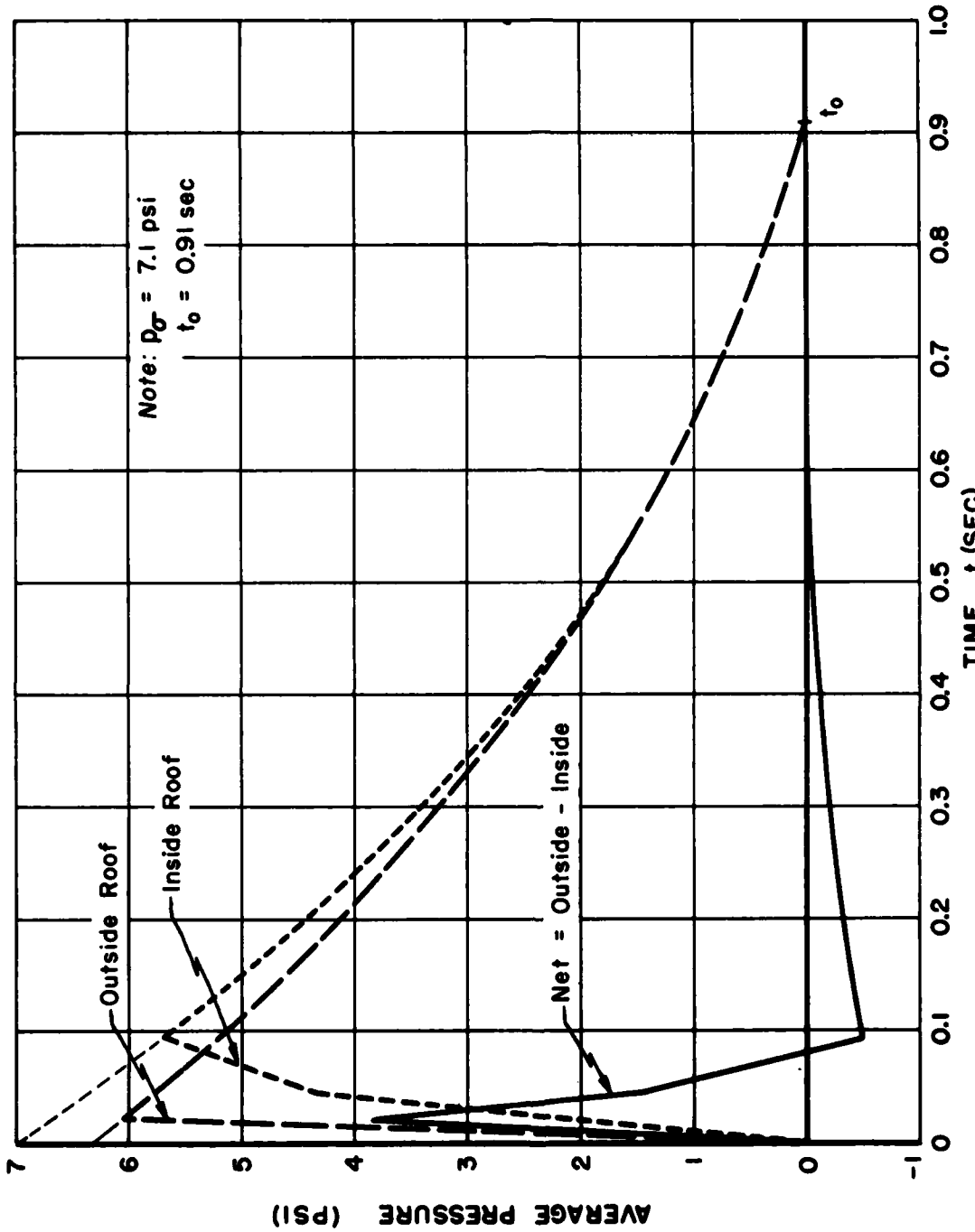

Fig. B.1 Predicted Loading on Flat Roof in Mach Region, 3.5 bb

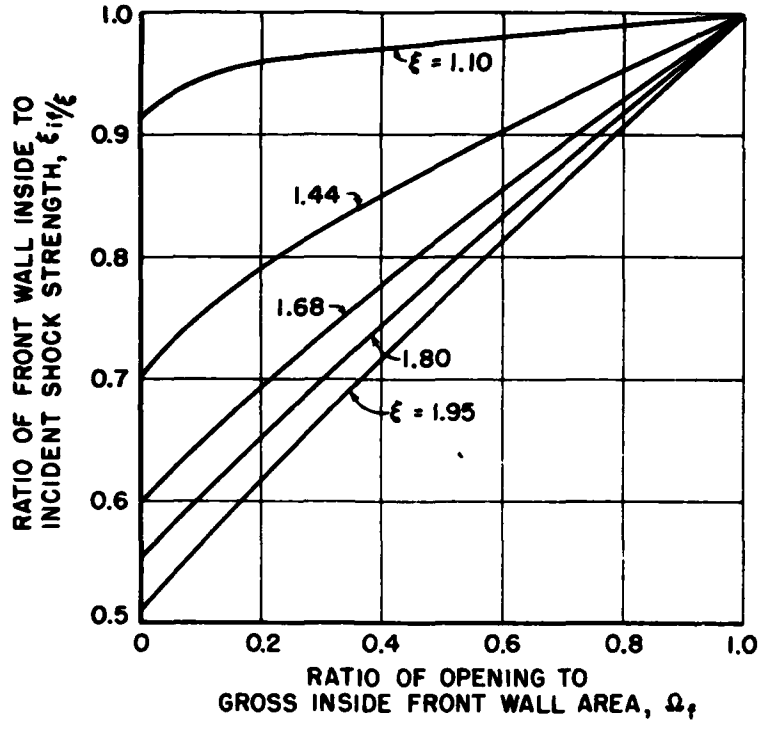

Fig. B.2 Shock Strength Ratio versus Percentage of Frontal Opening for Initial Inside Wave Front Near Front Wall

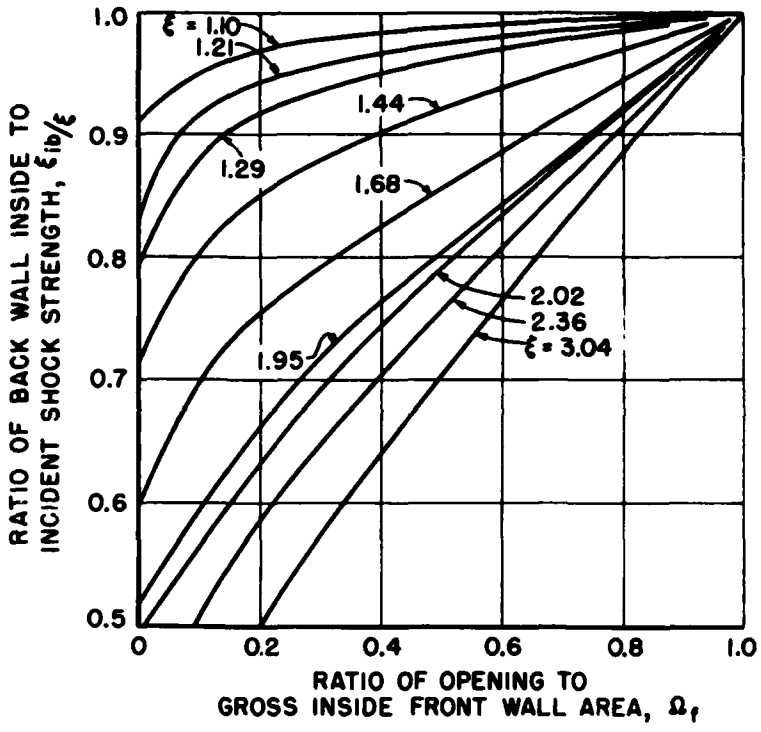

Fig. B.3 Shock Strength Ratio versus Percentage of Frontal Opening for Inside Wave That Strikes Back Wall

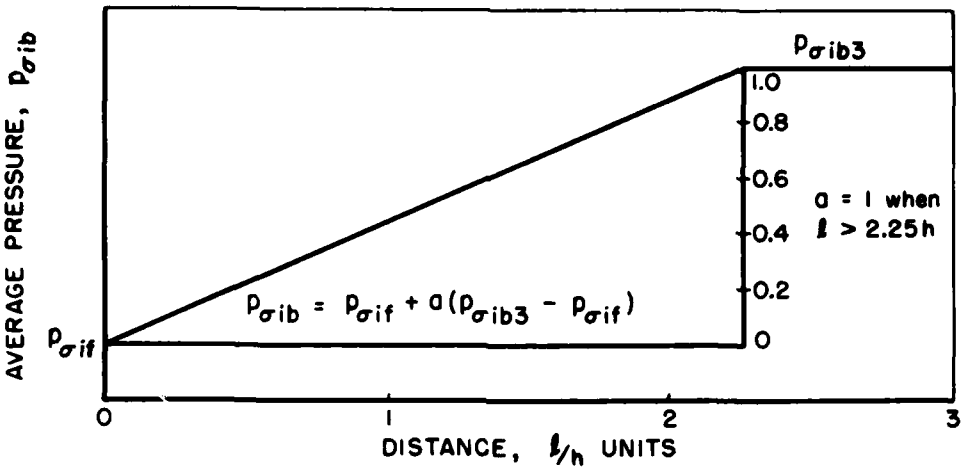

Fig. B.4 Overpressure Behind Inside Wall Just Before Striking Back Wall

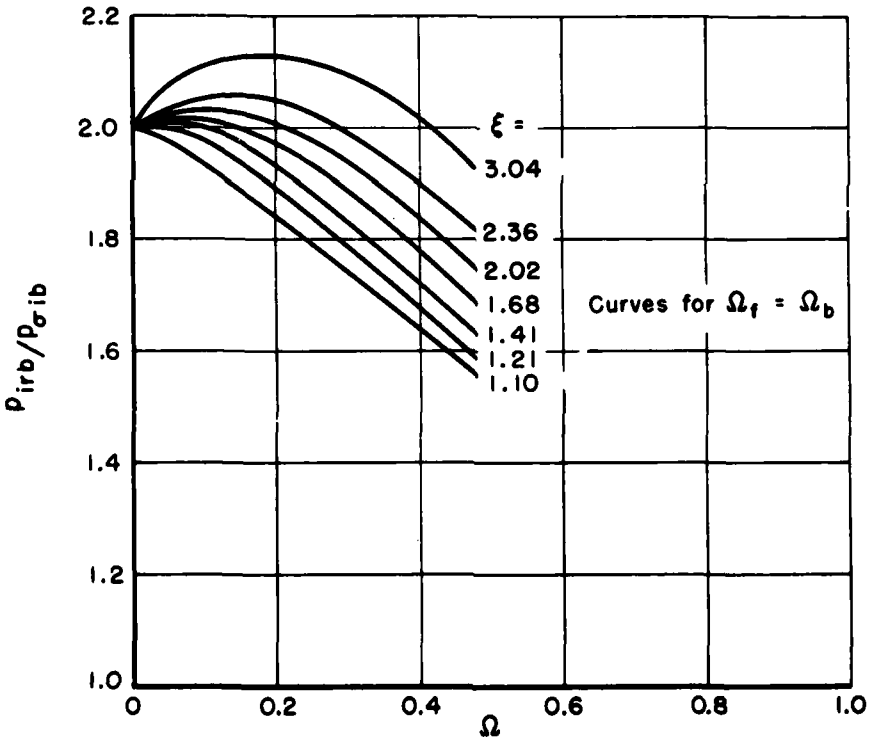

Fig. B.5 Inside Pressure Ratio After Reflection from Inside Back Wall

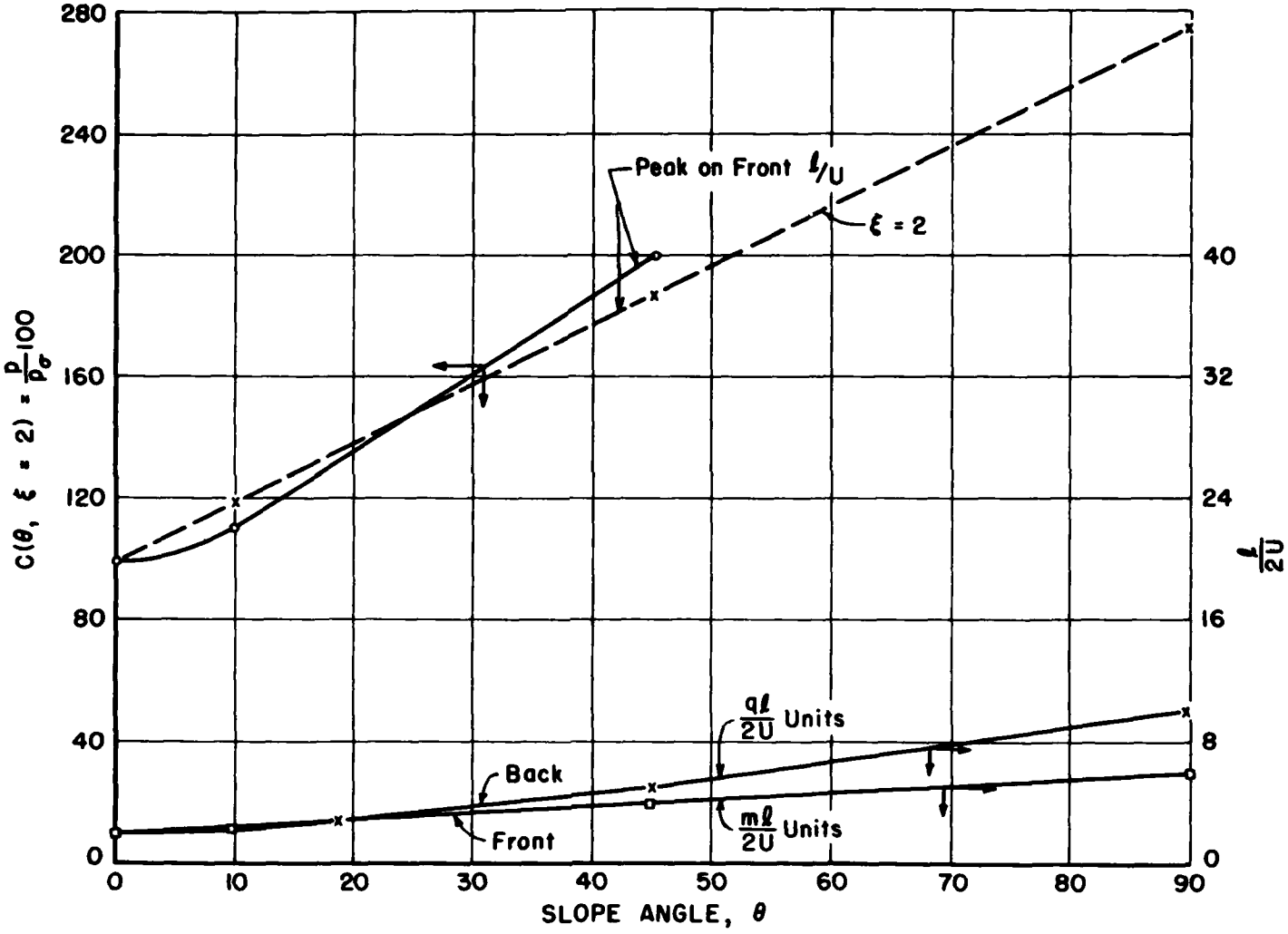

Fig. B.6 Reflection Coefficient and Time to Reach Pseudo Steady State for Pitched Roofs

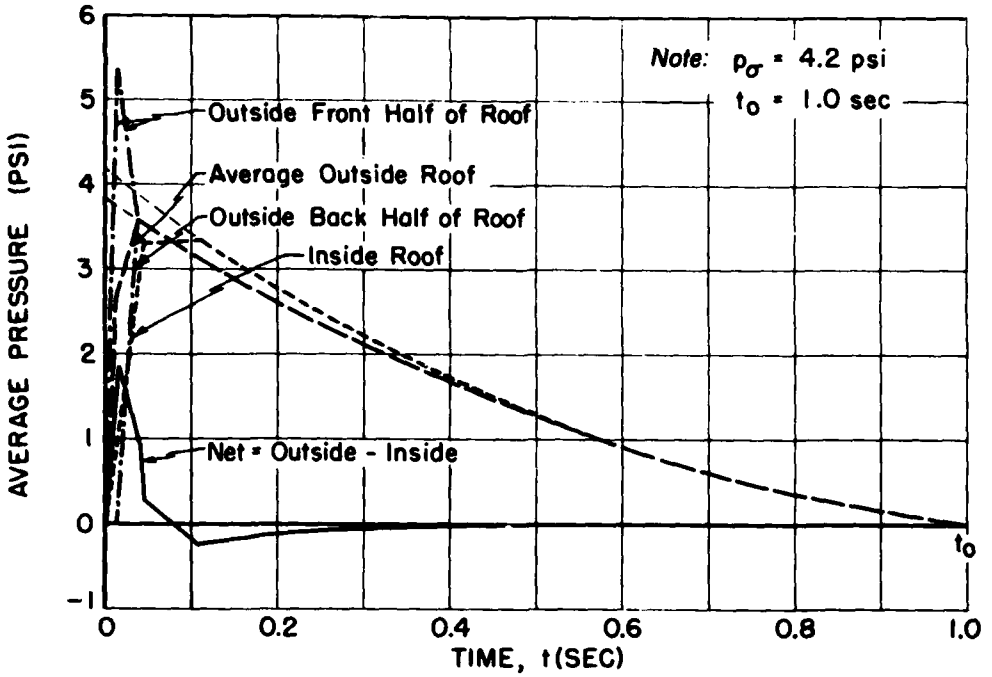

Fig. B.7 Predicted Loading on Pitched Roof in Mach Region, 3.5 ab

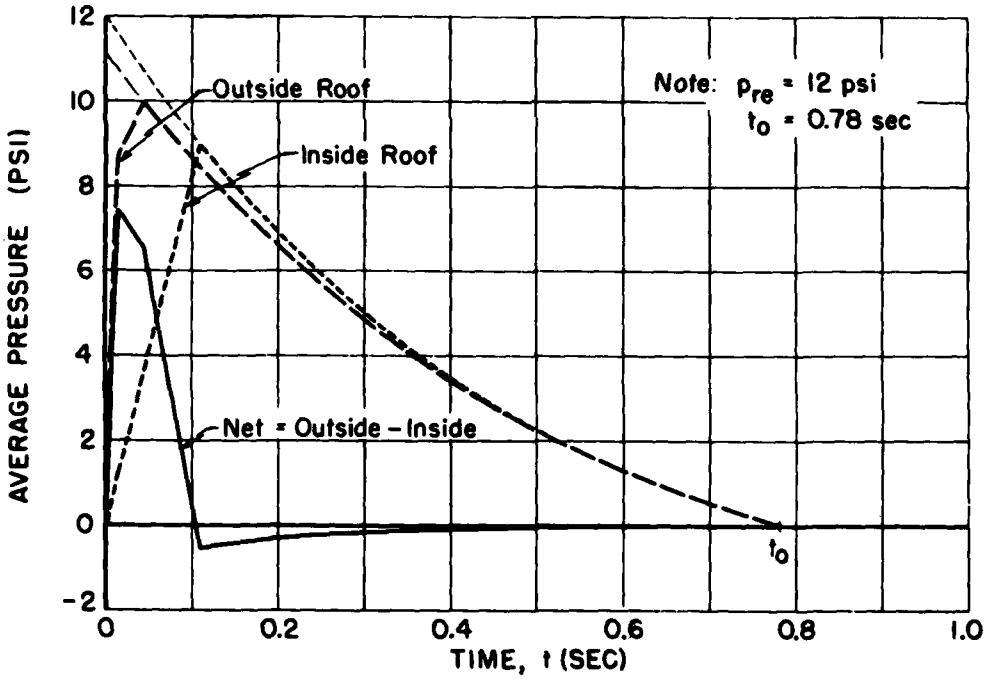

Fig. B.8 Predicted Loading on Flat Roof in Regular Reflection Region, 3.5 ca

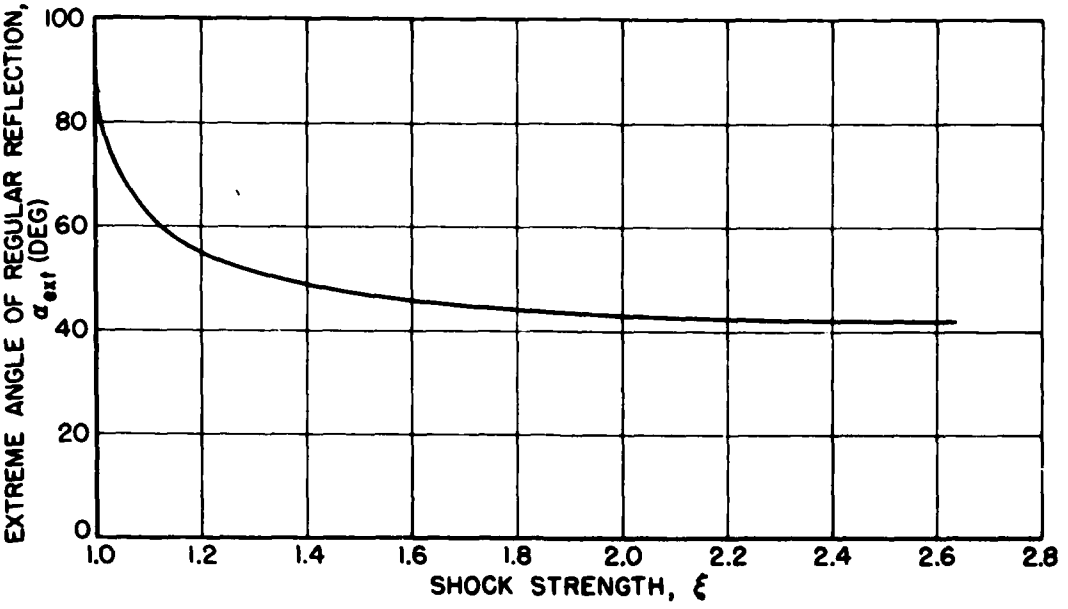

Fig. B.9 Limiting Angle at Regular Reflection, α_{ext}

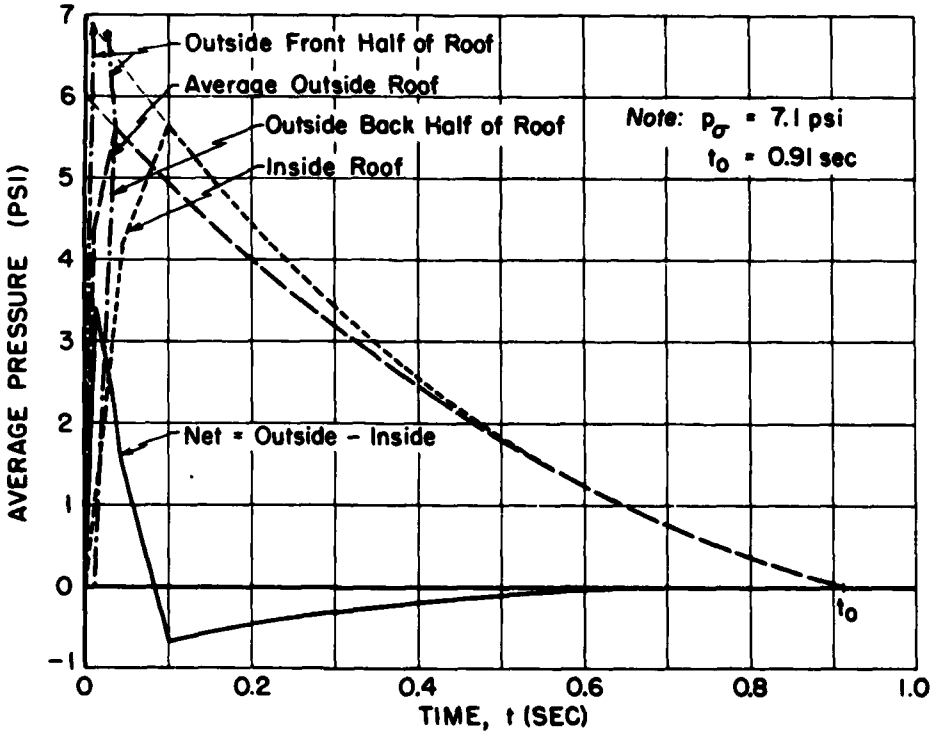

Fig. B.10 Predicted Loading on Curved Roof in Mach Region, 3.5 ba

BIBLIOGRAPHY

Air Force Structures Program, Final Pretest Report, Planning Program for Air Force Structures Tests, Part VII, Tests on Wall and Roof Panels, Armour Research Foundation, for Air Materiel Command, under Contract No. AF33(038)-30029. SECRET

Behavior of Wall Panels Under Static and Dynamic Loads II, Massachusetts Institute of Technology, AFSWP 113, Contract No. DA-49-129-ENG-158.

Development of Procedures for Rapid Computation of Dynamic Structural Response, by N. B. Brooks and N. M. Newmark, University of Illinois, Interim Progress Report, Contract No. AF33(600)-24994.

Military Effects Program, Summary Report of the Technical Director, WT-782.

Operation GREENHOUSE, Appendix I, Vol. I and II, Annex 3.3, Air Force Structures Program, Armour Final Results, WT-87. CONFIDENTIAL RESTRICTED DATA

Operation UPSHOT-KNOTHOLE, Project 1.1b, Air Pressure Versus Time, by L. M. Swift and D. C. Sachs, Stanford Research Institute, WT-711. SECRET-RESTRICTED DATA

Operation UPSHOT-KNOTHOLE, Project 3.1, Tests on Building and Equipment Shapes, T. H. Schiffman, Armour Research Foundation, WT SECRET-RESTRICTED DATA

Operation UPSHOT-KNOTHOLE, Project 3.28.1, Structures Instrumentation, Ballistic Research Laboratories, WT-738.

Operation UPSHOT-KNOTHOLE, Project 9.1, Technical Photography, WT-779.

[redacted] UNCLASSIFIED

DISTRIBUTION

Military Distribution Category 5-60

ARMY ACTIVITIES

1 Asst. Chief of Staff, G-3, D/A, Washington 25, D.C ATTN: Dep. CofS, G-3 (RR&SW)
2 Chief of Research and Development, D/A, Washington 25, D.C. ATTN: Special Weapons and Air Defense Division
3 Chief of Ordnance, D/A, Washington 25, D.C. ATTN: ORDTX-AR
4- 6 Chief Signal Officer, D/A, P&O Division, Washington 25, D.C. ATTN: SIGOP
7 The Surgeon General, D/A, Washington 25, D.C. ATTN: Chief, R&D Division
8- 9 Chief Chemical Officer, D/A, Washington 25, D.C.
10 The Quartermaster General, CBR, Liaison Officer, Research and Development Div., D/A, Washington 25, D.C.
11- 15 Chief of Engineers, D/A, Washington 25, D.C. ATTN: ENGNB
16 Chief of Transportation, Military Planning and Intelligence Div., Washington 25, D.C.
17- 19 Commanding General, Continental Army Command, Ft. Monroe, Va.
20 President, Board #1, Headquarters, Continental Army Command, Ft. Bragg, N.C.
21 President, Board #2, Headquarters, Continental Army Command, Ft. Knox, Ky.
22 President, Board #4, Headquarters, Continental Army Command, Ft. Bliss, Tex.
23 Commanding General, U.S. Army Caribbean, Ft. Amador, C.Z. ATTN: Cml. Off.
24 Commander-in-Chief, European Command, APO 128, c/o PM, New York, N.Y.
25- 26 Commander-in-Chief, Far East Command, APO 500, c/o PM, San Francisco, Calif. ATTN: ACofS, J-3
27- 28 Commanding General, U.S. Army Europe, APO 403, c/o PM, New York, N.Y. ATTN: OPOT Div., Combat Dev. Br.
29 Commandant, Command and General Staff College, Ft. Leavenworth, Kan. ATTN: ALLLS(AS)
30 Commandant, The Artillery and Guided Missile School, Ft. Sill, Okla.
31 Secretary, The Antiaircraft Artillery and Guided Missile School, Ft. Bliss, Texas. ATTN: Lt. Col. Albert D. Epley, Dept. of Tactics and Combined Arms
32 Commanding General, Medical Field Service School, Brooke Army Medical Center, Ft. Sam Houston, Tex.
33 Director, Special Weapons Development Office, Headquarters, CONARC, Ft. Bliss, Tex. ATTN: Lt. Arthur Jaskierny
34 Superintendent, U.S. Military Academy, West Point, N.Y. ATTN: Prof. of Ordnance
35 Commandant, Chemical Corps School, Chemical Corps Training Command, Ft. McClellan, Ala.
36 Commanding General, Research and Engineering Command, Army Chemical Center, Md. ATTN: Deputy for NW and Non-Toxic Material
37- 38 Commanding General, Aberdeen Proving Grounds, Md. (inner envelope) ATTN: RD Control Officer (for Director, Ballistics Research Laboratory)
39- 41 Commanding General, The Engineer Center, Ft. Belvoir, Va. ATTN: Asst. Commandant, Engineer School
42 Commanding Officer, Engineer Research and Development Laboratory, Ft. Belvoir, Va. ATTN: Chief, Technical Intelligence Branch
43 Commanding Officer, Picatinny Arsenal, Dover, N.J. ATTN: ORDBB-TK
44- 45 Commanding Officer, Chemical Corps Chemical and Radiological Laboratory, Army Chemical Center, Md. ATTN: Tech. Library
46 Commanding Officer, Transportation R&D Station, Ft. Eustis, Va.
47 Director, Technical Documents Center, Evans Signal Laboratory, Belmar, N.J.
48 Director, Waterways Experiment Station, PO Box 631, Vicksburg, Miss. ATTN: Library
49 Director, Operations Research Office, Johns Hopkins University, 7100 Connecticut Ave., Chevy Chase, Md., Washington 15, D.C. ATTN: Library
50- 56 Technical Information Service, Oak Ridge, Tenn. (Surplus)

NAVY ACTIVITIES

57- 58 Chief of Naval Operations, D/N, Washington 25, D.C. ATTN: OP-36
59 Chief of Naval Operations, D/N, Washington 25, D.C. ATTN: OP-03EG
60 Director of Naval Intelligence, D/N, Washington 25, D.C. ATTN: OP-922V
61 Chief, Bureau of Medicine and Surgery, D/N, Washington 25, D.C. ATTN: Special Weapons Defense Div.
62 Chief, Bureau of Ordnance, D/N, Washington 25, D.C.
63 Chief, Bureau of Ships, D/N, Washington 25, D.C. ATTN: Code 348
64 Chief, Bureau of Yards and Docks, D/N, Washington 25, D.C. ATTN: D-440
65 Chief, Bureau of Supplies and Accounts, D/N, Washington 25, D.C.
66- 67 Chief, Bureau of Aeronautics, D/N, Washington 25, D.C.
68 Chief of Naval Research, Department of the Navy Washington 25, D.C. ATTN: LT(jg) F. McKee, USN
69 Commander-in-Chief, U.S. Pacific Fleet, Fleet Post Office, San Francisco, Calif.
70 Commander-in-Chief, U.S. Atlantic Fleet, U.S. Naval Base, Norfolk 11, Va.
71- 74 Commandant, U.S. Marine Corps, Washington 25, D.C. ATTN: Code AO3H
75 Superintendent, U.S. Naval Postgraduate School, Monterey, Calif.
76 Commanding Officer, U.S. Naval Schools Command, U.S. Naval Station, Treasure Island, San Francisco, Calif.
77 Commanding Officer, U.S. Fleet Training Center, Naval Base, Norfolk 11, Va. ATTN: Special Weapons School
78- 79 Commanding Officer, U.S. Fleet Training Center, Naval Station, San Diego 36, Calif. ATTN: (SPWP School)
80 Commanding Officer, U.S. Naval Damage Control Training Center, Naval Base, Philadelphia 12, Pa. ATTN: ABC Defense Course
81 Commanding Officer, U.S. Naval Unit, Chemical Corps School, Army Chemical Training Center, Ft. McClellan, Ala.
82 Commander, U.S. Naval Ordnance Laboratory, Silver Spring 19, Md. ATTN: EE
83 Commander, U.S. Naval Ordnance Laboratory, Silver Spring 19, Md. ATTN: EH
84 Commander, U.S. Naval Ordnance Laboratory, Silver Spring 19, Md. ATTN: R
85 Commander, U.S. Naval Ordnance Test Station, Inyokern, China Lake, Calif.
86 Officer-in-Charge, U.S. Naval Civil Engineering Res. and Evaluation Lab., U.S. Naval Construction Battalion Center, Port Hueneme, Calif. ATTN: Code 753
87 Commanding Officer, U.S. Naval Medical Research Inst., National Naval Medical Center, Bethesda 14, Md.
88 Director, U.S. Naval Research Laboratory, Washington 25, D.C ATTN: Code 2029
89 Commanding Officer and Director, U.S. Navy Electronics Laboratory, San Diego 52, Calif. ATTN: Code 4223
90- 91 Commanding Officer, U.S. Naval Radiological Defense Laboratory, San Francisco 24, Calif. ATTN: Technical Information Division
92 Director, Naval Air Experimental Station, Air Material Center, U.S. Naval Base, Philadelphia, Penn.

[redacted]

[redacted] RESTRICTED DATA [redacted] CONFIDENTIAL

UNCLASSIFIED

[redacted]

93 Commanding Officer and Director, David W. Taylor Model Basin, Washington 7, D.C. ATTN: Library
94 Commander, U.S. Naval Air Development Center, Johnsville, Pa.
95 Director, Office of Naval Research Branch Office, 1000 Geary St., San Francisco, Calif.
96-102 Technical Information Service, Oak Ridge, Tenn. (Surplus)

AIR FORCE ACTIVITIES

103 Asst. for Atomic Energy, Headquarters, USAF, Washington 25, D.C. ATTN: DCS/O
104 Director of Operations, Headquarters, USAF, Washington 25, D.C. ATTN: Operations Analysis
105 Director of Plans, Headquarters, USAF, Washington 25, D.C. ATTN: War Plans Div.
106 Director of Research and Development, Headquarters, USAF, Washington 25, D.C. ATTN: Combat Components Div.
107-108 Director of Intelligence, Headquarters, USAF, Washington 25, D.C. ATTN: AFOIN-IB2
109 The Surgeon General, Headquarters, USAF, Washington 25, D.C. ATTN: Bio. Def. Br., Pre. Med. Div.
110 Deputy Chief of Staff, Intelligence, Headquarters, U.S. Air Forces Europe, APO 633, c/o PM, New York, N.Y. ATTN: Directorate of Air Targets
111 Commander, 497th Reconnaissance Technical Squadron (Augmented), APO 633, c/o PM, New York, N.Y.
112 Commander, Far East Air Forces, APO 925, c/o PM, San Francisco, Calif.
113 Commander-in-Chief, Strategic Air Command, Offutt Air Force Base, Omaha, Nebraska. ATTN: Special Weapons Branch, Inspection Div., Inspector General
114 Commander, Tactical Air Command, Langley AFB, Va. ATTN: Documents Security Branch
115 Commander, Air Defense Command, Ent AFB, Colo.
116-117 Commander, Wright Air Development Center, Wright-Patterson AFB, Dayton, O. ATTN: WCRRN, Blast Effects Research
118 Commander, Air Training Command, Scott AFB, Belleville, Ill. ATTN: DCS/O GTP
119 Assistant Chief of Staff, Installations, Headquarters, USAF, Washington 25, D.C. ATTN: AFCIE-E
120 Commander, Air Research and Development Command, PO Box 1395, Baltimore, Md. ATTN: RDDN
121 Commander, Air Proving Ground Command, Eglin AFB, Fla. ATTN: AG/TRB
122-123 Director, Air University Library, Maxwell AFB, Ala.
124-131 Commander, Flying Training Air Force, Waco, Tex. ATTN: Director of Observer Training
132 Commander, Crew Training Air Force, Randolph Field, Tex. ATTN: 2GTS, DCS/O
133 Commander, Headquarters, Technical Training Air Force, Gulfport, Miss. ATTN: TA&D
134-135 Commandant, Air Force School of Aviation Medicine, Randolph AFB, Tex.
136-141 Commander, Wright Air Development Center, Wright-Patterson AFB, Dayton, O. ATTN: WCOSI
142-143 Commander, Air Force Cambridge Research Center, 230 Albany Street, Cambridge 39, Mass. ATTN: CRQST-2
144-146 Commander, Air Force Special Weapons Center, Kirtland AFB, N. Mex. ATTN: Library
147 Commandant, USAF Institute of Technology, Wright-Patterson AFB, Dayton, O. ATTN: Resident College
148 Commander, Lowry AFB, Denver, Colo. ATTN: Department of Armament Training
149 Commander, 1009th Special Weapons Squadron, Headquarters, USAF, Washington 25, D.C.
150-151 The RAND Corporation, 1700 Main Street, Santa Monica, Calif. ATTN: Nuclear Energy Division
152 Commander, Second Air Force, Barksdale AFB, Louisiana. ATTN: Operations Anal. Office
153 Commander, Eighth Air Force, Westover AFB, Mass. ATTN: Operations Anal. Office
154 Commander, Fifteenth Air Force, March AFB, Calif. ATTN: Operations Anal. Office
155-161 Technical Information Service, Oak Ridge, Tenn. (Surplus)

OTHER DEPARTMENT OF DEFENSE ACTIVITIES

162 Asst. Secretary of Defense, Research and Development, D/D, Washington 25, D.C. ATTN: Tech. Library
163 U.S. Documents Officer, Office of the U.S. National Military Representative - SHAPE, APO 55, New York, New York
164 Director, Weapons Systems Evaluation Group, OSD, Rm 2E1006, Pentagon, Washington 25, D.C.
165 Armed Services Explosives Safety Board, D/D, Building T-7, Gravelly Point, Washington 25, D.C.
166 Commandant, Armed Forces Staff College, Norfolk 11, Va. ATTN: Secretary
167-172 Commanding General, Field Command, Armed Forces Special Weapons Project, PO Box 5100, Albuquerque, N. Mex.
173-174 Commanding General, Field Command, Armed Forces, Special Weapons Project, PO Box 5100, Albuquerque, N. Mex. ATTN: Technical Training Group
175-183 Chief, Armed Forces Special Weapons Project, Washington 25, D.C. ATTN: Document Library Branch
184 Office of the Technical Director, Directorate of Effects Tests, Field Command, AFSWP, PO Box 577, Menlo Park, Calif. ATTN: Dr. E. B. Doll
185-191 Technical Information Service, Oak Ridge, Tenn. (Surplus)

ATOMIC ENERGY COMMISSION ACTIVITIES

192-194 U.S. Atomic Energy Commission, Classified Technical Library, 1901 Constitution Ave., Washington 25, D.C. ATTN: Mrs. J. M. O'Leary (For DMA)
195-197 Los Alamos Scientific Laboratory, Report Library, PO Box 1663, Los Alamos, N. Mex. ATTN: Helen Redman
198-202 Sandia Corporation, Classified Document Division, Sandia Base, Albuquerque, N. Mex. ATTN: Martin Lucero
203-205 University of California Radiation Laboratory, PO Box 808, Livermore, Calif. ATTN: Margaret Edlund
206 Weapon Data Section, Technical Information Service, Oak Ridge, Tenn.
207-269 Technical Information Service, Oak Ridge, Tenn. (Surplus)

ADDITIONAL DISTRIBUTION

270 Prof. N. M. Newmark, 111 Talbot Laboratory, University of Ill., Urbana, Ill.

[redacted]